NASA TECHNICAL REPORT

NASA TR R-173
C.1

NASA TR R-173

THE STRUCTURE AND STRENGTH OF THE INNER PLANETS

by Gordon J. F. MacDonald
Goddard Space Flight Center
Greenbelt, Maryland

NATIONAL AERONAUTICS AND SPACE ADMINISTRATION • WASHINGTON, D. C. • DECEMBER 1963

THE STRUCTURE AND STRENGTH OF THE INNER PLANETS

By Gordon J. F. MacDonald

Goddard Space Flight Center
Greenbelt, Maryland

NATIONAL AERONAUTICS AND SPACE ADMINISTRATION

For sale by the Office of Technical Services, Department of Commerce,
Washington, D. C. 20230 -- Price $2.25

THE STRUCTURE AND STRENGTH OF THE INNER PLANETS

by
Gordon J. F. MacDonald
Goddard Space Flight Center

SUMMARY

Recent developments in seismology and geodesy provide data for an improved model of the earth's interior. This report examines the internal structures of the moon, Mars, Venus, and Mercury in the light of what is known about the internal constitution of the earth.

A review of the seismic determination of the elastic constitution of the earth's mantle, based on new results on the stability of silicates at high pressures, leads to the following interpretation that the rapid increase of elastic wave velocity beginning at a depth of 200 km depends on the olivine-spinel transition and the breakdown of silicates to oxides. Preliminary calculations of the stability field of periclase (MgO) and stishovite (very dense SiO_2) relative to olivine ($MgSiO_4$) indicate that the oxides are stable at pressures greater than 100,000 to 150,000 bars. The oxide transition produces a change in volume of about 20 percent.

The earth's gravitational figure, as obtained from satellite orbits, is used to estimate the possible deviations from hydrostatic equilibrium in other planets. The earth's response to tidal excitation provides information regarding the deviations of elasticity within the earth. The near coincidence of the present rate of heat production of a chondritic earth and the present surface heat flow is discussed as a limiting condition on the earth's internal thermal structure.

Observations of the moon's orbital and rotational motions provide data on its gravitational figure. The calculation of its thermal structure shows that a model moon with uniform radioactivity and chondritic composition is inconsistent with the present figure. The inferred strength of the moon requires either that the radioactivity be substantially less than that of chondrites or that heat sources are concentrated in the outer layers. The problem of differentiation without melting is noted. The average lunar material has a radioactivity perhaps one-half or less that of chondritic materials.

The astronomical information on the mean density and gravitational figure of Mars is critically examined. If the mean radius of Mars is taken to be 3310 km,

the planet must have a surface density of 3.8-3.9 gm/cm^3 and be nearly homogeneous. If Mars were homogeneous and had a radioactivity equal to that of chondrites, the interior would be molten and large scale gravitational differentiation would be expected. Since this differentiation is not apparent in the gravitational data, it is concluded that the radioactive composition of Mars differs from that of chondrites.

The internal structures of Mercury and Venus are examined in terms of their inferred rotational history.

It is finally concluded that the inner planets differ in their abundances both of the heavy elements and of potassium, uranium, and thorium. Chondritic meteorites may provide a satisfactory chemical model for the earth, but not for the other inner planets, with the possible exception of Venus. This qualification is due to our ignorance of the internal constitution of Venus.

CONTENTS

THE STRUCTURE AND STRENGTH OF THE INNER PLANETS

by
Gordon J. F. MacDonald
*Goddard Space Flight Center**

Chapter 1

INTRODUCTION

A number of developments in the past few years have stimulated interest in the nature and origin of the planets. In the nineteenth and the early twentieth centuries, investigation of the planetary system utilized the concepts and methods of celestial mechanics. The past 20 years have seen several major breaks with this tradition. Urey emphasized the chemical aspects of the problem of planetary origins and, using thermochemical considerations, provided powerful restraints on speculation (Reference 1). Alfvén insisted that the magnetic fields play a role comparable in importance with that of the gravitational fields (Reference 2). Alfvén's considerations have been extended and deepened, particularly by Lüst and Schlüter (Reference 3) and by Hoyle (Reference 4). Cameron (Reference 5) and Fowler, Greenstein, and Hoyle (Reference 6), after the discovery of xenon-129 in meteorites by Reynolds (References 7-9), demonstrated the constraints placed by nuclear physics on the early history of the solar system. But by far the greatest impetus to further study of the planets has been the promise of direct exploration of the moon, Mars, and Venus. The advent of planetary probes also provides numerous new tools for this study.

Knowledge of the earth and its interior has grown in the past few years. The determination of the constitution of the earth provides a framework within which the observations of the moon and terrestrial planets can be interpreted. Jeffreys first examined the constitution of the earth-like planets in the light of geophysical knowledge (Reference 10). During the past ten years the understanding of the internal constitution of the earth has increased. The study of the earth's gravitational field with artificial satellites and the investigation of its interior by means of observations of low frequency seismic waves have added a new dimension to this understanding. Although major problems still abound in the theory of the earth's interior, its internal distribution of mass and elasticity are relatively well determined. The question of its thermal regime remains a major problem. The origin of its surface features is closely tied to its anelastic behavior, and little progress has been made in this field. The origin of the geomagnetic field remains a mystery, though magnetohydrodynamic theories developed by Bullard and by Elsasser indicate a promising approach to the answer. This report will

*This work was done while the author was on leave from the Institute of Geophysics and Planetary Physics, University of California.

review those areas of the study of the earth that have contributed most heavily to the understanding of its internal constitution. The methods, concepts, and techniques applicable to the earth should also apply to the study of the moon and the other inner planets. Therefore, after considering the state of knowledge about the earth, we will discuss the current state of knowledge of the internal constitution of the moon, Mars, Venus, and Mercury. Particular attention will be paid to those problems about which a great deal will be discovered in the early stages of planetary exploration.

The determination of the earth's figure is the principal concern of geodesy. Since the external figure of the earth is the result of the internal mass distribution, a detailed knowledge of the earth's gravitational field sets limits on the possible internal mass distributions. The departure of the earth's gravitational field from that of a homogeneous sphere results in observable perturbations in the motions of the moon and of artificial satellites. The study of the orbits of artificial satellites has been particularly valuable in providing additional information regarding the earth's external potential. The deviations of the earth's figure from that which would be assumed by a fluid body rotating at the same angular velocity provide some measure either of the earth's strength in resisting long-period small-amplitude stress differences or of this strength and the internal dynamic processes that support the figure inequalities.

Gravitational forces of the moon and sun raise tides in the solid body of the earth; and these tidal forces are precisely known. Accurate observation of the earth's response to these forces yields information on the distribution of both elasticity and density within the earth and on anelasticity of the earth at the frequencies of the tidal forces. The variation of the earth's rotation – both in terms of the variation of position of the instantaneous axis of rotation and in terms of the length of day – also yields information regarding the internal elasticity and anelasticity.

The most powerful tool in the investigation of the earth's interior has been a determination of the time needed for elastic waves to travel through the earth. The source of such elastic waves is, for the most part, earthquakes, though in recent years artificial sources have become increasingly important. The determination of the travel time of these waves permits an estimation of their velocity variations, and this can be combined with geodetic data to obtain the distribution of elasticity and density within the earth. In recent years an additional powerful investigational tool has been the observation of the earth's free oscillations. Because free oscillations involve the planet as a whole, this method reduces the difficulties associated with analyzing many events on different seismographs for several earthquakes.

The variation of elastic wave velocity with depth, when combined with laboratory investigations, permits a first guess as to the temperature distribution in the interior of the earth. A more direct method involves measurements of the heat flowing from the interior through the surface. Locally, this surface heat flux depends on the vertical temperature gradient and thermal conductivity. The *total* surface heat flux is fixed by the internal distribution of radioactive heat sources and of thermal conductivity, and on thermal conditions during the early stages of the earth's formation. Models of the earth involving the distribution of radioactivity and initial thermal conditions can be constructed, leading to the observed total heat flux. These models also give some indication of possible internal temperature distributions. However, the actual distribution remains most uncertain.

A very important aspect of the investigation of the earth's interior concerns the behavior of materials at high pressures and temperatures. In the last few years great progress has been made in simulating deep-earth conditions in the laboratory. Materials that are stable at the earth's surface undergo a vast variety of changes when subjected to the conditions that prevail in the upper 100 km of the earth. It is likely that further changes in the structure of matter will occur in the laboratory experiments as they more closely approach conditions existing in the *deep* interior, where pressures are on the order of 10^6 bars at temperatures on the order of a few thousand degrees. Laboratory data can be combined with seismically derived velocity-depth variation data to construct chemical-physical models of the earth's interior. But the laboratory data do not yet cover a sufficient range, and most models depend heavily on untested theories of the behavior of matter at high temperatures and pressures.

After reviewing the state of knowledge of the earth in the fields considered above, we will examine the present state of ignorance regarding the moon and the other planets. Though it is by far the best known of the nearby bodies, the moon's internal character remains a mystery. The two small Martian satellites provide data on the gravitational figure of the Red Planet. These data are consistent with a number of possible models for the internal constitution of Mars, but a combination of arguments permits some further limits to be placed on the planet's internal character. The natures of Mercury and Venus are even more uncertain. Almost nothing is known about Venus because of its continuous cloud cover. Mercury remains anomalous with its much higher density than the other members of the solar system.

Chapter 2

THE EARTH'S GRAVITATIONAL FIELD

The earth's geometrical figure and its gravitational field are closely related, since the figure is defined in terms of the mean sea level and the mean sea level is fixed by the ocean surface, which is everywhere perpendicular to the direction of gravity. The dimensions of the earth can be estimated by geodetic surveys. Latitudes and longitudes are found by astronomical observation, and surveys along a meridian determine a length. A comparison of the length with the differences in latitude and longitude fixes the local figure. In recent years large arcs have been surveyed on land and geodetic measurements across oceans have been attempted.

A second way of determining the earth's figure involves the measurement of the gravitational field at various places on the surface. Prior to the advent of satellites this was the principal method of determination. It suffers from the fact that the earth's gravitational field contains power in all harmonics. Field irregularities, which can be described as high-wave-number gravitational noise, make it difficult to estimate the field from scattered surface observations. In recent years statistical methods have been applied to the reduction of the gravitational data. These lead to a far superior description of the field, yet they are still inadequate for the low-wave-number components in comparison with the determination made by using satellites.

On account of the flattening of the earth, the attraction of the earth and moon produces a couple which induces motion of the earth's rotation axis about the pole of the ecliptic. This motion is known as precession and the precessional constant H is given by

$$H = \frac{C - A}{C} ,$$

where C is the principal moment of inertia about the axis of rotation and A is the moment of inertia about an axis in the equatorial plane. H can be determined from the period of precession. The observed precession of the equinoxes yields a value of 1/305.3; the principal uncertainty in this value is due to the uncertainty in the mass of the moon.

Artificial satellites offer a powerful method for determining the earth's gravitational field. The orbit of a satellite about an isolated homogeneous spherical earth devoid of an atmosphere would be an exact ellipse. The size and shape of the ellipse would remain constant; the plane of the ellipse would be fixed relative to the stars and the orientation of the ellipse in its own plane would not change. But the earth does have an atmosphere, the sun and moon perturb the motion of a satellite, and, most importantly, the deviations of earth from a homogeneous sphere perturb the ellipse.

The two most important perturbations of the satellite's orbit which are due to the earth's internal density field are the steady rotation of the orbital plane about the earth's axis and the rotation of the major axis of the orbit in its own plane. These rotations are determined by the even order harmonics of the earth's gravitational field. Careful observations of many satellites have fixed the lower order even harmonics. In addition to the secular variation of the satellite orbit, there are long period oscillations due to the odd order harmonics.

Satellite orbits are also perturbed by the atmosphere and the tidal actions of the sun and moon. Fortunately, these effects can be removed for the most part. The main effect of the atmosphere is to make the orbit contract and become more circular; its effect on the rotation of the orbital plane is negligible.

DESCRIPTION OF THE EXTERIOR POTENTIAL

The earth's potential at a distance r from the center of mass of the earth can be expressed as a sum of spherical harmonics:

$$U = \frac{GM}{r}\left\{1 - \sum_{n=2}^{\infty}\left(\frac{a_e}{r}\right)^n\left[J_n^0 P_n^0 \sin\theta + \sum_{m=1}^{n}\left(J_n^m \cos m\lambda + K_n^m \sin m\lambda\right) P_n^m \sin\theta\right]\right\}, \tag{1}$$

where G is the gravitational constant, M the mass, and a_e the equatorial radius of the earth ($a_e = 6378.1 \pm 0.1$ km and $GM/a_e = 62.494 \pm 0.01$ km^2/sec^2), θ is the geocentric latitude, which differs only negligibly from the geodetic latitude in terms other than J_2, and λ is the longitude. The values P_n^m are the associated Legendre functions defined by

$$P_n^m \sin\theta = \frac{\cos^m\theta}{2^n n!}\sum_{l=0}^{k}\frac{(2m-2l)!}{(n-m-2l)!}(-1)^l \sin^{n-m-2l}\theta, \tag{2}$$

where

$$\left.\begin{aligned} k &= \frac{n-m}{2} \qquad (n-m \text{ even}), \\ k &= \frac{n-m-1}{2} \qquad (n-m \text{ odd}). \end{aligned}\right\} \tag{3}$$

Prior to artificial satellites only J_2^0 was known and the value used at that time has been found to be inaccurate by 1 part in 300.

The equation of motion of a satellite can be written in terms of the earth's potential U. A principal problem of celestial mechanics is to determine the effect that the various J_n^m and K_n^m values have on the orbital elements. Six orbital elements are required to describe the Kepler ellipse with one focus at the origin: a, the semimajor axis; e, the eccentricity; i, the inclination of the orbit to the equator; Ω, the angular coordinate of the node, or intersection of the orbit and the equatorial

plane; ω, the argument of perigee or the angle from the ascending node to the point (perigee) of closest approach on the ellipse to the origin; and f, the true anomaly, the angle from perigee to the satellite.

In writing the disturbing potential in terms of the elements of a Keplerian orbit it is apparent that J_n^0, n even, will give rise to secular changes in ω and Ω but have no effect on a, e, or i. J_n^0, n odd, will cause periodic variations with frequency ω in e, i, ω, and Ω.

Since the first satellite launching, a large number of papers have been devoted to the reduction of orbital data to obtain estimates of J. Table 1 lists estimates of the zonal harmonics derived from studies of satellite motion. The tesseral and sectorial harmonics give rise to daily and semidaily oscillations in the orbit. Using observations of the satellite Transit IV-A (1961 o1), R. R. Newton obtained $J_{22} = 2.2 \times 10^{-6}$ and $J_{41} = 1.25 \times 10^{-6}$ (Reference 16).

The errors caused by neglecting higher order terms in the expansion are not yet known, and there is no proof that the accumulated effect of these terms is negligible. Since the series must converge the coefficients must decrease, but the rate at which they decrease is unknown. The high order harmonics may be of more or less the same magnitude. It seems unlikely that any given harmonic would be much larger than those already found, since this would demand an unexpected asymmetrical concentration of mass.

A major result of satellite studies is the discovery that the earth's gravitational potential is irregular. This reduces the value of the concept of flattening, since the earth's geometrical figure cannot be expressed in terms of a single quantity as earlier theories presumed. The surprisingly large magnitude of the low order harmonics clearly shows that the earth's figure is complex.

Table 1

Estimates of Zonal Harmonics.

Source	$J_2^0 \times 10^6$	$J_3^0 \times 10^6$	$J_4^0 \times 10^6$	$J_5^0 \times 10^6$	$J_6^0 \times 10^6$	$J_7^0 \times 10^6$
O'Keefe, Eckels, and Squires (Reference 11)	1082.49 ± 0.06	-2.39 ± 0.26	-1.70 ± 0.06	-0.30 ± 0.53	–	–
Kozai (Reference 12)	1082.19 ± 0.02	-2.29 ± 0.02	-2.13 ± 0.04	-0.23 ± 0.02	–	–
King-Hele (Reference 13)	1082.79 ± 0.15	–	-1.4 ± 0.2	–	0.9 ± 0.8	–
Kaula (Reference 14)	1082.3 ± 0.2	-2.3 ± 0.1	-1.8 ± 0.2	-0.3 ± 0.2	–	–
King-Hele (Reference 15)	1082.7 ± 0.3	-2.4 ± 0.1	-1.7 ± 0.3	-0.1 ± 0.2	0.8 ± 0.1	-0.4 ± 0.2

FIGURE OF A FLUID EARTH

A rotating fluid develops a bulge represented in the gravitational potential by finite values of J_n^0, n even. The difference between observed J_n^0 values for the earth and the J_n^0 values for an equivalent rotating fluid indicates the deviation of the earth from a perfect fluid. The moment of inertia of

a fluid is related to the hydrostatic flattening f by:

$$\frac{C}{Ma_e^2} = \frac{2}{3}\left\{1 - \frac{2}{5}\left[\frac{5m}{2f}\left(1 - \frac{3}{2m}\right) - 1\right]^{\frac{1}{2}}\right\}, \tag{4}$$

to first order in the flattening, where m is the ratio of the centrifugal to the gravitational acceleration at the equator. With the observed value of C/Ma_e^2 the hydrostatic value of the flattening follows from the equation. Henriksen (Reference 17) and O'Keefe (Reference 18) noted that J_2^0 determines a much-improved estimate of the polar moment of inertia, since

$$\frac{J_2^0}{H} = \frac{\frac{C - A}{Ma_e^2}}{\frac{C - A}{C}} = \frac{C}{Ma_e^2}. \tag{5}$$

The hydrostatic flattening can then be used to obtain a value for the hydrostatic J_2^0:

$$J_2^0 = \frac{3}{2}f\left(1 - \frac{1}{2}f\right) - \frac{1}{3}m\left(1 - \frac{3}{2}m - \frac{2}{7}f\right). \tag{6}$$

This theory, carried to higher orders, provides improved estimates of the hydrostatic values for J_2^0, J_4^0, and J_6^0 (Reference 18). Thus the observed value of J_2^0 can be used to obtain a description of what would be the gravitational potential of the earth if the earth behaved as a perfect fluid in hydrostatic equilibrium. Table 2 lists the hydrostatic values of J_n^0. It should be noted that the values of J_n^0, n odd, vanish for a fluid earth, as do the sectorial and tesseral harmonics.

The observed and hydrostatic values for the gravitational potential are compared in the first two lines of Table 2. The third line gives the nonhydrostatic component of the potential computed as the difference between the observed J_n^0 and the J_n^0 for an equivalent rotating fluid. The nonhydrostatic J_n^0 represents density anomalies within the earth. The last line of the table lists values of J_n^0 arising from the continent-ocean structure provided the continents and oceans are in perfect isostatic equilibrium. The observed deviations from equilibrium are larger than and opposite in sign to those expected from the near-surface structure. These anomalies cannot be explained by near-surface or crustal variations in density (References 14 and 19). The negative correlation between the continent-ocean structure and the gravitational figure was anticipated by Jeffreys on the basis of the surface observation of gravity (Reference 20). But the magnitude of the deviations is surprisingly large. This negative correlation may have significance since it possibly reflects the process of formation of the continent-ocean system.

Table 2

Comparison of Observed and Equilibrium Values of J_n^0 in Parts per Million.

Method	J_2^0	J_3^0	J_4^0	J_5^0	J_6^0	J_7^0
Observed	1082.7	-2.4	-1.7	-0.1	0.8	-0.4
Hydrostatic	1071.0	0	-2.9	0	0.00	0
Nonhydrostatic	11.7	-2.4	1.2	-0.1	0.8	-0.4
Topography and Perfect Isostasy	–	0.20	-0.33	0.69	-0.23	–

STRENGTH OF THE EARTH

The interpretation of the deviation of the earth's potential from that expected for an equivalent rotating fluid raises the problem of the anelastic response of the deep earth to small stresses. The question of the earth's response to large-scale small-amplitude stress differences imposed for long periods has plagued geophysicists for a century. Kelvin assumed that the earth can be treated as an elastic body even for long period deformations, whereas Darwin proposed that the earth behaves plastically. Today, proponents for both points of view can be found; the gravitational field as determined from the satellite orbits has yielded important information on this problem but no decision is yet possible.

The simplest interpretation of the density anomalies within the earth supposes that the anomalies are supported by the finite strength of the rocks making up the mantle. The anomalies lead to stress differences, the magnitude of these differences depending on the radial distances over which the stress differences are supported. If the entire mantle is involved, the differences between the observed and hydrostatic J_n^0 values imply maximum stress differences of the order of tens of bars. If only the upper mantle supports the density anomalies then higher stress differences are implied.

An alternative to the finite-strength interpretation for the density anomalies is that the values of J_n^0 indirectly result from convection currents; the density variations are directly associated with temperature inhomogeneities, the anomalies being supported by viscous stresses developed in the convective motion. Many geologists and geophysicists argue that the large scale structure of the earth can be interpreted only in terms of convective motion (Reference 21). Perhaps the most striking evidence is that presented by Vacquier, Raff, and Warren who showed that great blocks of the Pacific Ocean floor off the California coast have moved as much as 1000 km relative to each other (Reference 22). This relative motion may be interpreted in terms of a crust being dragged along by subcrustal convective systems.

Prior to the acquisition of geodetic data from the analysis of satellite orbits the principal evidences for a mantle of zero strength were: (1) The figure of the earth closely approximates that of an equivalent rotating fluid; (2) Formerly glaciated areas in Scandinavia and North America have been rising – this was interpreted as a viscous rebound following the removal of ice.

The presatellite value used for the flattening of the earth, about 1/297.2, agrees closely with Bullard's calculation of the flattening of a rotating fluid having the estimated density distribution of the earth (Reference 23). This close agreement indicated that the earth behaves as a fluid for long term deformations. The new data obtained from satellites indicate that the actual bulge of the earth is about 1/2 percent larger than the surface of an equivalent rotating fluid. Munk and MacDonald show that the bulge is to be expected, in a sense, for a rotationally decelerating earth (References 19 and 24). At the present rate of deceleration, the bulge implies an equilibrium figure about 10^7 years ago. The adjustment of the bulge to the changing rotation rate can result from continuous creep of the mantle at the stress difference fixed by the creep strength, or from intermittent flow or fracture as the strength is exceeded locally. If the entire mantle is undergoing more or less continuous adjustment, the discrepancy between the actual and equilibrium bulge of the earth gives a good estimate of the creep strength of the mantle, about ten bars.

The classical estimate of the viscosity of the mantle depends on the interpretation of uplift in certain Pre-Cambrian shield areas. During the last glacial epoch, the Baltic and Canadian shields were depressed by the weight of ice; and isostatic uplift followed the removal of this glacial ice. Haskell solved the problem of loading and unloading of a layer of viscous fluid and determined the viscosity of the mantle from the rate of uplift (References 25 and 26). His value of 3×10^{21} in cgs units depends critically on the assumption that the uplift is due to the viscous response of a material possessing zero strength. This assumption has been severely criticized, particularly by Russian investigators (Reference 27). Gravity studies on the formerly glaciated regions reveal a close correlation of negative anomalies with uplift, in agreement with the hypothesis that the area is undergoing isostatic uplift. But there are large areas in Norway where positive anomalies are found in regions undergoing uplift. Furthermore, the uplift in Scandinavia is of approximately the same magnitude as the uplift in other shield areas that have not undergone glaciation. Lyustikh suggests that the uplift is of a general character and that the association with glaciation is accidental. A further difficulty in accepting a viscosity of the order proposed by Haskell is the short time scale implied for vertical motion. Large scale gravity anomalies should persist for longer than 10^4-10^5 years if the crust rested on a fluid with a viscosity of 10^{22} in cgs units. This is in direct contradiction to the existence of ancient geologic features associated with large gravity anomalies.

Chapter 3

BODILY TIDES AND THE ROTATION OF THE EARTH

The earth's gravitational potential provides information regarding its internal density distribution; and the difference between the observed potential and the potential calculated for an equivalent rotating fluid yields data on the earth's anelastic behavior. Because of the large scales involved, it is assumed that the long term anelastic responses are associated with the gravitational anomalies. As we shall see in the next section, data from seismology provide information on the anelastic response of the earth to oscillations with periods on the order of hours to seconds. The earth also yields to other distorting forces having periods intermediate between the very long secular changes and the high frequency seismic deformations.

The attraction of the moon and the sun produces deformations in the body of the earth analogous to the tides in the oceans. The attraction of an external body on a spherical earth may be considered to be of two parts. First, there is a net force attracting the earth toward the external body in question which is of such a magnitude that it would seem that all the earth's mass were concentrated at its center of gravity. This force is responsible for keeping the earth in its orbit around the sun or around the center of gravity of the earth-moon system. Second, there is a differential force on the various parts of the earth's volume because they are at slightly different angular positions from the center of the sun or moon. These differential or tide-raising forces produce the ocean tides. They also deform the solid earth, tending to elongate it into an ellipsoid whose major axis is directed toward the disturbing body. The ocean tides are large and more obvious, but the deformation of the solid earth also produces observable effects which can be measured. Therefore, these effects yield information on the interior of the earth. The "earth tides" yield readily to a mathematical treatment, whereas the ocean tides do not. The free periods of elastic vibrations in the earth are on the order of an hour and an equilibrium theory is therefore applicable to the slowly varying tidal deformations. In the oceans the free periods are probably on the order of days, so they cannot be treated as equilibrium phenomena. As we shall see, ocean tides complicate the analysis of body tides.

In addition to the forced motion induced by the action of the sun and moon, there is a free nutation of the earth's axis of rotation. Euler showed that a body symmetrical about its axis of rotation would rotate permanently about the axis of greatest moment. A small disturbance makes the axis of rotation move in a cone about the axis of greatest moment and it completes its revolution within the body in a period of $A/(C - A)$ times the period of rotation. The ratio $A/(C - A)$ is well known, from the precession of the equinoxes, to be 305. The wobble in the pole of rotation should show up in astronomical observations as a change in latitude with about a 10 month period. During the nineteenth century a number of astronomers searched for changes in latitude with a 10 month period. The results were

inconclusive. Chandler (Reference 28) announced a term in the latitude variation with a period of 428 days, 40 percent longer than Euler's classic value; in addition, Chandler detected a 12 month term. The discovery of the 428 day term was entirely unexpected and raised doubts concerning the validity of the observations. But only a year later Newcomb was able to demonstrate that the yielding of the earth and its oceans could bring about an increase in the period from 10 to 14 months. He attributed 1/4 of the increase to the mobility of the oceans, the remainder to the earth's anelasticity. The lengthening of the period can be understood to occur as follows: The rotation of the earth produces an elastic strain which is symmetrical about the instantaneous axis and does nothing to displace it. This is superimposed on a permanent flattening, the two together making up the total flattening. The permanent part affects the axis of rotation just as such a condition would affect a rigid body, and it is this part that determines the period; but both parts are attracted by the sun and moon and contribute to the precession. The lengthening of the period from 10 months to 14 months thus gives a measure of the elastic yielding of the earth. In addition, the Chandler nutation or wobble is not constant in time but decays. If a source is given, the rate of decay provides information regarding the anelasticity of the earth.

LOVE NUMBERS

A description of the deformation of the earth due both to the tide-raising forces of the sun and moon and to the 14 month wobble is best given in terms of certain numbers introduced by Love. Consider the earth's response to a disturbing potential $U(r)$ described in terms of a spherical harmonic of degree 2; the tidal forces of the moon and the sun and centrifugal forces arising from the earth's rotation can be written as gradients of such a potential U. The resulting deformation defines the Love numbers h and k as follows:

The ground is lifted by an amount hU/g, where g is the surface value for the gravitational acceleration. The additional gravitational potential at the displaced surface arising solely from this redistribution of mass is kU. The numbers h and k are the Love numbers of degree 2. Thus $1 + k$ is a factor allowing for the attraction of the bulge by itself and the response of hU/g takes this self-attraction into account. A fluid surface covering the globe would remain equipotential and be lifted by $(1 + k)U/g$ relative to the center of the earth and by $(1 + k - h)U/g$ relative to the sea bottom. In addition to the vertical displacement of the solid surface by hU/g there is horizontal displacement with the components

$$\left.\begin{aligned} &\frac{l}{g}\frac{\partial U}{\partial \theta}, \\ &\frac{l}{g}\frac{1}{\cos\theta}\frac{\partial U}{\partial \lambda}, \end{aligned}\right\} \qquad (7)$$

where the third Love number l describes the horizontal yielding of the surface.

The Love numbers are dimensionless parameters which neatly summarize some of the earth's elastic properties. Evaluation of them is somewhat difficult, and we will consider several sources of information in our discussion of them.

SECULAR LOVE NUMBERS

Consider the distortion of the earth due to any potential U of degree 2. The distortion gives rise to an exterior gravitational potential

$$k \frac{a^5}{r^5} U \quad . \tag{8}$$

The gravitational potential near the boundary of a nearly spherical body is given by MacCullagh's formula (Reference 29). In the present case, the deformation is a spherical harmonic of degree 2 and the pertinent terms in MacCullagh's formula can be written as:

$$\left.\begin{aligned} U &= \frac{GM}{r} + V \ , \\ V &= \frac{G}{2r^5}\left[C_{11}\left(x_2^2 + x_3^3 - 2x_1^2\right) + \cdots - 6C_{12}\, x_1 x_2 - \cdots\right] = k\frac{a^5}{r^5} U \ , \end{aligned}\right\} \tag{9}$$

where C_{ij} are the components of the moment of inertia tensor. The dots in Equations 9 indicate two additional terms that are obtained by the cyclic rotation of subscripts.

Now consider the special case of centrifugal potential,

$$\frac{1}{2}\left[\omega^2 r^2 - \left(\omega_i x_i\right)^2\right] \ , \tag{10}$$

where $\omega^2 = \omega_i \omega_i$ and $r^2 = x_i x_i$. Expression 10 can be organized into terms of the form

$$\frac{1}{3}\omega^2 r^2 + U \ , \tag{11}$$

where

$$U = \frac{1}{6}\left[\omega_1^2\left(x_2^2 + x_3^2 - 2x_1^2\right) + \cdots - 6\,\omega_1\omega_2\, x_1 x_2 - \cdots\right] \tag{12}$$

is a spherical harmonic of degree 2. The term $(1/3)\omega^2 r^2$ leads to a purely radial deformation which consists of a contraction near the center of the earth and extension in the outer parts. Combining Equation 12 with Equations 9 yields

$$C_{ij} = I\,\delta_{ij} + \frac{ka^5}{3G}\,\omega_i \omega_j + \text{constant} \ , \tag{13}$$

where

$$I = \frac{1}{3}\left(C_{11} + C_{22} + C_{33}\right) \tag{14}$$

is the inertia of the sphere in the absence of rotational deformation; and δ_{ij} vanishes except for $i = j$, when it is unity. This determines the constant so that, finally,

$$C_{ij} = I\,\delta_{ij} + \frac{ka^5}{3G}\left(\omega_i\,\omega_j - \frac{1}{3}\,\omega^2\,\delta_{ij}\right) . \tag{15}$$

The Love number k in Equation 15 can be interpreted as a measure of the earth's yield to centrifugal deformation during the last 5 million years. Without loss of generality, the x_3 axis can be placed along the rotation vector. Then $\omega_1 = 0$, $\omega_2 = 0$, $\omega_3 = \Omega$, and

$$\left.\begin{aligned} C_{11} = C_{22} = A &= I - \frac{k_s a^5}{9G}\,\Omega^2 , \\ C_{33} = C &= I + \frac{2k_s a^5}{9G}\,\Omega^2 , \\ k_s &= \frac{3GHC}{a^5\Omega^2} . \end{aligned}\right\} \tag{16}$$

For a homogeneous sphere, $C = (2/5)Ma^2$; then with $M = 5.98 \times 10^{27}$ gm for the mass of the earth, $k_s = 1.14$. In reducing the value of C from the satellite observations, the value for k_s becomes

$$k_s = 0.96 . \tag{17}$$

The foregoing calculation of k_s involves the observed rate of precession and the gravitational potential of the earth derived from the observations of satellites. No assumptions were made concerning the stress-strain relations within the earth.

The secular Love number measuring the response of the earth to very-long-period stresses is far different from the Love numbers obtained from studying the earth tides and the Chandler wobble. There can be no doubt that the earth responds far differently to tidal forces than it does to diurnal rotation.

TIDAL VARIATION OF GRAVITY

Consider an external disturbing function U_2. The total external gravitational potential is

$$U = \frac{ga^2}{r} + U_2 + \frac{ka^5}{r^5}\,U_2 . \tag{18}$$

The tidal deformation displaces the surface and to first order the acceleration at $r = a$ is

$$g\left[1 - \frac{2U_2}{ag}\left(1 - \frac{3}{2}\,k + h\right)\right] . \tag{19}$$

Thus, gravity measured at the surface of the earth will show a tidal variation. The effect of the yielding of the earth is to cause a larger variation of gravity than would otherwise be anticipated.

The tidal periods are very much longer than the longest free period of oscillation (see the next chapter), so the yielding should be nearly in phase with the tidal driving forces. The departure from perfectly elastic behavior, such as might result from energy dissipation due to frictional processes within the earth, produces a phase lag in the yielding and, hence, in its contribution to the total gravity variation.

Observations of the variation of gravity with a sensitive gravity meter provide data on the amplification factor $\left(1 - \frac{3}{2} k + h\right)$ and thus on the possible values of the Love numbers h and k. Tidal variations in gravity have been determined at a number of stations distributed over the earth's surface. Of particular interest are measurements carried out by the Institute of Geophysics of the University of California with the use of a LaCoste-Romberg gravimeter. The principal tides for which observations have been made are those having a period near 12 and 24 hours. Table 3 lists results obtained by the Institute during the International Geophysical Year from the measurements of twelve stations distributed around the earth. The determinations are based on observations of about 6 weeks duration at each station. Uncertainties are due primarily to the perturbing influence of ocean tides. Ocean tides, unlike body tides, are not an equilibrium phenomenon, and since they differ in phase from the disturbing potential the local value of acceleration is perturbed.

Table 3

Amplification of Diurnal and Semidiurnal Tides by Elastic Yielding of the Earth (from unpublished data of Harrison, Ness, and Slichter).

Tidal Component	Period (hours)	$1 - \frac{3}{2} k + h$	Phase Lag (degrees)
O_1	25.84	1.177 ± 0.018	+0.64 ± 1.07
P_1 K_1	23.92	1.140 ± 0.012	+0.26 ± 1.85
M_2	12.42	1.1821 ± 0.007	+0.86 ± 0.74
S_2 K_2	12.00	1.1849 ± 0.0072	+0.12 ± 0.72

CHANDLER WOBBLE

Observations of the latitude of stations belonging to the International Latitude Service determine the wobble of the instantaneous axis of rotation. A spectral analysis of the variation of latitude shows two principal peaks, one with a period of a year and another with a period of 429 days (Reference 19). The lengthening of the period over that of a Eulerian rigid body is due both to the elastic yield of the earth and to the fluid yield of the core and ocean.

The period of wobble can be interpreted in terms of a tidal effective Love number $k = 0.29 \pm 0.01$. In interpreting this value it is important to realize that the earth as a whole is involved, including both the oceans and the fluid inner core. The oscillations excited by the wobble are only in part communicated to a liquid core so that the inertia of the core plays only a minor role in determining the period. Indeed, if the core were a perfect fluid occupying a spherical cavity in a rigid shell, the core would not partake in the wobble at all. The fraction of the core involved in the wobble depends on the

ellipticity, density distribution, and viscosity of the core, and on the electromagnetic forces acting on the core and mantle. Only the variations in ellipticity and density due to the finite elasticity of the shell have been investigated. The subtraction of the inertia of the core reduces the period of the Chandler wobble, as compared to a static model in which the earth is taken to be an elastic body. The reduction is in the ratio of the inertia of the core to the inertia of the core plus the shell. For a rigid outer earth the ratio is 1/10 and the reduction in the period is 30 days.

In quite the same way an inviscid ocean covering the whole earth would shorten the period, though only by a very small amount since the ocean's moment of inertia would be minute. If, on the other hand, this ocean remained always aligned with respect to the wobbling axis, then the ocean would lengthen the period. The lengthening due to such an equilibrium tide would be 33 days. If, without any real evidence, we assumed an equilibrium pole tide, then the value of the effective Love number would change from 0.29 to 0.23. Jeffreys and Vincente showed that the effects of the core increase k by about 0.08 (Reference 30). The Love number due to the elastic deformation of the earth would then be $k = 0.31$.

The observed Chandler wobble frequency of 0.85 cycles per year (cpy) can be interpreted as the earth's Eulerian frequency of nutation (1.20 cpy) diminished by about 0.25 cpy because of the elastic yield of the earth and by about 0.1 cpy because of the fluid yield of the oceans. The last value is very uncertain since it is questionable whether the response of the ocean is an equilibrium response at these low frequencies.

In addition to the frequency of the Chandler wobble and its interpretation in terms of the elastic properties, it is of interest to examine the problem of dissipation and generation of the wobble. Dissipation is important since the anelastic response of the elastic mantle to a 14 month excitation is involved, though the interpretation involves subtracting the contributions of the core and oceans to the dissipation. The Chandler wobble may be regarded as a resonance amplification of some unknown excitation. In this sense, it is like playing a relatively broad-band noise through a filter with a fairly narrow passband. The relative bandwidth of the filter, Q^{-1}, can be obtained from the latitude observations. The resulting value depends on what series of data are used and the value ranges from 18 to 60.

First we need to estimate the rate of energy dissipation. The kinetic energy of a rigid body freely wobbling about a mean axis, x_3, is

$$K = \frac{1}{2}\left(A\omega_1^2 + A\omega_2^2 + C\omega_3^2\right) . \tag{20}$$

The kinetic energy of the rigid body in steady rotation having the same angular momentum is

$$K_0 = \frac{1}{2C}\left[A^2\left(\omega_1^2 + \omega_2^2\right) + C^2\omega_3^2\right] . \tag{21}$$

The time variance of the kinetic energy is then

$$\begin{aligned} \Delta K &= K - K_0 \\ &= \frac{1}{2} HA\Omega^2\left(m_1^2 + m_2^2\right) , \end{aligned} \tag{22}$$

where

$$m_i = \frac{\omega_i}{\Omega} \quad . \tag{23}$$

For a root-mean-square amplitude of 0.14 seconds of arc for the Chandler wobble,

$$\begin{aligned} 2\Delta K &= Q \times 10^{21} \text{ ergs} \\ &= 4 \times 10^{-15} \text{ K} \end{aligned} \tag{24}$$

is the mean kinetic energy of the Chandler wobble; and

$$2\Delta K \sigma_0 Q^{-1} = 10^{15} Q^{-1} \frac{\text{ergs}}{\text{sec}} \quad , \tag{25}$$

(where σ_0 is the frequency of the wobble) is the mean rate of energy dissipation. This rate is very small compared to the energy dissipated by tides and to the energy loss due to radioactivity.

Interpretation of the damping of the wobble has had a long and complex history. It was first attributed by Jeffreys to tidal friction in the oceans. Bondi and Gold dismissed the core and oceans as a possible sink, since neither has a sufficient moment of inertia to affect the mantle (Reference 31). However, Munk and MacDonald argue that either the core or mantle is sufficient to account for the damping and that the low Q observed for a Chandler wobble does not represent the anelastic response of the mantle.

The excitation of the Chandler wobble remains a problem. Early researchers thought that the wobble was due to variations in mass distribution on the earth's surface. These variations would produce time-dependent products of inertia which in turn would result in a shift of position of the axis of rotation. However, a detailed study by Munk and Hassan shows that the computed spectral density of the atmospheric variation at the Chandler frequency falls short of the energy required in the wobble by one or two orders of magnitude (Reference 32) MacDonald (unpublished data) has repeated the analysis of the meteorological forcing function, using somewhat improved methods of data reduction. The results of Munk and Hassan have been confirmed. However, a bispectral analysis shows that the energy at one cycle per year interacts nonlinearly with energy at 0.15 cycle per year. The excitation of the Chandler wobble is due to nonlinear coupling. Deviations from perfect elasticity or magnetohydrodynamic coupling of the core and mantle can provide the nonlinearity. The latter possibility is consistent with present theories regarding the core-mantle interaction (Reference 42).

VALUES FOR THE ELASTIC LOVE NUMBERS

The calculation of the Love numbers for an elastic earth is a straightforward problem in elastic theory. The methods are similar to those used in treating the earth's free oscillations and will be considered in the following chapter. Takeuchi, Saito, and Kobayashi (Reference 33) have determined the Love numbers for a model of the earth having a velocity distribution given by Gutenberg (Table 4).

Table 4

Love Numbers for an Elastic Earth for the Gutenberg Model.

n	k_n	h_n	l_n
2	0.280	0.592	0.076
3	0.083	0.274	0.010
4	0.035	0.161	0.007
5	0.020	0.116	0.006
6	0.013	0.094	0.005
7	0.009	0.081	0.004
8	0.007	0.073	0.003
10	0.005	0.063	0.002
12	0.003	0.055	0.002
14	0.003	0.051	0.001
16	0.002	0.048	0.001

The Love number k calculated for an elastic earth can be compared with k for the Chandler wobble. They are in close agreement, but this agreement is fictitious since the Love number for the Chandler wobble involves the response of the oceans and fluid core, neither of which are considered in the calculation of the elastic Love number. The gravitational amplification $\left(1 - \frac{3}{2}k + h\right)$ for an elastic earth is 1.172. This value can be compared with the values listed in Table 3. The differences do not imply uncertainties in the elastic constitution of the earth, but rather, the nonequilibrium response of the ocean tides complicates the interpretation of the semidiurnal and diurnal tides.

From the study of earth tides and the Chandler wobble, we find $h = 0.59$ and $k = 0.29$. These are in marked contrast with the values of the *secular* Love numbers $h_s = 1.96$, $k_s = 0.96$ obtained from the figure of the earth. A number of hypotheses have been suggested to explain the difference and it is not known which, if any, is correct. One hypothesis is based on the relative magnitude of stresses, with the secular Love numbers referring to stress differences above the critical strength, and tidal effective Love numbers to stress differences below the critical strength. A second hypothesis is based on the relative duration of stresses. In this case the secular Love numbers refer to stresses much more prolonged than some critical duration and the tidal effective Love numbers refer to stresses much less prolonged than this critical duration. Still another possibility is that the earth was originally molten and now has the hydrostatic figure appropriate at the time of congealment. This last hypothesis is extremely unlikely, both on the grounds of the thermal history of the earth and also because of the observed deceleration of the earth due to the lunar tide.

LOAD LOVE NUMBERS

In many geophysical problems it is convenient to express the effect of surface load in terms of dimensionless numbers analogous to the Love numbers. Consider the effect of a variable surface slope, $q(t)$ gm/cm^2. We are concerned with the term q_n of degree n in the surface spherical harmonic

Table 5

Load Love Numbers.

n	h_n'	k_n'
2	-1.034	-0.312
3	-1.078	-0.191
4	-1.083	-0.126
5	-1.121	-0.096
6	-1.185	-0.081
7	-1.260	-0.072
8	-1.338	-0.066
10	-1.486	-0.058
12	-1.622	-0.052
14	-1.750	-0.048
16	-1.872	-0.045

expansion of q. The interior potential resulting from a gravitating layer q_n is

$$U_n = \frac{4\pi G a q_n}{2n + 1} \left(\frac{r}{a}\right)^n . \tag{26}$$

Deformation is due to two opposing effects: a normal stress due to the load, which will depress the surface; and a gravitational attraction of the earth on the load, which will raise the ground. The combined effect of pressure and attraction raises the surface by $h_n' U_n/g$ and the gravitational potential arising from the distortion is $k_n' u_n'$. This defines h_n' and k_n'. The depression is found to be somewhat larger than the gravitational uplift and the load Love numbers are negative. The calculated values for the load Love numbers are shown in Table 5.

Chapter 4

ELASTICITY OF THE EARTH AT HIGH FREQUENCIES

In modern analysis the variation, with depth, of the two seismic body waves (compressional and shear) is used to determine the internal constitution of the earth. Velocity-depth curves may be derived from distance-time curves; the latter are constructed by identifying, interpreting, and analyzing the various phases of the seismogram (Reference 34). The variable quality of the records, the local effects, and the regional grouping of stations all complicate the analysis. Moreover, the conversion of a distance-time curve to a velocity-depth curve depends upon the mathematical methods applied.

The observation analysis of the earth's free oscillations provides another method for determining the general features of the velocity-depth curves. Since the oscillations involve the earth as a whole, difficulties associated with analyzing many events on different seismographs for several earthquakes should vanish. The results from the Chilean earthquake of May 22, 1960, show that Gutenberg's solution for the variation of velocity with depth in the mantle fits the observations very well (Figure 1). Before discussing the earth's free oscillations, it would be well to consider the features of the velocity-depth curves on which most seismologists agree.

Under continental areas the velocity in the upper few tenths of a kilometer varies markedly with depth and location. The velocities, C_p, of the compressional wave range from 5 to 7 km/sec. At a depth averaging some 30-35 km there is a discontinuity in the seismic velocity, and below this discontinuity the velocity is usually above about 8 km/sec. The material above this discontinuity, first recognized by Mohovovicic, is termed the crust. The crust is much thinner under oceans, with some 6 km of water underlain by some 4 km of rock. At this depth (10 km) the velocities undergo a transition. The region below the crust, termed the mantle, extends to a depth of 2898 km. In the Gutenberg solution for the variation of velocity with depth, the velocity initially decreases, reaching a minimum at a depth of 150 km; then it rapidly increases, to a depth of 900 km. Below this it increases more gradually. The existence of two velocities throughout the mantle is significant and suggests a normal type of elasticity.

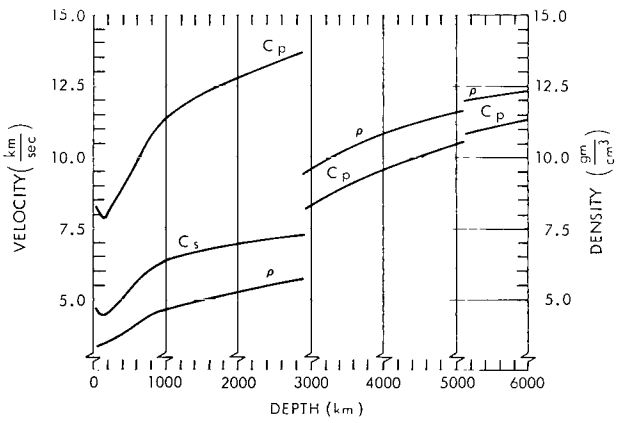

Figure 1—Variation of the compressional wave velocity C_p, the shear wave velocity C_s, and the density ρ within the earth (Reference 35).

The absence of shear waves below the mantle is the principal reason for believing this region to be liquid. The absence of this velocity and the drastic decrease of the compressional wave velocity are the outstanding seismic features which distinguish the core from the mantle. The surface of separation of the core and mantle is usually considered to be sharp and is the best located, as well as the largest, discontinuity in the earth's interior. At a depth of 5121 km another discontinuity is encountered. The velocity distribution within the inner core is not known.

THE EARTH'S FREE OSCILLATIONS

During the great Chilean earthquake of May 22, 1960, the earth's free modes of vibration were observed for the first time. Their detection broadened the spectrum over which a geophysicist may study the earth's interior. Prior to 1960 almost all information regarding the earth's interior had been derived from detailed investigations of the arrival of the elastic body waves as recorded by seismographs. These waves travel different paths through the earth and contain most of the energy in the high frequency part of the spectrum (10-0.1 cps). The interpretation of arrival times is based on a ray theory similar to that of geometrical optics (Reference 34). The use of low frequency normal modes as a tool for investigating the earth is somewhat analogous to the astronomers' use of radio frequencies as a supplement to observations in the visual range. In the following sections we will consider the general features of the earth's free oscillations. The detailed calculations are contained in Appendix A.

THE FREE VIBRATIONS OF AN ELASTIC SPHERE

A small-amplitude disturbance in an elastic solid is carried outward by two traveling waves. The fast (compressional) wave carries the compression and rarefaction of ordinary sound at a phase velocity of

$$C_p^2 = \frac{\lambda + 2\mu}{\rho} , \tag{27}$$

where λ and μ are the Lamé constants and ρ is again the density. The slow (shear) wave transmits particle motion at right angles to the direction of propagation with a phase velocity of

$$C_s^2 = \frac{\mu}{\rho} . \tag{28}$$

The adiabatic bulk modulus k is given by

$$\frac{k}{\rho} = C_p^2 - \frac{4}{3} C_s^2 . \tag{29}$$

If an elastic solid is sufficiently isolated from its surroundings, reflections from boundaries may set up standing waves. Lamb showed that the vibrations of an elastic sphere can be classified into two

groups: In the *toroidal* or torsional oscillations, a particle executes motion on the spherical surface; there is no radial component of motion. The toroidal oscillations unite to form the familiar horizontally polarized shear waves of classical seismology. The *spheroidal* oscillations combine both radial and tangential motions to produce compression and rarefaction. A degenerate spheroidal oscillation involves only radial motion; the entire sphere expands or contracts.

The notation adopted to describe the earth's free oscillations is similar in many ways to the notation used in spectroscopy. This reflects the common mathematical structure of these two fields. The solution to the equations of motion of an elastic sphere can be separated into a function dependent upon the angular coordinates and a function dependent upon radius. The angular function is written as a sum of spherical harmonics,

$$X_l^m = P_l^m(\sin\theta)e^{im\lambda} , \tag{30}$$

where P_l^m is the associated Legendre function, θ is the latitude, λ is the longitude, and m and l are the magnetic and azimuthal quantum numbers, respectively. The time dependence can be included in the exponential:

$$\exp\left[i(m\lambda - \omega t)\right] , \tag{31}$$

where ω is the angular frequency. This represents a wave traveling with a speed of m/ω radians per second. If m is positive the wave travels from west to east; if m is negative it travels from east to west. The two signs of m are symmetrical in a stationary sphere; however, rotation destroys this symmetry and creates important differences between waves traveling from west to east and those traveling from east to west. The values m and l must assume integral values because of the conditions on the outer boundary and the conditions for regularity at the center of the sphere. These integral values determine the surface pattern of deformation associated with a particular free oscillation. The number of lines of vanishing displacement associated with the angular coordinate θ is $l - m$; the number of nodal lines associated with the angular coordinate λ is m. There will also be surfaces of zero particle displacement associated with the radial function. The description of the radial function is in terms of n, the radial quantum number.

The free oscillations can thus be characterized by three values: l and m determine the pattern of displacement on the spherical surface and n determines the number of internal nodal surfaces. The notation that has been adopted is ${}_nS_l^m$ and ${}_nT_l^m$, for spheroidal and toroidal oscillations, respectively. The expression ${}_nT_l^m$ denotes a toroidal oscillation with n radial nodal surfaces and a displacement pattern on the surface of the sphere fixed by the spherical harmonic with ordinal numbers l and m. In the ${}_0S_2$ oscillation a sphere alternately assumes a prolate and oblate form; this is sometimes termed the "football" mode. In the ${}_0T_2$ oscillation one hemisphere differentially rotates or twists relative to the other.

The eigen frequencies for an inhomogeneous spherical shell can be determined by numerical computation (Appendix A). The distribution of elasticity and density is taken to be that of the Gutenberg model of the earth (Figure 1). The effects of the inhomogeneous elasticity and density on the earth's

free oscillations are illustrated in Figures 2 and 3 where the Gutenberg earth model is contrasted to a homogeneous model in which the elasticity equals the average elasticity of the Gutenberg model. The energy levels shown in Figure 2 are normalized to provide a 1 centimeter displacement at the surface (the observed displacement is much less, on the order of 10^{-6} cm). About 3×10^{21} ergs are required to produce this displacement with a ${}_0T_2$ surface pattern in both the homogeneous and inhomogeneous models. At higher modes and frequencies (Figure 3) it takes more energy to form the complicated surface pattern of displacement and still maintain this maximum surface amplitude of 1 centimeter. The needed energy is greater in the homogeneous model since the near-surface rigidity is larger. The difference increases with greater values of the mode number l.

The elastic energy is more or less evenly distributed over the entire mantle at low mode numbers (Figure 4). At higher mode numbers it is concentrated in the outer layers of the mantle. The ${}_0T_2$ oscillation involves the mantle, but the ${}_0T_{18}$ oscillation is confined to the upper few hundred km.

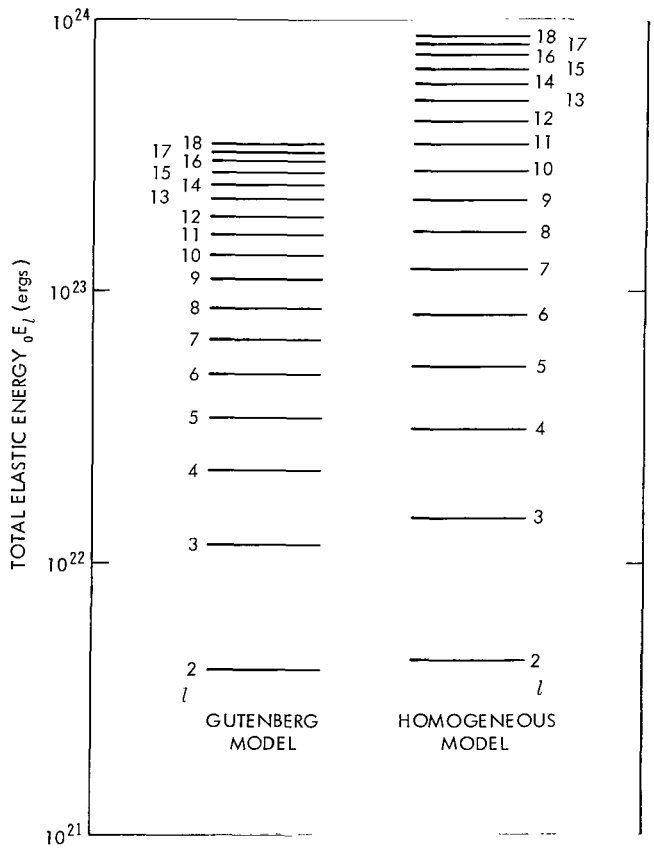

Figure 2—Total elastic energy in the toroidal oscillation (${}_0T_l$). The energy is normalized to a 1 cm surface displacement.

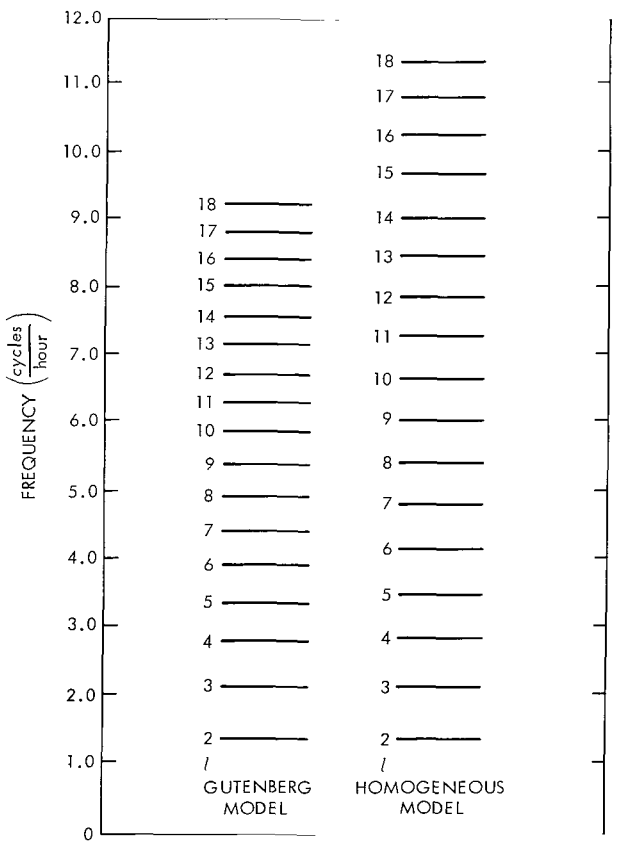

Figure 3—Comparison of the resonant frequencies for the toroidal oscillations (${}_0T_l$) in the Gutenberg and homogeneous models.

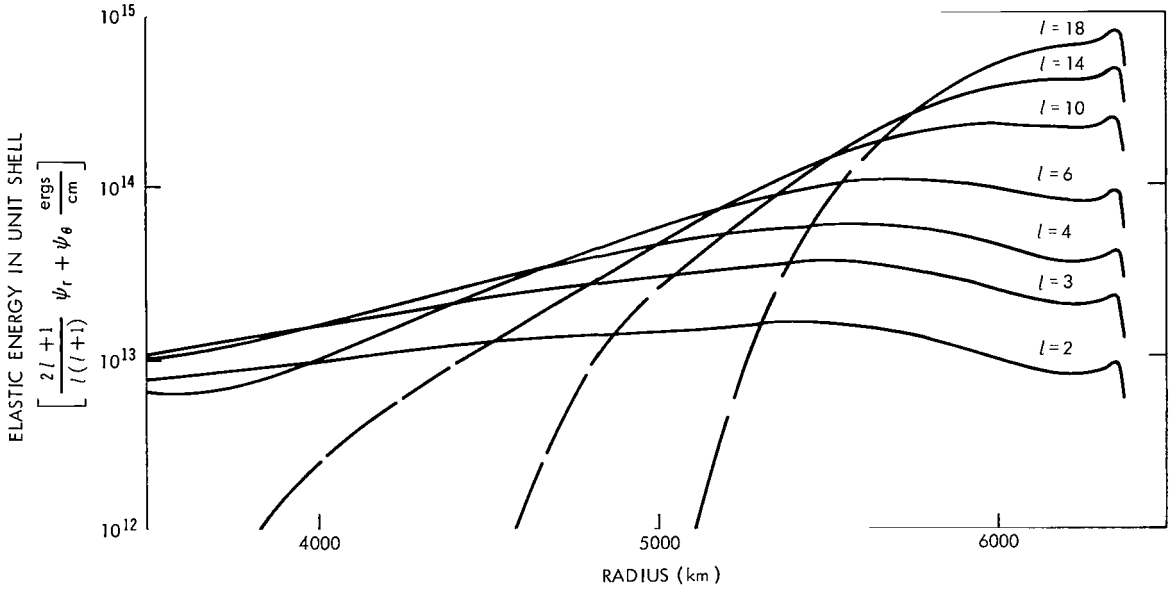

Figure 4—Elastic energy per unit radius in the toroidal oscillations for the Gutenberg earth model.

OBSERVATIONS OF THE EARTH'S FREE OSCILLATIONS

Despite considerable theoretical efforts the first attempt to observe the earth's oscillations was made only recently. Benioff constructed a strain-measuring seismometer, a silica glass rod 24 meters long, to investigate the low frequency spectrum. He suggested that an apparent 57 minute periodicity visible on the strain records of the Kamchatka earthquake of 1952 was the ${}_0S_2$ mode. This suggestion prompted extensive computational work. A second attempt at detecting the free oscillations was made in 1958 by spectral analysis of the background noise in the strain seismometer and measurement of the changes of the local gravitational field. The results were negative.

Several instrumental developments during 1958 and 1960 made possible the observation of the free oscillations excited by the Chilean earthquake of May 22, 1960. Benioff modified the circuitry associated with the seismometer so that the effect of the finite amplitude of the earth tides was reduced and a greater magnification achieved. A lower noise level was achieved on the LaCoste-Romberg gravimeter at the University of California. In addition, the Lamont Geological Observatory installed a strain gauge of the Benioff type in a mine shaft near Ogdensburg, New Jersey. The strain seismometer and the gravimeter complement each other. The strain seismometer is sensitive to strain produced by both vertical and horizontal motion; it, therefore, records both spheroidal and toroidal oscillations. On the other hand, the gravimeter records only vertical accelerations and spheroidal oscillations. A combination of observations from the two instruments permits a separation and identification of vertical and horizontal motion. The free oscillations excited by the Chilean earthquake were detected on both instruments.

The power spectrum of the gravity variations in Los Angeles for 4 days following the Chilean earthquake is shown in Figure 5. This figure should be compared with Figure 6, a record of a quiet interval of 116 hours, 1 month after the earthquake, which is almost structureless except for a significant peak at 20.5 minutes.

Thus the spectrum of a seismic disturbance is characterized by well-defined short peaks for periods between about 8 minutes and 1 hour. At higher frequencies the isolated peaks begin to merge into a continuum as a result of the finite width of the individual peaks and the increased number of peaks. Similar analyses were carried out on the records of strain by Benioff, Press, and Smith (Reference 36) and by Alsop, Sutton, and Ewing (Reference 37).

COMPARISON BETWEEN THEORY AND OBSERVATION

A comparison between the spheroidal modes calculated by Pekeris, Alterman, and Jarosch (Reference 38) and those measured by Ness, Harrison, and Slichter (Reference 39) is shown in Figure 7. At low frequencies the observations favor neither model, since only the average properties of the earth are involved; but at higher frequencies the observations closely fit the Gutenberg model. A similar comparison can be made with the toroidal oscillations, and again (Table 6) the fit is better with the Gutenberg model.

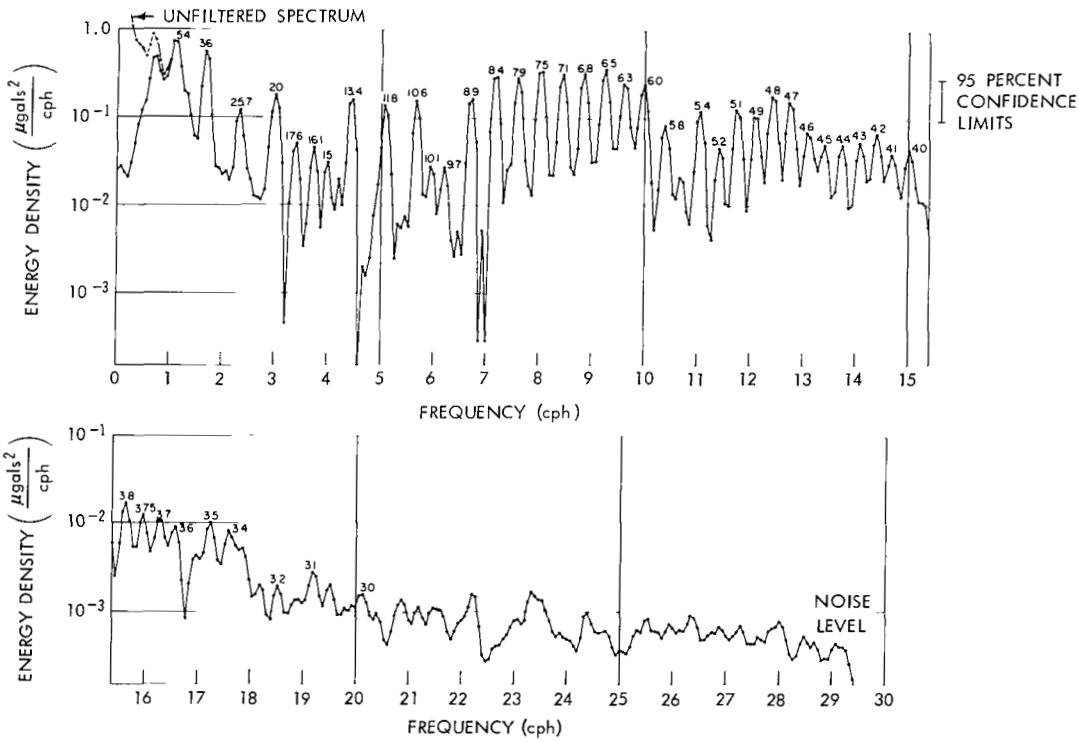

Figure 5—Power spectrum of the gravity record after the Chilean earthquake of May 22, 1960, made with the University of California (Los Angeles) earth tide gravimeter; recording period, 110 hours, May 23-27; interval, one minute; sensitivity, 0.1 microgal.

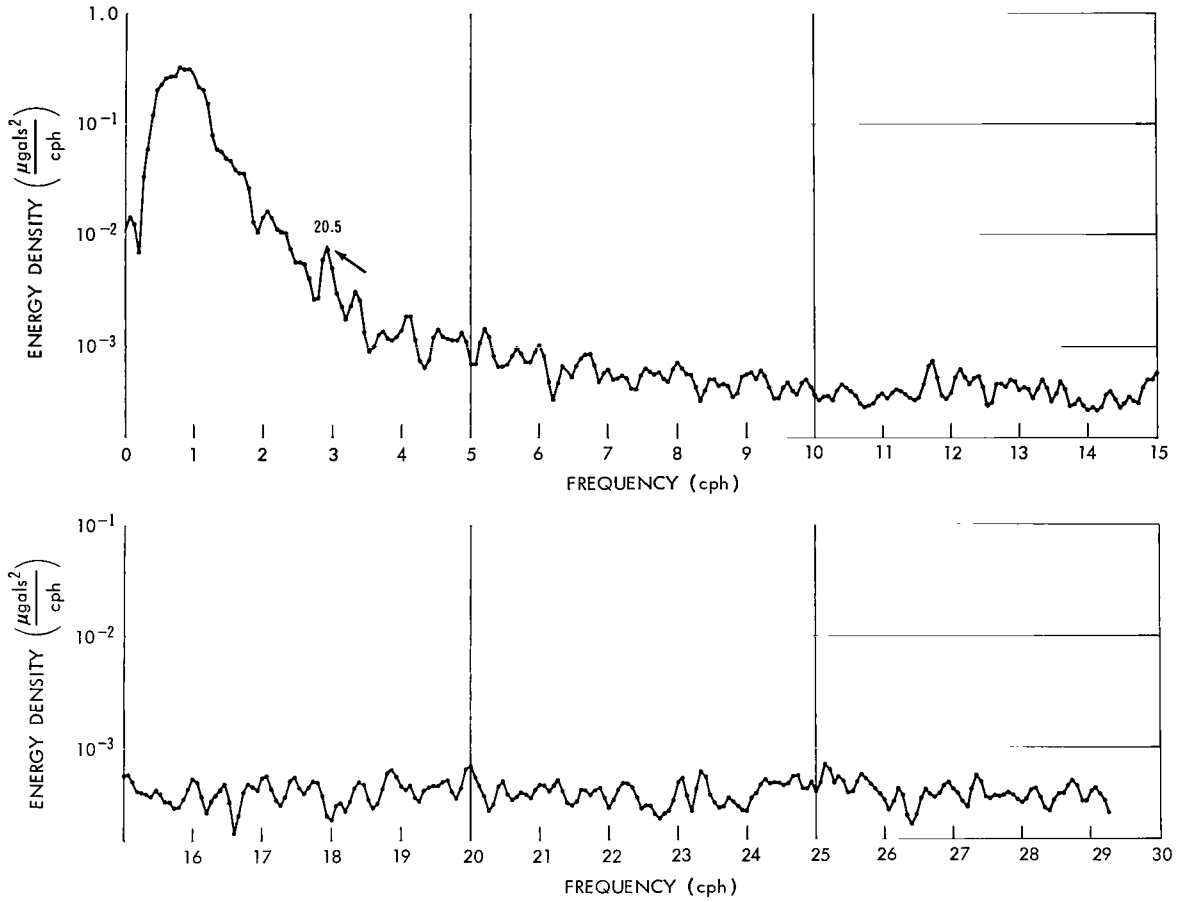

Figure 6—Power spectrum of a quiet period 1 month after the Chilean earthquake made with the University of California (Los Angeles) earth tide gravimeter; recording period, 116 hours, June 23-28; interval, 1 minute; sensitivity, 0.1 microgal.

LINE STRUCTURE

The detailed reduction of the Chilean earthquake records shows that the low frequency spectral peaks appear as multiples instead of as the single lines that would be expected for a stationary elastic sphere. Rotation destroys the symmetry with respect to the integer m, and a degeneracy associated with the symmetry is removed. The effect of rotation on the oscillations can be qualitatively understood by recalling that a free oscillation is composed of a number of running waves. Waves traveling in the direction of the earth's rotation are carried forward relative to waves traveling in the opposite direction. The net effect is that the total pattern of surface deformation rotates relative to the earth. The local effect is to cause the vibrating particles to precess much in the manner of the Foucault pendulum. The rotational splitting is analogous to the Zeeman effect of spectroscopy, where a magnetic field removes the degeneracy with respect to the quantum number m. Detailed calculations of the splitting in the spheroidal oscillations have been made by Backus and Gilbert (Reference 41), Pekeris, Alterman, and Jarosch (Reference 38), and MacDonald and Ness (Reference 42). Calculated

Table 6

Comparison of Observed and Calculated Toroidal Frequencies (Reference 40).

Order	Bullen B	Gutenberg	Observed
2	44.2	43.6	42.9
3	28.6	28.2	28.6
4	21.9	21.6	21.9
5	18.1	17.9	18.0
6	15.6	15.4	15.5
7	13.7	13.6	13.6
8	12.3	12.2	12.3
9	11.2	11.2	11.2
10	10.3	10.3	10.3
11	9.59	9.66	9.61
12	8.95	8.94	9.06

splitting is in agreement with the splitting observed in the low order spheroidal oscillations, an oscillation of order l being split into $2l + 1$ peaks. The fine structure of the lowest order toroidal oscillations is in doubt and the line ${}_0T_2$ presents a number of problems.

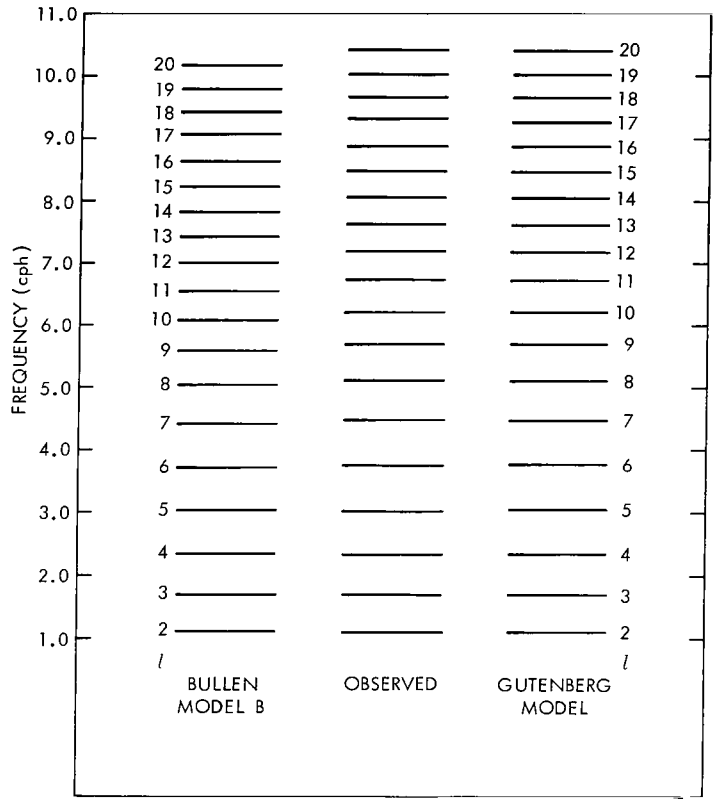

Figure 7—Comparison of the calculated and observed frequencies of the spheroidal oscillations ${}_0S_l{}^0$.

If the earth were a perfectly elastic body, then the spectral peaks should show up as individual lines broadened only by the data reduction techniques (instrumental broadening). The deviations from perfect elasticity and fluidity result in a natural broadening of the lines. The degree to which a given line is broadened, or alternatively the rate at which a given peak decays, provides, in time, a measure of the anelastic properties of the earth at the frequencies of the free oscillations. The distribution of the anelastic properties can be obtained by comparing the decay rate at various frequencies, since different frequencies are affected by different portions of the earth. Furthermore, several mechanisms of dissipation will be prominent in the various oscillations. The spheroidal oscillation of order 2 involves the entire earth, including the core, and the motion contains components of compression and shear. The radial oscillation ${}_0S_0$ involves only compressional motion; this oscillation provides a measure of the earth's dissipation in compression. The broadening of the toroidal lines is due primarily to dissipative processes within the mantle. The interaction of the core and mantle provides an additional sink of energy. But a detailed study of possible viscous and hydromagnetic effects rules out the core-mantle boundary as a major contributor to the energy loss (Reference 42).

The half-width of the lines, Q, or the rate of energy dissipated per peak elastic energy, is found to be about 350 for spheroidal oscillations. Thus, in spheroidal oscillation the earth rings as a rather poor bell. The estimates of the Q for toroidal oscillations are not as good, somewhat lower figures

being indicated, and the Q for ${}_0T_2$ is very uncertain. The highest Q of all is shown by the radial oscillation. As may be noted by comparing Figures 5 and 6, the earth appears to be ringing in this mode of oscillation a month after the earthquake. The indicated Q is greater than 5000. Thus the dissipation due to compressional motion is much less than in shear.

THE PROBLEM OF THE INTERACTION OF THE CORE AND MANTLE

The period of the fundamental toroidal oscillation is 42.9 minutes. This is more than a minute less than the period predicted for a theoretical model which gives a good fit to the other oscillation. The deviation is in the direction that one would expect if the core-mantle boundary were partly rigid; the resonant period for a mantle with a rigid inner surface is 32.1 minutes. A possible explanation for the apparent stiffness involves the earth's magnetic field. A component of the magnetic field tangential to the core-mantle boundary leaks out of the core into the conducting lower mantle. This component combines with the dipole component to give a Maxwell stress. The lower mantle is then partially glued to the core and this leads to an apparent stiffness. If this interpretation is correct, an estimate can be made of the conductivity of the lower mantle and the strength of the magnetic field. Thus detailed studies of the low frequency toroidal oscillations may lead to fundamental information regarding the electromagnetic properties of the core and mantle.

Chapter 5

THERMAL CONSTITUTION OF THE EARTH

The earth is a thermal engine. Any theory of the origin of the principal surface features of the earth must include assumptions or deductions for its thermal history. Since Kelvin's classic investigation, several important studies have been devoted to the determination of the earth's thermal character. Despite advances on many fronts, the distribution of temperature with depth remains uncertain, as does the principal mechanism by which heat is transported. At low temperatures, solids transport heat by ordinary thermal conduction. At high temperatures, large amounts of heat may be transported by radiation in optically transparent silicates. However, the combined effects of ordinary conduction plus radiation may be far exceeded by convection provided that the material making up the mantle can undergo mass motion. The problems of heat transport within the earth are thus closely tied to the question of the anelastic character of the earth's material (see Chapter 2). If the earth behaves as an elastic solid with a certain critical stress, up to which only elastic deformations are possible, then thermal transport probably takes place solely by conduction and radiation. If, on the other hand, the material of the mantle, subjected to small stresses for a long time, undergoes creep, then convection is the dominant mechanism by which heat is transported. The ratio of heat transported by radiation and conduction to that transported by convection is $K/L\rho CV_r$, where K is the total conductivity including radiation, L is the scale length, ρ is the density, C is the heat capacity, and V_r is the radial velocity. Substituting numerical values we see that velocities on the order of 10^{-9} cm/sec are required for convection to dominate radiation and conduction. Because of the uncertainly in the mechanical behavior of the material, the nature of the thermal conditions in the earth remains most uncertain.

In the present chapter we consider the major factors which influence the internal distribution of temperatures. It is useful to base the discussion in terms of the problem of the development of the temperature distribution within the earth. Knowledge of the initial conditions are then required as well as the distribution of the heat sources in the earth and the radial variation of thermal conductivity, heat capacity, and density. The calculations then predict the present-day thermal distribution and surface heat flux.

A number of observations serve to limit the possible models of the earth's thermal history. The flow of heat from the interior of the earth averages about 50 ergs/cm^2-sec over both oceans and continents. Large regional variations exist but the impressive feature is the apparent equality of the average continental and oceanic heat flows. Seismology has established that the outer 2900 km of the earth is solid and that the material immediately underlying this mantle is fluid. A more accurate estimate of the melting points within the earth is now possible because of laboratory studies of

the melting relations of geologically important materials at high pressures. The solid nature of the mantle thus limits the possible hypotheses of thermal distributions. In addition, the details of the variation of elastic velocity with depth and, in particular, the existence of a region of low velocity immediately under the crust, may provide a further indication of the thermal conditions within the earth.

AGE OF THE EARTH

The age of the oldest rock provides a lower limit to the age of the earth. Gerling and Polkanov report a Pre-Cambrian rock evincing an age of 3.4×10^9 years (Reference 43). The ratios of the stable lead isotopes have been used in numerous attempts to estimate the earth's age (Reference 44). It has been established that the isotopic compositions of primordial lead in the earth appears to be identical to that in meteorites (Reference 45). Patterson obtained the value of 4.5×10^9 years for the earth's age on the basis of lead isotopes (Reference 46).

The age of chondritic meteorites has been determined by a number of workers by using both the strontium-rubidium method and the potassium-argon method. The ages scatter somewhat but are clustered around 4.0×10^9 to 4.4×10^9 years. For purposes of considering the earth's thermal history, the value of 4.5×10^9 years is here adopted as the age. This age is taken to be the time from the initial formation.

HEAT GENERATION BY LONG-LIFE RADIOACTIVE ISOTOPES

Radioactive isotopes that have produced significant amounts of heat throughout the earth's history are distinguished by two characteristics: (1) The product of the abundance of the isotope and the rate of heat generation is relatively large; (2) The half-life of the isotope is of the same order as the age of the earth. The known isotopes that meet these requirements are U^{238}, U^{235}, Th^{232}, and K^{40}. Table 7 lists the half-lives and heat generation of the important isotopes. Isotopes with shorter half-lives may have played an important role in the initial stages of the development of the earth.

Table 7

Half-Life and Heat Generation of Important Heat-Producing Isotopes.

Isotope	Half-Life (years)	Heat Generation (joules/gm-year)	Percentage of Element's Abundance
U^{238}	4.51×10^9	2.97	99.27
U^{235}	0.71×10^9	18.0	0.72
Th^{232}	13.9×10^9	0.82	100.0
K^{40}	1.25×10^9	0.92	0.0119

RADIOACTIVE COMPOSITION OF THE EARTH

In accordance with a suggestion by Urey, most discussions of the earth's thermal history assume that the earth and the chondrites have the same abundances of the radioactive elements. Strong

supporting evidence for such an assumption follows a comparison of the present heat flow and production of heat that would exist in an earth of chondritic composition ($K = 8.0 \times 10^{-4}$ gm/gm, $U = 1.1 \times 10^{-8}$ gm/gm, $Th = 4.0 \times 10^{-8}$ gm/gm). If all the heat produced by radioactivity instantaneously reached the surface, then the present heat flow in a chondritic earth would be 59.0 ergs/cm^2-sec (Table 8). If only the mantle were chondritic then the present rate of heat production would be equivalent to a heat flux of 40.2 ergs/cm^2-sec. The average of the observed heat flow is about 50 ergs/cm^2-sec.

Table 8

Heat Production and Surface Heat Flux for a Chondritic Earth.

Measurement	Chondritic Earth		Chondritic Mantle	
	Today	Initially	Today	Initially
Heat Production (ergs/sec)	3.01×10^{20}	24.3×10^{20}	2.04×10^{20}	16.5×10^{20}
"Equilibrium" Surface Heat Flow (ergs/cm^2-sec)	59.0	476	40.2	324

The relative production of heat, by the various isotopes, for a chondritic model of the earth is shown in Table 9. At present, about 60 percent of the heat is due to K^{40}, U^{238}, and Th^{232}, each contributing about 20 percent. The relative heat production of K^{40} was much greater in the early stages of the earth's history.

Table 9

Heat Production by Isotopes.

Isotope	Today (ergs/gm-year)	4.5×10^9 Years Ago (ergs/gm-year)
U^{238}	0.32	0.64
U^{235}	0.014	1.14
Th^{232}	0.36	0.45
K^{40}	0.90	10.6

SURFACE HEAT FLOW MEASUREMENTS

A most important quantity in any discussion of the thermal character of the earth is the amount of heat that is presently escaping from the earth's interior. The outward flux of heat by conduction per unit area per unit time is equal to the product of the thermal conductivity and the temperature gradient:

$$\frac{dQ}{dt} = -K\left(\frac{\partial T}{\partial r}\right) . \qquad (32)$$

The observation of heat flow requires separate measurements of thermal conductivity and of the temperature gradient.

Systematic studies of thermal conductivities and temperature gradients have been carried out only since 1939. Birch reviewed the measurements on heat flow (Reference 47). At that time (1954) about

40 determinations had been made on land areas and 25 at sea. The land areas showed a variation, roughly, of 20 to 120 ergs/cm^2-sec. The variation in ocean measurements was somewhat greater, ranging from 15 to 140 ergs/cm^2-sec. The mean of these measurements indicated an average heat flow of about 50 ergs/cm^2-sec. Since that time the number of measurements at sea has more than doubled; and new measurements have also been made in continental areas. The new sea measurements indicate that the mean heat flow through the Pacific Ocean is about 50 ergs/cm^2-sec (Reference 48) but there is a far wider range in individual values, 10 to 370 ergs/cm^2-sec. A partial explanation of this greater range in oceanic values may be that it is far easier to avoid thermally active regions on land than it is at sea. However, there is no simple explanation of the rather widespread lower values that have been found.

THERMAL CONDUCTIVITY OF SILICATE MATERIALS

Birch and Clark demonstrated that the thermal conductivities of a wide variety of rocks show surprisingly small variation with composition (Reference 49). Recent measurements at room temperature further establish the small variation (References 50 and 51). Birch and Clark measured thermal conductivities up to 400° C and found that the conductivities of poor conductors such as feldspar and quartz increase with temperature, whereas the thermal conductivities of most materials decrease as the temperature increases. Studies of dielectric solids at somewhat higher temperatures show that thermal conductivity decreases approximately inversely with temperature, in accordance with phonon theory. No experimental studies have been carried out on the variation of thermal conductivity with pressure.

At high temperatures energy may be transferred within the solid by radiation rather than by lattice vibrations. Clark (Reference 52) shows that the contribution of radiation to thermal conductivity is approximately

$$K_R = 16\, n^2 \frac{sT^3}{3\epsilon} , \tag{33}$$

where n is the effective index of refraction of the material, s is the Stefan-Boltzmann constant, T is the temperature in degrees Kelvin, and ϵ is the sum of the absorption and scattering coefficients averaged over all wavelengths. The striking feature of the contribution of radiation to conductivity is the strong temperature dependence. The higher the temperature the greater will be the amount of energy transferred by radiation, provided that the variation of the index of refraction and opacity do not overwhelm the T^3 dependence.

The opacity ϵ and the index of refraction are determined by the properties of the material, and in general they will be functions of temperature and pressure. The variation of the index of refraction of a given material with pressure has not been investigated experimentally. An estimate can be obtained by noting that, for materials of different compositions, the index varies linearly with density. If a law of corresponding states holds, then the index should vary linearly with pressure. Within the mantle the density varies from about 3.3 to 5.7, so that over the earth's mantle variation by a

factor of 2 would be expected, with material at a depth having a higher index of refraction than that near the surface.

The rate at which radiation is transferred through a solid depends on the frequency of the radiation. Various mechanisms are known by which solids can absorb radiation, and these become important at different frequencies. Absorption due to excitation of lattice vibrations by radiation is strong in the infrared. This lattice absorption is relatively unimportant since at high temperatures the energy density is low at these long wavelengths. Intrinsic absorption is due to the excitation of valence electrons to the conduction band across the fundamental energy gap. Intrinsic absorption is important in the ultraviolet for wavelengths less than about 0.4 microns. The transparency of silicates to radiation is thus limited at long wavelengths by the infrared absorption due to lattice vibrations, and at short wavelengths by the absorption in the ultraviolet due to the excitation of electrons to the conduction band.

The region of high transparency in silicates lies in the visible to near infrared. This is not true for some of the conductors such as silicon and germanium which are opaque in the visible. Because of a lower energy gap the absorption edge in these materials lies in a much longer wavelength than in silicates. Within the visible and near infrared region of transparency, two processes can lead to absorption. Characteristic absorption peaks are associated with the presence of transition elements. The energy levels of the unfilled electron shells are split by the crystalline field and certain transitions between these split levels are allowed. These transitions lead to characteristic absorption bands of the transition elements. In silicates the most important transition element is iron, which has a strong absorption peak about one micron. Titanium, manganese, and other elements will also give rise to absorption bands. It is these bands that give color to the crystals.

The absorption between the peaks determines the contribution of radiation to thermal conductivity. If there is one perfectly transparent region, then the material has an infinite thermal conductivity. The general level of absorption between absorption bands limits the energy transported by radiation. This general absorption is primarily due to free electrons. In the classical theory, free electrons will absorb at all wavelengths. The dependence of the opacity on electrical conductivity is given by

$$\frac{60\pi\sigma}{n} , \tag{34}$$

where both the electrical conductivity σ and the index of refraction n vary with frequency. If we assume that the dc electrical conductivity is a sufficiently good approximation, the variation with opacity can be written as

$$\epsilon = \epsilon_0 + \frac{60\pi\sigma_0}{n} e^{-E/kT} , \tag{35}$$

where ϵ_0 is the opacity at low temperatures and the second term on the right-hand side takes into account the temperature dependence of the conductivity; E is a characteristic excitation energy.

From the preceding discussion, it is apparent that the region of transparency in the near infrared and in the visible (between the ultraviolet absorption and the infrared lattice absorption) can be closed

by: (1) the presence of absorption peaks due to transition elements; or (2) a high level of general absorption due to free carriers, and, in particular, free electrons. Furthermore, it must be expected that changes in temperature and pressure will affect the nature of the region of transmission.

A few direct measurements of thermal conductivities at high temperatures suggest the importance of radiation. Most estimates of the contribution of radiation are based on determination of the absorption spectra rather than on actual measurements. In a few cases the measurements of spectra can be made as a function of temperatures; these indicate the closing, at high temperatures, of the region of transparency for glasses containing transition elements. Clark measured the room temperature absorption spectra of several silicates in the visible and near infrared (Reference 52). Radiative conductivities calculated from the absorption spectra are shown in Table 10. It should be noted that the ordinary conductivities at room temperature are on the order of 0.02-0.03 joules/cm-sec-deg.

Table 10

Radiative Conductivities Calculated from Absorption Spectra.

Mineral	K_R (joules/cm-sec-deg)			
	1000°K	1500°K	2000°K	2500°K
Olivine, $(Mg,Fe)_2SiO_4$	0.297	0.86	1.45	2.02
Diopside, $CaMgSi_2O_6$	0.067	0.238	0.44	0.725
Pyrope, $Mg_3Al_2Si_3O_{12}$	0.004	0.021	0.075	0.184
Almandine, $Fe_3Al_2Si_3O_{12}$	0.004	0.017	0.042	0.212

The absorption spectra of olivine and diopside are similar. Each has a peak at about one micron due to the ferric ion. The ultraviolet absorption edge lies at about 0.35 microns. Clark concluded that ferromagnesium silicates are sufficiently transparent for radiation to make an important contribution to the radioactivity. The results suggest a value of about 10 cm^{-1} or less as appropriate for the opacity of silicates at room temperature.

Data on the shift of absorption with an increase in temperature and pressure are still incomplete. It seems probable that increases both in temperature and pressure will tend to move the absorption edge toward longer wavelengths and reduce the region of transparency. An additional effect is the marked increase of electrical conductivity with an increase in temperature. If this increase is interpreted in terms of intrinsic conduction by free electrons, then the opacity will increase with an increase in temperature. Equation 35 illustrates the exponential dependence of the opacity and temperature through the mechanism of electrical conductivity.

MELTING RELATIONS AT HIGH PRESSURE

The fact that the mantle is solid can be used to limit the possible temperature distribution if the dependence of the melting point on pressure is known. Data on the increase of the melting point with pressure are still scanty. Boyd and England (Reference 53) have determined the melting curves of diopside and albite ($NaAlSi_3O_8$). The measurements on diopside extend from 5 to 50 kilobars and those on albite from 10 to 32 kilobars. The melting curve of albite is intersected by the transition of albite to jadeite plus quartz at a pressure slightly in excess of 32 kilobars.

It is customary to represent the melting relations in terms of the Simon semiempirical equation. The pressure and temperature along a fusion curve are given by

$$P = \frac{a}{B}\left[\left(\frac{T}{T_0}\right)^B - 1\right] , \tag{36}$$

where a and B are empirical constants. T_0 is the melting temperature at 1 bar pressure. The initial slope of the melting curve can be used to determine a, and B is determined by the initial curvature. Values for the coefficients in the Simon equation are given in Table 11 for diopside and albite.

If the diopside melting curve is extrapolated to a pressure of 1.3×10^6 bars, the pressure of the core-mantle boundary, the melting point is 3900° C. It should be noted that the melting points give estimates of the possible maximum temperatures. The melting points refer to a system that can be treated as a single component. Naturally occurring silicate materials form multicomponent systems, and the melting points are lowered.

Table 11

Coefficients for the Simon Equation (see Reference 53).

Mineral	T_0 (° K)	Calculated Initial Slope (deg/kilobar)	a	B
Albite	1391	14	19.3	5.1
Diopside	1665	15	25.2	4.4

CALCULATION OF INTERNAL THERMAL CONDITIONS

The internal thermal state of the earth can be investigated by assuming an initial temperature distribution, a distribution of heat sources, and a distribution, with depth, of the parameters determining density, heat capacity, and thermal conductivity. The temperature at the surface of the earth will be assumed to be known and taken as constant in time. The problem is then to determine the distribution at later times. If volume changes associated with the changes in temperature are neglected, the equation governing the temperature distribution in a spherical symmetrical body is

$$\rho C_p \frac{\partial T}{\partial t}(r, t) = \frac{1}{r^2}\frac{\partial}{\partial r}\left(r^2 K \frac{\partial T}{\partial r}\right) + A(r, t) . \tag{37}$$

The rate of heat production per unit volume, A, is a function of time as well as radius, since if a radioactive element is producing heat at a rate dQ/dt today, it produced heat at a rate $e^{\lambda t}(dQ/dt)$ at

a time t years ago; λ is the disintegration constant of the radioactive element. Analytical solutions to this equation can be obtained for special problems if the thermal conductivity is assumed to be independent of temperature (Reference 54). If radiative transfer of heat is important, the conductivity depends on temperature and the equation becomes a nonlinear partial differential equation. In this case there are no known solutions for the general problem and numerical methods have been used.

Lubimova (Reference 55) and MacDonald (Reference 56) have carried out detailed calculations on the development of temperature within the earth. Several general features of the calculation are important. The principal effect of radiative transfer of energy on the distribution of temperature in the earth is the flattening of the temperature gradient with depth. Near the surface the temperature gradient is dependent only on the lattice conductivity of the solids, and a near-surface gradient on the order of 10-20° C per km results in a wide variety of distributions of heat sources and thermal parameters. Because of the contribution from radiation the temperature required to remove heat from the deep interior decreases as the effect of conductivity increases with temperature. As a result the melting temperatures are most closely approached in the outer few hundred km of the earth. If the heat sources are distributed throughout the mantle the melting temperature is most closely approached or exceeded at depths on the order of 400-800 km. If the radioactivity is concentrated in the upper mantle (upper few hundred km) the melting point is approached or exceeded in the range 200-600 km.

The increase of opacity due to the increase of the number of free electrons at high temperatures does not influence the temperature distribution in a major way. Therefore the temperature distribution is relatively insensitive to the parameters that determine the electrical conductivity in the earth. The rapid increase of temperature in the outer few hundred km may contribute to a rapid rise of electrical conductivity in this region.

The prediction of today's heat flow for a number of earth models having a chondritic radioactive composition, and vastly different initial conditions and distributions of heat sources, falls within a factor of 2 of 50 ergs/cm^2-sec. The contribution of initial heat to the present heat flow is sufficiently great that the heat flow in any model in which the earth has passed through a molten stage is greater than the observed heat flow. The concentration of heat sources near the surface further increases the heat flow. A differentiated earth in which the differentiation is the by-product of melting is inconsistent with the hypothesis of an earth with a total radioactivity equal to that of chondritic meteorites. This is illustrated in Table 12 where the heat flow for various models of the earth is shown as a function of the depth to which the radioactive heat sources are concentrated. The parameters describing the models are shown in Table 13.

A differentiated once-molten earth could contain a radioactivity of, at most, half that of the chondritic radioactivity and remain solid. This conclusion is independent of the mode of the transport of heat, unless substantial amounts of heat can be transported by convection at temperatures well below the melting point of the solids.

The coincidence of the present surface heat flow with the present rate of heat production in chondritic materials may be explained in a number of ways. Radioactivity corresponding to a chondritic earth is entirely concentrated within the upper few hundred km. The initial temperature of the

Table 12

Present Surface Heat Flow in Differentiated Earth (Reference 57).

Heat Source Depth of Burial (uniform distrib.) in km	Surface Heat Flow (ergs/cm^2-sec)
100	69.4
200	79.4
300	83.2
400	85.7
500	87.8
600	89.7

Table 13

Parameters for Models Listed in Table 12.

Opacity ϵ_0	10 cm^{-1}
Surface Temperature	0 ° C
Index of Refraction	1.7
Heat Capacity	1.3 joules/gm-deg
Lattice Conductivity	0.025 joules/cm-sec-deg

Depth (km)	Initial Temperature (° C)
100	1880
200	1970
300	2050
500	2180
1000	2490
1500	2640
2000	2930

earth must have been less than some 1000°C; and heat is transported both by convection and conduction-radiation. Alternatively, chondritic radioactivity is distributed so that an appreciable proportion of the heat sources lie well below 600 km. The average initial temperature must be low. The contribution of initial heat and the higher rate of heat production in the past compensate for the heat produced but not reaching the surface. Still another possibility is that the radioactivity is, at most, half that of the chondrites. Heat sources can then be near the surface and the initial temperature relatively high.

A further feature of the thermal calculations is the shallow depth from which heat can be reaching the surface. Even with a high contribution of the radiation to the conductivity, heat produced at depths greater than about 1000 km does not reach the surface. The earth has a large thermal inertia and the time scale associated with the diffusion of heat within the earth is long compared with the time scale for the earth's history.

Chapter 6

INTERPRETATION OF THE VARIATIONS OF SEISMIC VELOCITIES IN THE MANTLE

Several features of the variation of seismic velocity with depth require explanation. First, there is the discontinuity between crustal material and material underlying the crust. This discontinuity can be interpreted either in terms of a relatively sharp change in the chemical composition of the material or in terms of a phase transition in which materials of low density transform to high density compounds.

Below the crust the velocity decreases with depth, reaching a minimum at a depth of 150 km. The decrease of velocity with depth can result either from the effect of changing temperature and pressure or from a change of chemical composition. Between 200 and 900 km the rate of the rise of velocity is much larger than below 900 km. The rapid rise of velocity again indicates a gradual change of composition, phase, or both. The discontinuity between the elastic mantle and the fluid core can also be interpreted in terms of phase transitions or a sharp break in chemical compositions. The present chapter discusses the laboratory evidence that bears on the problem of interpreting the variation of seismic velocities. It should be emphasized that the velocities shown in Figure 1 are only average velocities and there is no reason to expect that material in the upper regions of the mantle is homogeneous. Indeed, the inhomogeneity of the near-surface material strongly suggests that the upper mantle, at least, will show major inhomogeneities.

THE CRUST-MANTLE BOUNDARY

Seismic investigations on crustal structure have shown that the average thickness of the normal continental crust is approximately 35 km. The compressional and shear wave velocities are about 6.2 and 3.6 km/sec, respectively, near the surface, and increase with depth to approximately 7.0 and 3.8 km/sec. The seismic velocities for the subcrustal mantle material center about 8.1 and 4.7 km/sec. The seismic results for the oceanic regions indicate that the discontinuities separating the crustal material from the mantle lie at depths approximately 10 to 12 km below the surface of the sea. In general, the oceanic crust is somewhat less than 5 km thick with seismic velocities for compressional waves of 6.3 to 7.0 km/sec. The rocks below the discontinuity have compressional wave velocities centering around 8.1 km/sec, although a larger variation in these velocities is observed in the oceanic mantle than in the continental mantle.

The interpretation of the seismic data in terms of chemical composition cannot be unique. The seismic data must be combined with other independent sources of data in order to obtain an

interpretation of the composition of the crust and upper mantle. At present, the hypothesis of an oceanic crust of basaltic composition is compatible with both gravity and seismic results. Oceanic islands give no evidence for large amounts of any other material and hence it is generally assumed that the crust is predominantly basaltic. The continental crust is inferred to be of a far more complicated character. Surface outcrops indicate a wide variety of compositions and the observed variations of seismic velocities indicate a variation with depth. Subcrustal material in both oceanic and continental regions is generally assumed to be peridotite or similar rock. In this interpretation the crust-mantle boundary is the result of a sharp change in chemical composition, the crustal material having a greater proportion of Na, K, Ca, Al, and Si than the subcrustal material.

An alternative hypothesis about the nature of the seismic discontinuity between crustal and mantle material is that of phase transition. The phase transition would involve the breakdown of the feldspar to a denser form such as jadeitic pyroxene. The principal rearrangement involved in such transitions is the change in the local coordination of aluminum. In phases stable at high temperature aluminum is found in four coordination (four nearest neighbors); in phases stable at high pressure, aluminum takes on six coordination. Associated with the structural rearrangement is a 10-15 percent change in density. The laboratory results shown in Table 14 and Figure 8 indicate that the low density albite and nepheline will transform to higher density jadeite at a pressure equivalent to a depth of 30 km in the crust, provided the temperature is on the order of 400° C. Other materials undergo transitions at nearly the same conditions.

Table 14

Constants for Solid-Solid Transitions at High Pressures.

Constants	$NaAlSi_3O_8$ + $NaAlSiO_4$ (albite) (nepheline) $\rightarrow 2NaAlSi_2O_6$ (jadeite)	$NaAlSi_3O_8$ (albite) $\rightarrow NaAlSi_2O_6$ + SiO_2 (jadeite) (quartz)	SiO_2 (quartz) $\rightarrow SiO_2$ (coesite)	Al_2SiO_5 (sillimanite) $\rightarrow Al_2SiO_5$ (kyanite)	Sapphirine + Enstatite (+Sillimanite?) $\rightarrow$ Pyrope
T = bp - c					
b (°C/bar)	0.054	0.049	0.089	0.11	0.11
c (°C)	54	273	1740	1020	780
ΔV (cm^3/gm)	-0.083	-0.075	-0.046	-0.035	–
ΔS (joules/gm-deg)	-0.17	-0.15	-0.051	-0.031	–

The laboratory results are only suggestive since the exact thermal conditions at the crust-mantle boundary are not known, and since the experimental work has been carried out on chemically idealized systems. The effect of other components on the transition is still uncertain.

The simple suggestion that the seismic discontinuities represent a phase transition from a basalt-like material into a high pressure form faces serious difficulties. Since basalts form a multi-component system, a transition would be anticipated to occur over a wide range of temperatures and pressures rather than along a single curve on the temperature-pressure plane. Although the width of the transition zone is uncertain, it might be on the order of a few thousand bars; in this case the

transition zone would be spread over several km or tens of km. The seismic evidence on the sharpness of the transition is still unclear, but most investigators would assume that the transition from crust to mantle takes place over a relatively sharp interval, a few km at most.

An additional difficulty for a phase transition in oceanic areas follows from recent studies of the heat flow in the Pacific Ocean. Large regional variations in the surface heat flow correspond to variations in temperature of several hundred degrees at a depth of a few tens of km. Initial seismic studies over the same region show no comparable variation in the depth of the seismic discontinuity. Indeed the experimental data and assumed thermal gradients cannot be reconciled with the hypothesis of identical phase transitions under both oceans and continents. The depths of the seismic discontinuity can be explained in terms of a phase transition only if the crust and mantle have different compositions under oceans and continents.

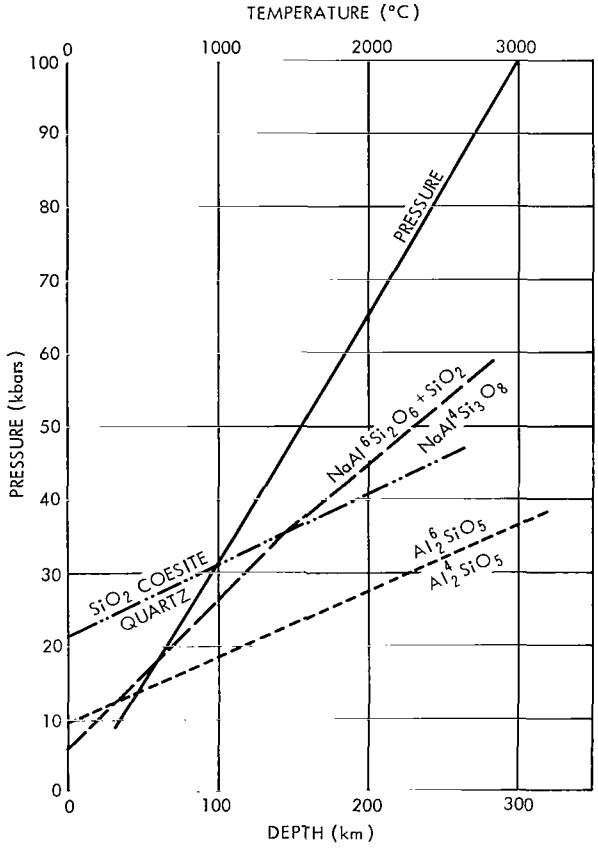

Figure 8–Stability relations between sillimanite and kyanite (Al_2SiO_5), quartz and coesite (SiO_2), and albite ($NaAlSi_3O_8$), jadeite ($NaAlSi_2O_6$), and quartz.

INTERPRETATION OF THE LOW VELOCITY LAYER

The physical conditions which give rise to the anomalous decrease in velocity below the crust are of great interest. Laboratory measurements show that in silicates the velocity increases with pressure; pressure stiffens a rock. An increase in temperature has the opposite effect, a decrease in the wave velocity. In the outer regions of the earth both pressure and temperature increase; thus velocity decreases if the increase in temperature is more effective than the increase in pressure. An extrapolation of laboratory data indicates that a gradient of 6° to 7°C per km is sufficient to produce a decrease in velocity.

If the low velocity zone is indeed due to the greater effect of the increase of temperature, then the existence of this zone indicates the magnitude of the temperature gradient in the upper regions of the mantle. The gradient between 30 and 150 km must be at least 6° to 7° C per km; and below 150 km the gradient must be less.

The low velocity zone might be due to large scale chemical inhomogeneity in the upper mantle. Presently available methods are insufficient to resolve the problem.

STRUCTURE OF THE MANTLE BETWEEN 200 AND 900 KILOMETERS

Understanding the variation of velocity between 200 and 900 km is important in any discussion of the internal make-up of the inner planets. The terrestrial pressure at 200 km is 0.65×10^5 bars and this pressure is reached within Venus, Mars, and Mercury.

The present interpretation of seismic results proposes a gradual increase in velocity over the region of 200 to 900 km. Earlier, Jeffreys presented a solution with the discontinuity in velocity at the depth of 480 km (Reference 58). Bernal proposed that the 480 km discontinuity was due to a phase change in which silicates transform from a lower density olivine structure to a higher density spinel structure. This suggestion was based on the similarity in chemical properties of silicon and germanium. The compound Mg_2GeO_4 was thought by Bernal to exist both in the olivine and in a higher density spinel structure. If silicon and germanium behave similarly, then olivine should also show a transition to spinel structure. The reality of the transition in Mg_2GeO_4 remained an open question until 1954 when Roy and Roy synthesized the high pressure, high density spinel phase (Reference 59). In addition, recent results of high pressure experiments indicate other transitions.

Olivine and Spinel Structures

Olivine, $(Mg,Fe)_2SiO_4$, has a zero-pressure density ranging from 3.2 gm/cm^3 for the pure magnesium end member to 4.3 gm/cm^3 for the pure iron end member. The main features of the olivine structure are (Reference 60):

1. The volume is largely determined by the arrangement of the oxygen. The oxygen atoms are in approximate hexagonal closest packing. They lie on sheets.
2. The silicon atoms are in tetrahedral coordination.
3. The magnesium or iron atoms are in octahedral coordination.

In spinel structure the oxygen atoms are approximately in cubic closest packing. In the interstices of the oxygen atoms are positions for metal atoms in four coordination between a tetrahedral group of oxygen atoms, and two sets of positions with an octahedral arrangement of nearest oxygen neighbors.

In the spinel structure one octahedron shares four edges with octahedra of the same kind and two with the tetrahedra. The other octahedron shares one edge with a tetrahedron and two with other octahedra. The spinel thus differs from the olivine structure, in which each tetrahedron shares three edges with an octahedron and does not share the other three.

In the spinel form of Mg_2SiO_4 the magnesium atoms fill the octahedral positions and the silicon atoms fill the tetrahedral positions (Reference 61). Each oxygen atom is linked to one silicon atom

and to three magnesium atoms. The structure of the silicate spinel differs from the germanate, since in Mg_2GeO_4 the germanium occupies the six coordinated position and the magnesiums are split between the tetrahedral and octahedral positions.

Stability Relations for the Olivine-Spinel Transition

The stability relations between the olivine and spinel forms of Mg_2SiO_4 have been extensively studied by Dachille and Roy (References 61-63) and by Ringwood (References 64 and 65). They studied the temperature and pressure stability of solid solutions of $Mg_2(Si,Ge)O_4$. The transition of the pure iron end member has been similarly examined. Dachille and Roy found that the maximum silicate content of the spinel solid solution increases steadily with pressure from about 10 mole percent at 700 bars to 50 mole percent at 60,000 bars and 540° C (Reference 61). They extrapolated these data to obtain the transition of the pure end member Mg_2SiO_4 at 100,000 bars, with an uncertainty of at least 15,000 bars. Ringwood synthesized the spinel form of Fe_2SiO_4 at 38,000 bars and 600° C (Reference 66).

The volume change in the olivine-spinel transition is a matter of some uncertainty. It may be appreciably lower than the 8.2 percent volume change for the transition in Mg_2GeO_4. Dachille and Roy (Reference 61) estimate that the change in volume is 2.0 cm^3/mole or 4.6 percent, whereas Ringwood uses 4 cm^3/mole for the change in volume.

Dachille and Roy estimate that the slope of the transition curve is on the order of 13° per kilobar (Reference 61). The presence of iron in the olivine will lower the transition pressure so that at temperatures on the order of 1000-2000° C an olivine with Mg/Fe = 9 would transform from the olivine form to the spinel form at depths on the order of 200-300 km.

Decomposition of Silicates to Oxides Under Pressure

A further possible transition involves the conversion of olivine or spinel forms of magnesium-iron silicate to oxide phases. Birch considered this possibility while noting that the ratio of the incompressibility to density (K_s/ρ) for a close-packed metal oxide such as MgO approaches the observed ratio of K_s/ρ within the earth at depths on the order of several hundred km (Reference 67). At room pressure, the stable oxides chemically equivalent to Mg_2SiO_4 are quartz, SiO_2, and periclase, MgO. In periclase, the oxygen atoms are in approximate cubic closest packing with the magnesium and oxygen atoms at alternate corners of a set of cubes (NaCl structure). In quartz, each silicon atom is surrounded by four oxygen atoms. The tetrahedra of oxygen atoms, each with a central silicon atom, are joined together to form groups which combine in a low density, open framework.

The open framework of quartz is unstable at moderate pressures. At a temperature of 930° C, 30,000 atmospheres are required to convert quartz to coesite; coesite has a density of 3.02 gm/cm^3 (References 68 and 69). In coesite, each silicon atom has as its neighbors four oxygen atoms in tetrahedral arrangement, as in quartz (Reference 70). The structure of coesite differs from that of quartz in having a more compact arrangement of the silica tetrahedra. Birch suggested still another possible form for SiO_2, the rutile structure assumed by TiO_2 (Reference 67). In this structure each

silicon atom has as its nearest neighbors six oxygen atoms, approximately in the corners of a regular octahedron, and each oxygen atom is next to three silicon atoms, approximately at the corners of an equilateral triangle. The oxygen atoms are in approximate closest packing. The rutile structure thus assumes the general structure for AB_2 compounds, in which the A atom has six coordination. TiO_2 is also found in two other structures in which Ti is in six coordination but the oxygen atoms show slightly different arrangements. MacDonald, considering the transition of quartz to coesite, estimated the density of the rutile form of SiO_2 to be about 4.5-5.0 gm/cm^3 (Reference 68). Stishov and Popova synthesized the high pressure rutile form of SiO_2 (Reference 71). The density of the new compound was found to be 4.35 gm/cm^3. Chao, Fahey, et al. later discovered the new high pressure form of SiO_2 in coesite-bearing rocks near Meteor Crater, Arizona, where the high pressure form, stishovite, formed during the impact of the meteor (Reference 72).

The combination of SiO_2 and MgO is 21 percent denser than Mg_2SiO_4 in the olivine structure. The difference in density results from the fact that oxygen atoms in the two oxides are very nearly in closest packing with the largest change in density associated with the change in the coordination of silicon from four to six. The instability of the rutile form of SiO_2 at low temperature may be associated with the distance of nearest approach of the silicon atoms, each carrying a nominal charge of +4. In the quartz and coesite structures the silica tetrahedra are joined in such a way that each oxygen is shared by two silicon atoms. A pair of silicon atoms are shielded from each other by the presence of the intervening oxygen atom. In the rutile structure the octahedra surrounding the silicon atoms are joined together by shared edges. This results in the much closer approach of the silicon atoms without direct shielding of an oxygen atom. Silicon and titanium differ in behavior because titanium is a transition group element and the larger titanium ion forms bands that are less localized than those of silicon. Further, it may be noted that the anatase and brookite structures may be much less stable for SiO_2 than for TiO_2. In the anatase structure three edges are shared, and in both forms there is greater opportunity for the cations to interact directly with each other. Moreover, these other possible arrangements of octahedrally coordinated silicon lead to no saving in volume.

Stability Relations for the Oxide Transitions

Estimates of the possible conditions under which the breakdown of Mg_2SiO_4 to the oxides takes place depend upon recent, fragmentary data.

Stishov and Popova synthesized the rutile form of SiO_2 at a quoted pressure of 1.6×10^5 bars and a temperature between 1200 and 1400° C (Reference 71). The estimate of pressure is probably high because friction in the apparatus was undervalued (Reference 73). Let us assume that the coesite-stishovite transition pressure is 1.12×10^5 bars (30 percent less than the published value) and that the temperature is 1300° C. These values, and the thermochemical properties for the various phases listed in Table 15, give a rough estimate of the equilibrium conditions for the reaction

$$Mg_2Si^4O_4 \longrightarrow 2MgO + Si^6O_2 \quad , \tag{38}$$

where the superscripts 4 and 6 on Si denote the coordination number. The change in internal energy

Table 15

Thermochemical Properties for MgO, SiO_2, and Mg_2SiO_4.*

Material	Volume (cm^3/mole)	Density (gm/cm^3)	Entropy (joules/deg-mole)
MgO	11.2	3.59	27.2
Si^4O_2 (quartz)	22.6	2.65	41.8
Si^4O_2 (coesite)	19.9	3.02	38.9
Si^6O_2 (stishovite)	13.8†	4.35	28.0‡ - 33.0‖
Mg_2SiO_4 (olivine)	43.8	3.22	95.2
Mg_2SiO_4 (spinel)	39.8	3.37	–

*Reference 74.
†Reference 71.
‡Estimated on the basis of the "law of corresponding states" for quartz-coesite-stishovite.
‖Estimated on the basis of ≈ 2.4 joules/deg-cm^3 found for many close-packed oxides at temperatures above the Debye temperature.

in the transition of coesite to stishovite ($Si^4O_2 \longrightarrow Si^6O_2$) is

$$\Delta E = -P\Delta V + T\Delta S \approx (6.6 - 1.7) \times 10^4 = 4.9 \times 10^4 \frac{\text{joules}}{\text{mole}}, \quad (39)$$

for a heat of formation of Mg_2SiO_4, from the oxides, of 6.3×10^4 joules/mole; the change in internal energy for Reaction 38 is 11.2×10^4 joules/mole. The pressure required for the work term in Equation 39 to equal $T\Delta S - \Delta E$ is then 1.7×10^5 bars at 1300° C. It should be noted that $T\Delta S$ for the transition is small compared to $P\Delta V$.

Estimated phase transition curves for the coesite-stishovite, olivine-spinel, and olivine-oxides transitions are shown in Figures 9 and 10.

In the breakdown of the iron end member, Fe_2SiO_4, to the oxides, there is a volume change of 17.7 percent (Table 16). Using thermochemical data listed for fayalite (Reference 75) we find that the olivine to oxides transition pressure is about 10^5 bars. A summary of the volume changes associated with the various reactions is presented in Table 16.

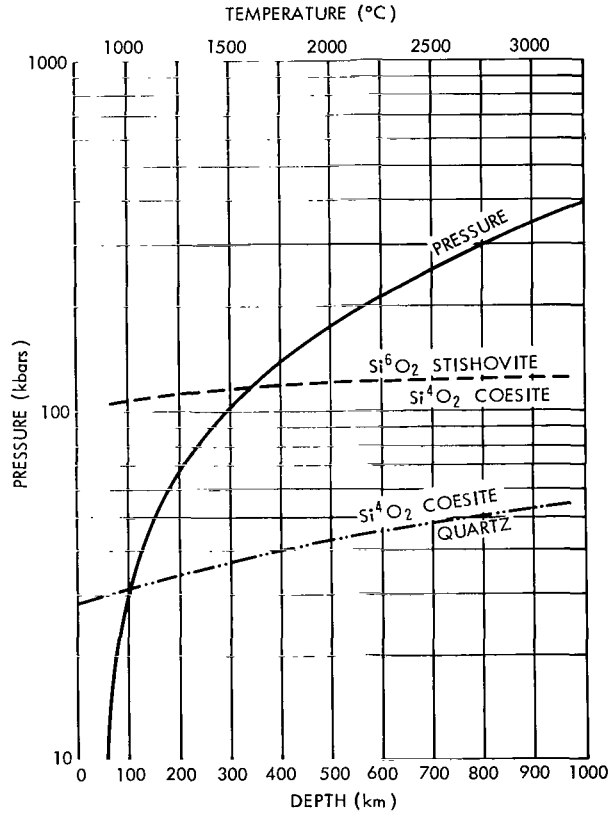

Figure 9—Calculated stability relations between stishovite and coesite and stability relations between coesite and quartz extrapolated from data of Boyd and England (Reference 69).

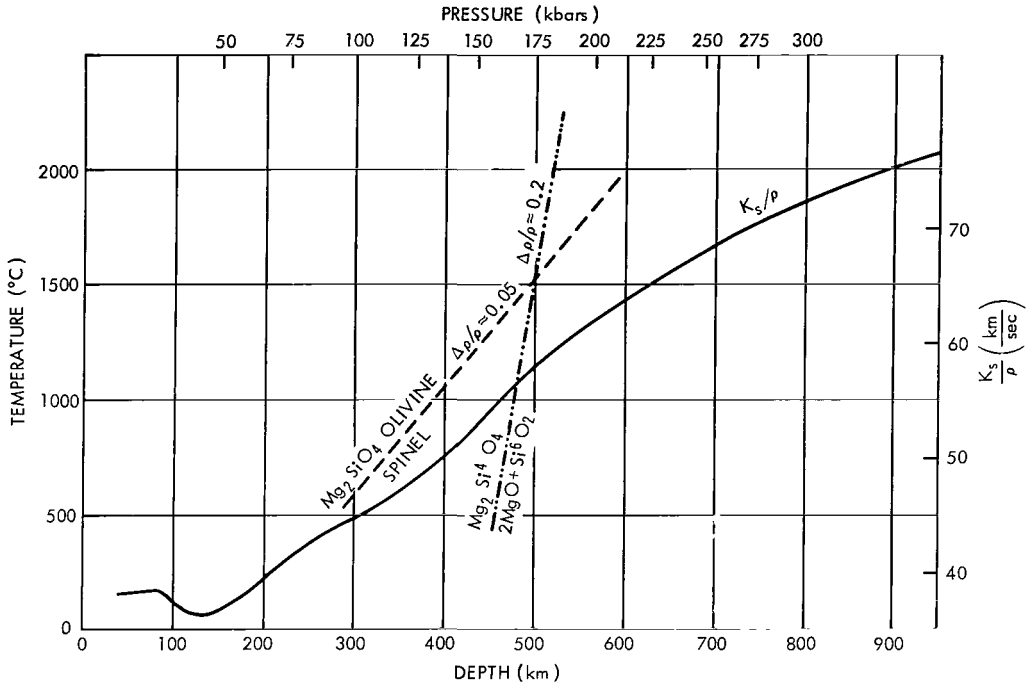

Figure 10—Calculated curve for the breakdown of olivine to periclase plus stishovite. The variation of $\phi = K_s/\rho$ is derived from the Gutenberg model earth shown in Figure 1.

Table 16

Summary of Volume Changes for High Pressure Transitions in Mg_2SiO_4 and Fe_2SiO_4.

Material	Density of Low Pressure Assemblage (gm/cm^3)	Density of High Pressure Assemblage (gm/cm^3)	Percentage Change in Volume
Mg_2SiO_4 (olivine) → Mg_2SiO_4 (spinel)	3.22	3.54*	11.0
Fe_2SiO_4 (olivine) → Fe_2SiO_4 (spinel)	4.3	4.85	12.0
$Mg_2Si^4O_4$ → $2MgO + Si^6O_2$	3.22	3.89	21.0
$Fe_2Si^4O_4$ → $2FeO + Si^6O_2$	4.3	5.06	17.7

*The values used are those given by Ringwood (Reference 66). Dachille and Roy obtained a 4.6 percent volume change (Reference 61). The origin of the discrepancy is not clear.

The temperature-pressure conditions under which high pressure transitions take place are still very uncertain. However, it is clear that under conditions existing at depths on the order of 200-500 km, the common silicate phases undergo transitions to new phases with structures in which the oxygen atoms lie in closest packing. Since the oxygen atoms occupy almost the entire volume within silicates, it is unlikely that the silicates will undergo further structural rearrangements. Any further decrease in volume can only result through a distortion of the outer electron orbits, i.e., pressure ionization. The pressure required for such transitions is on the order of 10^6 bars or greater, reached only within the cores of the larger planets. The density changes in these transitions are likely to be small compared to density shifts in the geometric rearrangements. The collapse of the silicate structures at a pressure of about 10^5 bars, however, can happen in Mars, Venus, and Mercury, since a pressure of this order is reached at moderate depths within the planets.

CHEMICAL COMPOSITION OF THE EARTH'S CORE

The discovery of the earth's core by Oldham in 1906 has provoked much speculation on its physical and chemical properties. The difficulty in determining the physical and chemical nature of the earth's core with any degree of certainty is connected with the difficulty of compressing materials to the pressure within the core. The pressure at the core-mantle boundary is 1.3×10^6 bars. This pressure is much greater than the highest pressure that can be obtained in static experiments at the earth's surface. However, it is possible to reach these pressures for short periods of time during the shock wave experiments, and data on the compressibility of solids obtained by using shock waves is of importance in establishing an equation of state for the core.

The core of the earth is generally assumed to be liquid iron-nickel alloy. Evidence advanced in support of this view includes: (1) the existence of iron meteorites; (2) the fact that the density of iron is in general agreement with the density of the core as estimated from seismology and from the theory of the figure of the earth; and (3) the fact that iron would probably be liquid at the temperatures and pressures of the core, whereas silicate materials would be solid. In addition, a recent investigation of the abundance of elements in the solar system suggests that iron is an abundant heavy element and a planet with an iron core would have the proper heavy element abundances.

The hypothesis of an iron core has not gone unchallenged. Kuhn and Rittmann propose a core of undifferentiated solar matter, arguing that an iron core is inconsistent with the relative abundances of the elements (Reference 76). Ramsey suggests that the seismic discontinuity at 2900 km represents a change in phase from $(Mg, Fe)_2SiO_4$ in the olivine form in the mantle to the metallic phase in the core (References 77-79). Birch critically reviews these suggestions and concludes that the core is principally iron-nickel with minor amounts of silicon and carbons, since the apparent density of the core is somewhat less than the expected density of pure iron (Reference 67). The view that the 2900 km discontinuity is a phase change has many attractive features. However, a phase change in a multicomponent system will almost certainly be spread out over a range of pressures. The sharpness of the 2900 km discontinuity plus the large change in density at the core-mantle boundary favor a compositional discontinuity rather than a change of phase.

Estimates for the mean density of the core and for the density of the core at the core-mantle boundary follow from the estimates of the incompressibility, obtained from seismic velocities in the mantle (Chapter 4) and from the moment of inertia (Chapter 2). The satellite determination of J_2^0 leads to a much improved estimate of the mean moment of inertia, about 0.9 percent less than the value previously accepted. The new value of the moment of inertia implies a somewhat greater central concentration of mass. Table 17 lists the masses and moments of inertia of the principal structural units of the earth. The continental crust is taken to have a thickness of 35 km with a mean density of 2.8 gm/cm^3. The oceanic crust consists of a layer of 6 km of water underlain by 4 km of rock of a density of 3.0 gm/cm^3. The continent-ocean boundary is taken to be the 1000 fathom line (Reference 19). The layer underneath the oceanic region extending to 35 km is assumed to have a density of 3.3 gm/cm^3.

Table 17

Masses and Moments of Inertia of the Major Structural Units of the Earth.

Structural Unit	Mass $\times 10^{-25}$ (gm)	Moment of Inertia $\times 10^{-43}$ (gm cm^2)
Crust	2.45	0.616
Continental	1.88	0.453
Oceanic	0.570	0.163
Layer Above 35 km	5.07	1.35
Mantle and Core	593	79.3
Mantle (below 35 km)	398	70.3
Core	194	8.99
Earth	597.7	80.68

The mass and moment of inertia of the mantle plus core follow by subtraction. Estimates of the individual moments of the core and mantle can be obtained from the Gutenberg velocity distribution (Figure 1). The resulting mean density of the core is 11.28 gm/cm^3 and the density of the core-mantle boundary is 10.17 gm/cm^3.

Shock wave measurements on the equations of state of iron (References 80 and 81) indicate that the density of iron at 1.3 megabars and about 2000° C is 11.2 gm/cm^3. Compare this value with the core-mantle boundary density of 10.17 gm/cm^3. The core material is about 10 percent less dense than iron. Nickel would raise the mean density whereas lighter elements, in particular silicon and carbon, would lower it. MacDonald and Knopoff suggest that perhaps silicon is the principal alloying element in the core (Reference 82).

Chapter 7

INTERNAL CONSTITUTION OF THE MOON

Almost all inferences regarding the internal constitution of the moon follow from the data on its orbital and rotational motion. A possible additional limitation to the thermal constitution is derived from a comparison of the radio emission temperatures of the lunar surface at several wavelengths (Reference 83).

The mean density is well established as 3.34 gm/cm^3. The density at 1 bar pressure and 25° C is uncertain because of the unknown thermal conditions and phase transformations within the moon. Urey estimates that the density is about 3.4 gm/cm^3 (Reference 84), significantly less than the density of chondrites (3.57-3.76). He has pointed out that the moon's density is consistent with a material having about half the total iron content of the chondritic meteorites and has considered several chemical models. In particular, the abundance of the elements in the moon may be similar to the heavy element abundance in the sun's atmosphere. This possibility is illustrated in Table 18 where the ratios of the chondritic to solar abundances are given. Note that iron is about 6 times, and potassium 1/4, as abundant in chondrites as in the solar atmosphere.

Table 18

Ratio of Chondritic to Solar Abundances for the Heavy Elements. Chondritic Abundances are the Averages of High and Low Iron Groups from Reference 85. Solar Abundances are from Reference 86.

Element	Ratio	Element	Ratio
Na	0.77	Ca	1.23
Mg	1.59	Ti	1.52
Al	1.18	Cr	1.07
Si	1.00	Mn	2.24
P	0.66	Fe	6.03
S	0.17	Co	1.59
K	3.72	Ni	1.02

The moon's density is almost equal to that of the upper part of the earth's mantle. The density of the upper mantle is usually interpreted in terms of a peridotitic or eclogitic composition, the chemical composition of which is almost identical to the composition of the silicate phase of chondrites. The maximum pressure within the moon is about 46,000 bars; the pressure is too low for either the olivine-spinel or olivine-oxides transition.

THE MOON'S GRAVITATIONAL FIELD

Urey emphasized that the figure of the moon sets limits on the internal constitution (Reference 1). The basic argument is that the present gravitational figure of the moon is not in hydrostatic

equilibrium. The inequalities in figure must be supported by internal strength. If the moon were partially molten or if a large part of it were nearly at the melting stage, then the figure should be close to hydrostatic. But the possible inferences about the internal thermal state are complicated by the fact that the stress differences may be supported in a sufficiently thick and cold outer shell, and the interior may be molten or nearly so. However, it is difficult to suggest a distribution of radioactivity that would lead to such a thermal configuration in a body the size of the moon. This point will be discussed in detail later.

We denote the moment of inertia about the axis of rotation by C. The least moment of inertia, A, is the moment about the axis pointing toward the earth. The moment B is along the tangent to the orbit. The ratios

$$\left.\begin{aligned} \alpha &= \frac{C - B}{A} , \\ \beta &= \frac{C - A}{B} , \\ \gamma &= \frac{B - A}{C} , \end{aligned}\right\} \qquad (40)$$

are determined from data on the moon's rotational and physical libration. The value for β depends on the angle of inclination between the mean axis of rotation and the pole of the orbit. Since the direction of the axis of rotation has been well observed, this ratio is accurately determined. A recent discussion by Jeffreys (Reference 87) gives

$$\beta = 0.0006270 \pm 0.0000015 . \qquad (41)$$

The value of α depends on observations of the libration in longitude. Difficulties in observation have led to a wide scattering of results. Table 19 lists the relevant values (References 87 and 88). Table 19 also lists the values for α and β, under the assumption that the moon is in hydrostatic equilibrium. The moon's equatorial bulge is much too large to be accounted for by its present rate of rotation and the bulge toward and away from the earth is much greater than would be expected from tidal theory.

If the moon is supposed to be an elastic body supporting the inequalities in figure, the maximum stress differences at its center are on the order of 20 bars, provided the inequalities are supported by the whole body. Urey, Elsasser, and Rochester suggest that near-surface density inhomogeneities can lead to the observed figure (Reference 89). The stress differences associated with these near-surface inhomogeneities will be larger than the 20 bars calculated for a homogeneous moon. It might be supposed that the outer layers of the moon are cold and could support the required stress differences. However, calculations of the possible temperature distribution within the moon bring the temperature close to the melting point at depths on the order of 300 to 400 km. The density inhomogeneities would then have to be concentrated in the outer 300 or 400 km.

Jeffreys proposed that the departure of the figure from equilibrium is due to the solidification of the moon at a time when it was much nearer to the earth (Reference 20). The present figure then

Table 19

Data on the Moon's Figure (Reference 87).

Computation	Observed Value	Theoretical Value		Ratio of Observed to Theoretical
		Hydrostatic Equilibrium	Uniform Density	
$\frac{C-B}{C}$	0.0004	0.0000094	–	42
$\frac{C-A}{C}$	0.0006279	0.0000375	–	16.7
$\frac{C-A}{Ma^2}$	0.000364	–	0.000251	1.45
$\frac{B-A}{Ma^2}$	0.000071	–	0.000084	0.84
$\frac{C}{Ma^2}$	0.56	–	0.4	1.4

would represent a frozen tidal wave. However, on the tidal wave hypothesis the ratio α/β is independent of distance of the moon from the earth and has a theoretical value of 0.25. The observed ratio is 0.64 (Reference 87). Thus, the present figure cannot be explained solely by supposing that the moon solidified when it was much closer to the earth. A further difficulty follows from its thermal history. If the moon were initially molten, a uniformly distributed radioactivity only one-fourth that of chondrites would keep the moon near or at the melting point. The frozen tidal wave could not be maintained.

The ratios of the differences in moment of inertia to Ma^2 are determined by the orbital motion of the moon and in particular by the mean motion of perigee and node. The observed values are listed in Table 19. Also listed are theoretical values obtained from α and β by assuming that the moon is of uniform density (Reference 87). Combining the observed values of $(C - A)/Ma^2$ with β results in the ratio of the principal moment of inertia to the product of the mass and the square of the radius. For a uniform moon this ratio should be 0.4. The observed value is 0.56. Jeffreys considers the uncertainties in the observational material to be sufficiently large that the discrepancy with the theory for a homogeneous moon is not significant.

The data on rotation, libration, and orbital motion suggest a model which supports stress differences on the order of 10 bars, and in which the density distribution is either uniform or slightly increasing toward the surface. The presently available dynamical data are not consistent with a moon in which gravity-controlled density stratification on a large scale has taken place.

LUNAR TIDES

Both the earth and the sun produce significant tides on the moon. If the moon were spherical, the effect of these tides would be to distort the sphere into an ellipsoid whose long axis would be toward the tide-raising body. The moon rotates once per month relative to the line joining the centers of the sun and moon. Therefore, the long axis of the solar tidal ellipsoid rotates once per month relative to a system of axes fixed within the moon, giving rise to a predominantly fortnightly tide similar to the semidiurnal tides on the earth. The moon, however, does not rotate relative to the line joining the centers of the earth and the moon but wobbles about this line in a range of about 7 degrees. The tides due to the earth have, therefore, two causes: the changing distance of the earth which causes the ellipticity of the tidal ellipsoid to increase as the earth comes closer to the moon and decrease as the earth recedes, and the moon's wobble about the line of centers. The relative importance of these effects varies with the position of the moon's surface. Close to points of intersection of the line of centers with the moon's surface, the distance variation is the more important. The monthly variation of the earth-moon distance is the most important factor leading to large monthly tides.

The response of the moon to tide-raising potential can be calculated by using the Love numbers h and k. These Love numbers are determined by the distribution of density and rigidity in the moon's interior.

The moon's density of 3.34 gm/cm^3 is close to that of the upper parts of the earth's mantle and suggests that the moon is made out of silicate materials similar to those in the mantle. A possible model of the moon, and the one usually considered, is a moon with a homogeneous composition. For a homogeneous incompressible spherical body the Love numbers are

$$\left.\begin{aligned} h &= \frac{5f}{2f + 1}\,, \\ k &= \frac{3f}{2f + 1}\,, \end{aligned}\right\} \tag{42}$$

where $f = g\rho a/19\mu$, with g the surface gravity, a the outer radius, and μ the rigidity. If the density is taken as 3.34 gm/cm^3 and the rigidity as 7.38×10^{11} dynes/cm^2 (the rigidity of the upper mantle), we obtain $h = 0.0331$ and $k = 0.0199$, and the tidal gravity variation $\left(1 + h - \frac{3}{2}k\right)$ is increased by 3.3 parts per thousand as compared with the variation on a perfectly rigid moon. If the moon were perfectly fluid, then h would equal 2.5 and k would be 1.5. If the moon has a fluid inner core with a core radius equal to half the outer radius then $h = 0.0639$, $k = 0.0384$, and there is a change in the moon's gravitational yielding of 6 parts in 1000.

The investigation of the elasticity of the moon by observations of the change of the tidal gravimetric acceleration is a possible experiment, but it is of marginal value because of the small effect.

LUNAR SEISMOLOGY

Seismic exploration of the moon will yield valuable information regarding its internal constitution. Prior to the actual landing of seismometers on the moon there are two important areas of investigation to consider. One is concerned with obtaining an estimate of eigen frequencies for the spheroidal oscillations. These long period oscillations can be detected by long period vertical seismometers, and they are an especially valuable source for information on the internal distribution of elasticity. A second investigation concerns elastic energy built up through differential heating and cooling associated with the internal release of radioactive heat and with the surface heat flow. The object in this case would be to estimate the magnitude of release of this elastic energy.

Computations of the expected spheroidal oscillations of the moon have been made by Bolt (Reference 90) and by Takeuchi, Saito, and Kobayashi (Reference 91). The results from Reference 91 are listed in Table 20 where the model of the moon is taken to be homogeneous, the elasticity being that of the upper mantle of the earth.

Table 20

Computed Periods of Spheroidal Oscillation of the Moon (Reference 91).

Order	Period (min.)
2	14.7
3	9.9
4	7.7
5	6.4
6	5.5
7	4.8
8	4.3
9	3.9
10	3.6

MacDonald determined the average rate of increase of the principal stress differences for several thermal models of the moon (Reference 92). This increase was on the order of 10 bars per million years. Using this figure we can estimate the average rate of release of strain energy, provided some assumption is made on the strength of the lunar materials. The rate of increase of strain energy will be a maximum when the stress differences are of the order of the strength. For a strength of 100 bars the maximum strain energy per unit volume is on the order of 1.4×10^3 ergs/cm^2. The rate of release of strain energy by failure at 100 bars maximum stress difference will be approximately 4×10^{24} ergs/year. At present, the moon should have a high degree of seismic activity, unless the radioactivity of the moon is concentrated in a thin layer near the surface or is far less than that of chondritic materials.

The degree of seismic activity varies among various models of the distribution of heat sources with depth. In the models considered in Reference 92 the greatest release of strain energy is at depths of 100 to 700 km. The assumption of deeply buried radioactivity implies deep foci for lunar seismic disturbances.

A determination of the average rate of seismic activity on the moon can be used to estimate the amount of radioactivity on the moon and possibly its distribution.

THERMAL CONSTITUTION OF THE MOON

Thermal Radiation from the Moon

Baldwin has made a study of the thermal radiation of the moon at radio wavelengths, in order to place a limit on the possible heat flow at the moon's surface (Reference 83). High frequency radio and infrared emission determines the temperature at and within a few cm of the surface. Baldwin has carried out observations at 178 Mc (168 cm), where the depth of penetration is greater than for the shorter wavelength emission. He estimates that the depth of penetration is greater than 25 meters and may be on the order of 200 meters. The uncertainty is due to the sensitive dependence of the penetration depth on the unknown dielectric constant of the lunar surface material.

Baldwin obtains a temperature of 233 ± 8°K at 178 Mc. This temperature is within 25° K of various estimates of the surface temperature. The indicated temperature gradient, when combined with various estimates of thermal conductivity, gives upper limits to the heat flow ranging from 1 to 10 ergs/cm^2-sec. Any limit in this range can be compared with the surface heat flow for a moon of chondritic composition. The present rate of heat production in a chondritic moon would be 3.7×10^{18} ergs/sec which is equivalent to an "equilibrium" surface heat flow of 9.6 ergs/cm^2-sec. The extreme upper limit of the heat flow obtained from the study of the radio wave emission is then barely consistent with the assumption of a chondritic moon; on the whole a lower heat flow is indicated.

Calculations on the Thermal Structure of the Moon

The present thermal state of the moon is determined by the distribution of: (1) radioactive elements; (2) thermal conductivity; and (3) initial temperature. Of these parameters, the expected variations of the thermal conductivity exercise the least influence on the present temperature distribution; the distribution of radioactivity and of the initial temperature are much more important.

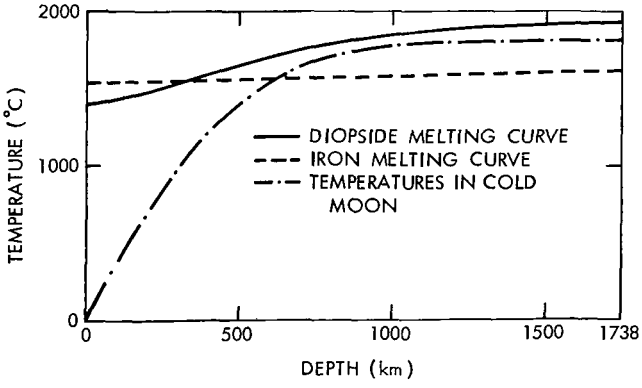

Figure 11—Variation of temperature in a moon having chondritic radioactivity which is uniformly distributed. The initial temperature is 0°C.

A number of calculations on the internal temperature distribution within the moon have been made with methods developed for the study of the thermal history of the earth (References 1, 56, and 93). If the moon were initially at a uniform temperature of 0° C, then the present temperature distribution (after 4.5×10^9 years) would be as shown in Figure 11. The radioactivity is taken to be equal to that of chondritic meteorites and assumed to be uniformly distributed throughout the moon. For comparison, Figure 11 also shows the melting point curves of diopside ($CaMgSi_2O_6$) and iron. The melting point of a multicomponent silicate material will be

lower than that of diopside. The close approach of the diopside melting point curve and the calculated temperature indicates that much, if not all, of the moon would be near or at the melting point. A uniform chondritic composition results in temperatures above the estimated melting temperatures of silicates even if the assumed initial temperature is low.

A large number of other models have been constructed in which the radioactivity is uniformly distributed and different thermal parameters have been assumed (References 88 and 92). The outstanding feature of the temperature-depth curves for models of the moon is the shallow depth at which the melting points are reached or exceeded. Since the moon is a relatively small body the central pressure is low, on the order of 46,000 bars. This low central pressure does not markedly raise the melting point of the possible constituents. The thermal conductivity is sufficiently low that only the outer portions of the moon are cooling to any extent. The combination of these two circumstances results in the close approach of the melting point curve to the calculated temperature distribution illustrated in Figure 11. In the earth the rate of increase of pressure with depth is much larger and raises the melting point, with the result that the earth's mantle is solid.

In a homogeneous moon, the melting temperature of silicates is approached or exceeded, provided that the moon has the composition of chondritic meteorites. The assumptions of chondritic radioactivity and of homogeneity are, then, inconsistent with the astronomical data on the figure of the moon, if these data are interpreted in terms of internal strength. There are two possible solutions: (1) The total radioactivity of the moon is less than that of chondritic meteorites. (2) The moon is a differentiated body whose radioactivity is concentrated toward the surface. In the latter case the suggestion of homogeneity in the orbital data must be disregarded. Both of these alternatives have been noticed by Urey (Reference 93); he has carried out calculations on the effect of a lower radioactivity.

In investigating the two alternatives to a homogeneous chondritic moon, we will first consider the temperature distribution in a differentiated moon with the radioactivity concentrated toward the surface. Figure 12 shows the maximum temperature and the depth at which this temperature is reached, for a moon in which the radioactivity is equal to that of chondritic meteorites but concentrated near surface layers. The initial temperature is taken to be 600° C. In the upper curve, the opacity is 1000 cm^{-1} and corresponds to a case where the radiative transport heat is unimportant. In the lower curve, the opacity is 10 cm^{-1} and radiation begins to dominate ordinary thermal conduction at temperatures on the order of 700° C. If the radioactivity is concentrated in the outer 100 km, then the maximum temperature is the

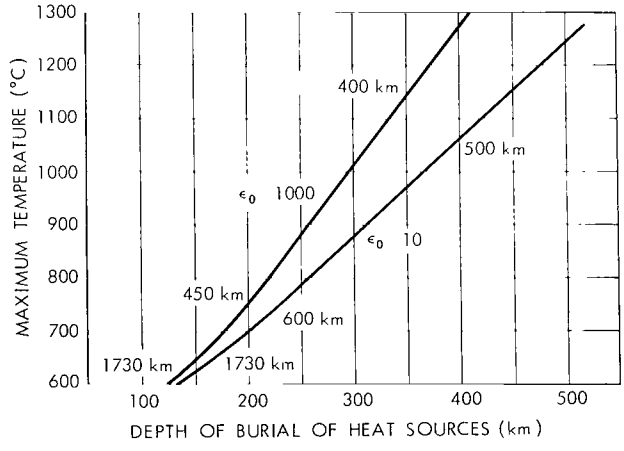

Figure 12—Maximum temperature within the moon as a function of the depth of burial of heat sources. The depth at which the maximum temperature is reached is shown for the various depths of burial. The initial temperature is 600°C and the total radioactivity equals that of chondrites.

initial 600° C since the central regions do not lose heat. These calculations illustrate that in a differentiated moon the melting point is not reached. The assumption of a differentiated moon removes the difficulty of a present-day partially molten moon, but raises the problem of how differentiation could proceed without the moon's passing through a molten stage. If the actual accretion of the moon is such as to permit a differentiated body, then the thermal difficulties are removed. However, there is no indication of density stratification in the orbital data.

In Figure 13 the temperature is a function of the depth of burial of the heat sources, with an initial temperature of 1200° C. Even for this high initial temperature the maximum temperatures lie well below the melting temperatures at the depths involved.

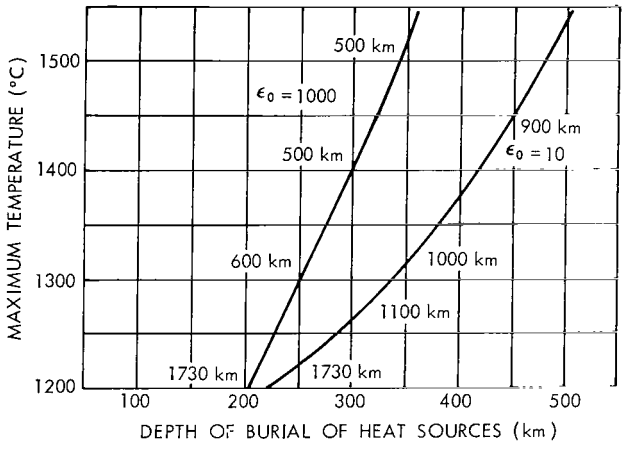

Figure 13—Maximum temperature within the moon as a function of depth of burial of heat sources. This figure is similar to Figure 12, but the initial temperature is 1200° C.

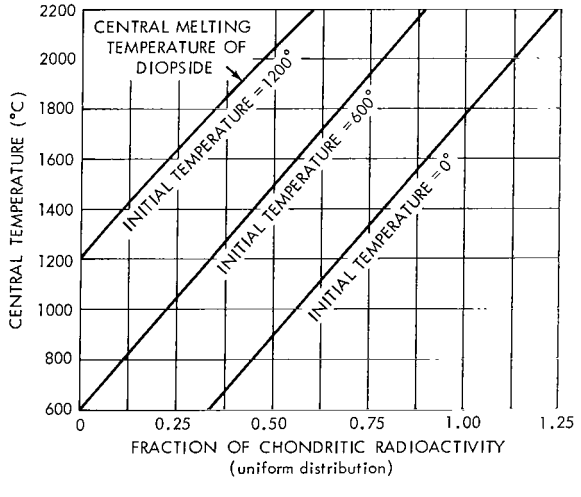

Figure 14—The maximum temperature within the moon as a function of the total radioactivity of the moon. Radioactivity is uniformly distributed.

Figure 14 shows the effect upon the maximum temperature of lowering the total radioactivity. The radioactivity is assumed to be uniformly distributed. In this case the maximum temperature is reached at the center of the moon. The central temperature is plotted as a function of the fraction of chondritic radioactivity maintaining the chondritic ratio among the heat-producing elements. It is to be noted that the solar abundance of potassium corresponds to about 1/4 of the chondritic radioactivity. If the initial temperature is 0, the central temperature lies below the melting temperature for a total radioactivity equal to that of chondritic meteorites. If the initial temperature is 600° C, then the moon remains solid throughout if the radioactivity is 0.75 that of chondrites or less. An initial temperature of 1200° C requires that the radioactivity be less than 0.4 that of chondritic meteorites for the present central temperature to lie below the melting point of diopside. If the radioactivity were as low as that indicated by the potassium content of the solar atmosphere, then the initial temperature could have been rather high, greater than 1200° C, and the lunar material would still have remained solid.

A differentiated moon removes the problem of the conflict between the inferred strength of the moon and the high temperatures within a uniform chondritic moon. Difficulties with the thermal emission may be raised in that the heat flow

in a partially differentiated moon will be greater than in a uniform moon. Figure 15 shows the surface heat flow as a function of the depth of burial of heat sources, by assuming a chondritic radioactivity and an initial temperature of 600° C. Two values for the opacity are shown and these indicate that the detailed assumptions regarding thermal conductivity are not important in the determination of the surface heat flow. If the heat sources extend to a depth of some 500 km, then the surface heat flow is twice that of the model in which the heat sources are located within the upper 70 km. The near-surface concentration of heat sources permits heat produced during the early stages of the history of the moon to escape rather than be trapped. If the heat sources are buried to a depth of some 500 km most of the heat is reaching the surface. This high heat flow may be in conflict with the results of radio emission at long wavelengths, but the point should not be held too strongly since the radio result involves rather arbitrary assumptions regarding the electrical properties of the near-surface lunar materials.

Figure 16 illustrates the dependence of the surface heat flow upon the depth of burial of sources when the initial temperature is at 1200° C. If the moon were initially molten, then the heat flow would be considerably higher, as in Figure 17.

The alternative to concentration of heat sources near the surface is that the radioactivity of the moon is substantially less than that of chondritic meteorites. The dependence of surface heat flow on the amount of radioactivity

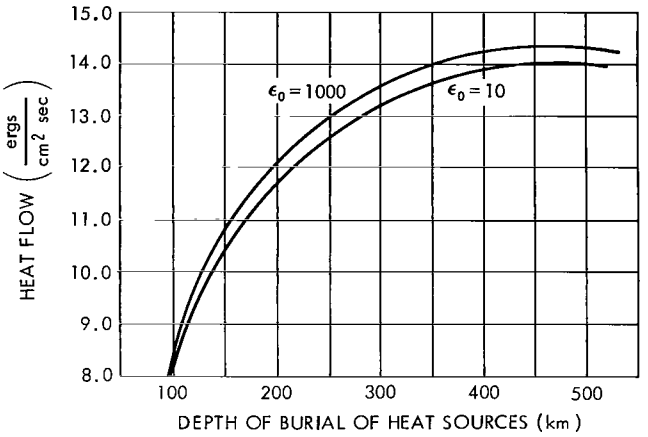

Figure 15—The dependence of surface heat flow on the depth of burial of heat sources. Total radioactivity equals that of chondrites. The initial temperature is 600° C.

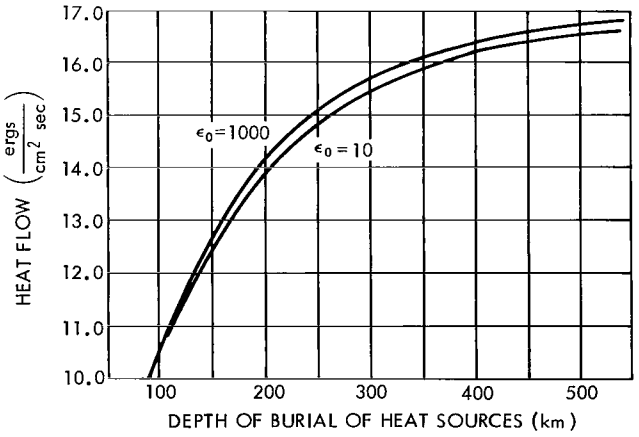

Figure 16—Dependence of the surface heat flow on the depth of burial of heat sources. Total radioactivity equals that of chondrites. The initial temperature is 1200°C.

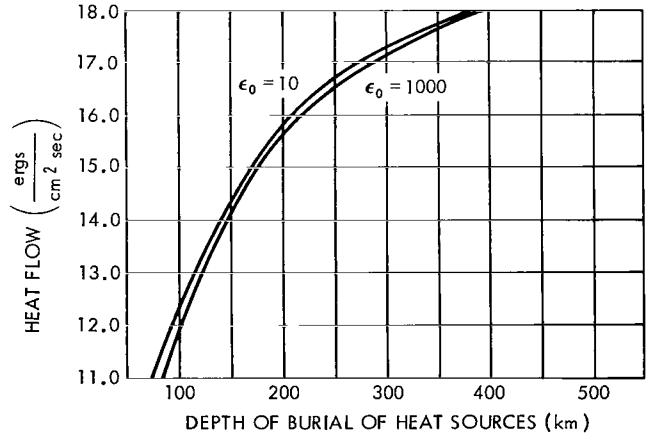

Figure 17—Dependence of surface heat flow on the depth of burial of heat sources. Total radioactivity equals that of chondrites. Initial temperature is the temperature along the diopside melting curve shown in Figure 11.

is shown in Figure 18 for two initial temperature distributions. In these models the radioactivity is assumed to be uniformly distributed throughout the moon.

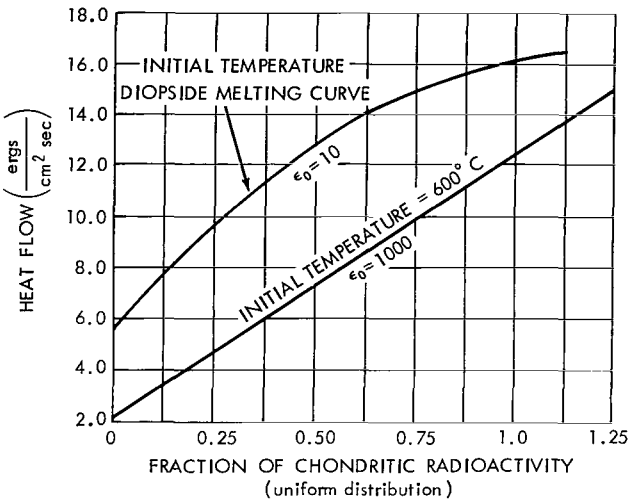

Figure 18—Variation of surface heat flow with total radioactivity.

The hypothesis that the moon is differentiated provides a solution to the discrepancy between its figure and the inferred high temperature of a moon of chondritic composition. There is no evidence in the astronomical data that the moon is indeed differentiated but the orbital data are not conclusive. The alternative supposition is that the radioactive element composition of the moon differs from that of meteorites. This hypothesis is strengthened by the fact that the density of the moon is appreciably less than the density of chondritic materials. The data on the moon can perhaps best be interpreted in terms of a heavy element composition like that of the solar atmosphere. This would explain the present density of the moon (Reference 84). Further, the potassium content in the solar atmosphere is about a quarter that of the chondritic meteorites through this value is very uncertain. If the potassium content were indeed so low, and if the uranium and thorium were similarly reduced, then the radioactivity would be low enough to permit a chemically uniform moon without melting.

Chapter 8

INTERNAL STRUCTURE OF MARS

The mass of Mars is well determined from the orbital constants of the satellites Phobos and Deimos. Its density is uncertain because the diameter is disputed. The orbital constants for Phobos and Deimos also provide an accurate value of $(C - A)/Ma^2$. This ratio can be used to estimate the moment of inertia C, if hydrostatic equilibrium is assumed. One problem is then to construct such a model of the density distribution within the planet that the variation of density yields the observed mass and moment of inertia. Since there is no definitive value for the radius, the problem is unsolved and there are a number of possible models of the density distribution within Mars.

THE GRAVITATIONAL POTENTIAL OF MARS

Urey has discussed the difficult problem of obtaining the radius of the solid surface of Mars (Reference 1). Rabe obtained a value of 3415 km (Reference 94); this value is usually accepted as the correct visual radius. Later workers have shown that Mars exhibits a different radius for light at different wavelengths. Trumpler found that the radius in yellow light is 3310 km and obtained a value agreeing with that of Rabe for white light (Reference 95). Dollfus arrived at a value 25 km greater (Reference 96). Camichel, in a detailed study, obtained results which appear to confirm Trumpler's value (Reference 97). Table 21 lists values for the radius and mean density of Mars obtained by the principal investigators. Though it appears that Trumpler's smaller radius value has been confirmed and is now generally accepted, we will show that it leads to difficulties in constructing a density-thermal model for Mars.

From Trumpler's value for the radius and Woolard's study of the motion of Phobos (Reference 98), we obtain

$$J_2 \cdot \frac{C - A}{Ma^2} = 0.00203 .$$

This value is obtained from observed quantities and does not depend on any assumptions regarding the attainment of hydrostatic equilibrium within the planet. By assuming the planet is in hydrostatic equilibrium it is possible to arrive at a value for the flattening, f (see Equation 6), and, from the flattening,

Table 21

Radius and Mean Density of Mars.

Source	Radius (km)	Mean Density (gm/cm^3)
Rabe (Reference 94)	3415	3.84
Trumpler (Reference 95)	3310	4.21
Dollfus (Reference 96)	3335	4.12

a value for C/Ma^2 (see Equation 4). The hydrostatic flattening for Mars is 0.0052. It should be emphasized that this value is not the observed flattening, but rather the flattening calculated from J_2 with the assumption that the interior of Mars is in hydrostatic equilibrium.

In the earth the difference, ΔJ_2, between the observed value of 1.0823×10^{-3} and the hydrostatic value of 1.0711×10^{-3} requires that stress differences on the order of ten bars or greater are supported within the interior of the planet. The difference between the moon's radii as found from its dynamical effects is about 1.8 km and hardly any of it is explained by the hydrostatic hypothesis; it must be supported by the strength of the interior. The true value of the flattening of Mars may also differ from the hydrostatic value. In the earth the fractional difference between the observed and the theoretical flattening is

$$\frac{\Delta f}{f} = 0.0053 \ . \tag{43}$$

Similar or even somewhat larger differences might be expected on Mars. On the earth the actual flattening is greater than the hydrostatic value and this has been interpreted to result from the secular deceleration of the earth (see Chapter 2 and References 19 and 24). For Mars the rate of rotational deceleration due to tidal interaction with Phobos is far less than for the earth. Nonetheless, we would expect the hydrostatic flattening on Mars to be less than the observed flattening. Percentage deviation can be larger on Mars since the maximum stress differences are proportional to gravity and gravity on Mars is about 0.38 that on the earth. On Mars $\Delta f/f$ might be on the order of 0.01 to 0.03 but probably is not much larger. The range of acceptable values of f is then about 0.005 to 0.0055. A much larger or much smaller value would lead to stress differences on the order of hundreds of bars rather than tens of bars and it is unlikely that any silicate material can support these stress differences for long periods of time.

DENSITY DISTRIBUTION WITHIN MARS

The construction of a density model for Mars requires the assumption of a surface density and a law of variation of density with pressure. To meet the requirements due to the total mass and J_2, an additional degree of freedom is necessary. Jeffreys suggested a chemically distinct core (Reference 10). The free parameter to be determined for a given surface density is the core radius. In addition, the laboratory data and the interpretation of the structure of the earth's mantle suggest that phase transitions and major changes in density take place in silicates at pressures on the order of 1.0×10^5-1.5×10^5 bars.

MacDonald has carried out detailed calculations on possible density distributions for Mars, assuming that the equation of state for the material is that for the material in the earth's mantle (Reference 99). If a lower value for the radius of Mars is adopted, it would appear that the only model consistent with the dynamically obtained value of J_2 is one in which the surface density is large, about 3.8-4.0, and in which there is no large scale chemical inhomogeneity in the form of an inner metallic core. The indicated density is large compared with the density of the moon and chondrites.

If the Trumpler value for the radius of Mars is adopted then the chemical composition of Mars must differ significantly from the chemical composition of the moon. An alternative possibility is that the outer radius is somewhat larger. In this case, the surface density of about 3.5 coupled with phase transitions would lead to an acceptable value of J_2. In such a model there could be a small core although its mass would be 1 percent or less that of the total body. The composition of Mars would then differ from the presumed chondritic composition of the earth in which the core contains 31 percent of the total mass of the earth. Possible density models are shown in Figures 19 and 20. An additional restriction is introduced by the fact that Mars has an observable atmosphere. The atmosphere implies that the planet has undergone some sort of differentiation.

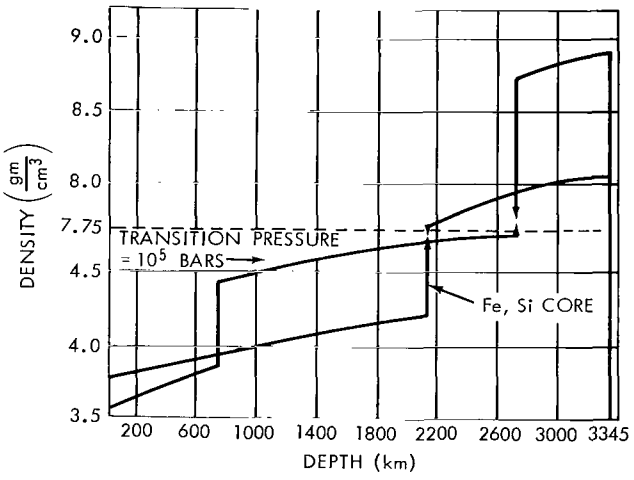

Figure 19—Density models for Mars with an outer radius of 3345 km and a flattening of 5×10^{-3}. In one model phase transition takes place at a pressure of 10^5 bars and there is a relative change in volume of 15 percent. In the other model no phase transition is assumed. The mass of the chemically distinct core is 0.01 of the total mass in the phase transition model and 0.093 of the total mass in the other model.

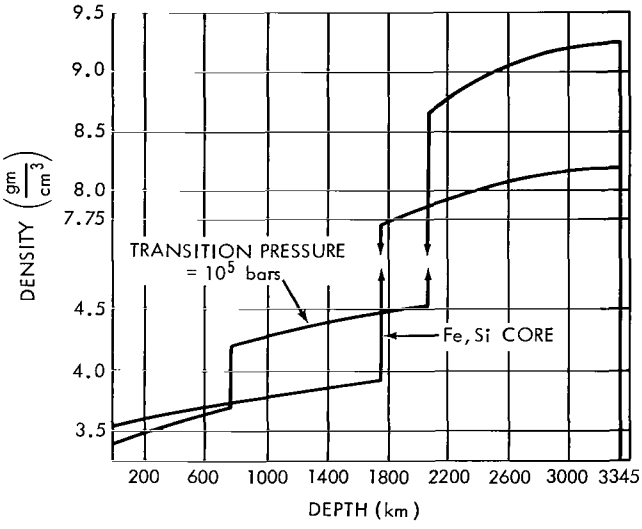

Figure 20—Density models for Mars with an outer radius of 3345 km and a flattening of 4.70×10^{-3}. In one model phase transition takes place at a pressure of 10^5 bars and there is a relative change in volume of 15 percent. In the other model no phase transition is assumed. The mass of the core is 0.117 of the total mass in the phase transition model and 0.20 of the total mass in the other model.

THERMAL CONSTITUTION OF MARS

Detailed calculations have been carried out on the possible temperature distribution within Mars under the assumption that the composition is chondritic. These calculations are illustrated in Figures 21-24 for the parameters listed in Tables 22 and 23. The outstanding feature of the temperature distribution is that if a chondritic radioactivity is assumed then the temperature exceeds the melting temperature of iron at shallow depths. Chondrites are about 12 percent metallic iron. If Mars were indeed of chondritic composition, the radioactivity would lead to the melting of the iron, and the iron would gravitationally differentiate to form a core composed of about 10 percent of the total mass of the planet. Such a core is too large for the observed value of J_2, if the outer radius is 3313 km.

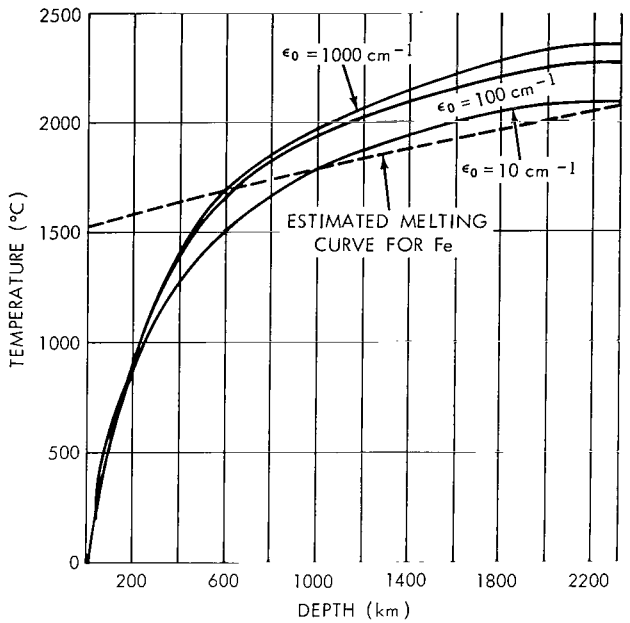

Figure 21–Calculated temperature distribution in Mars I model (uniform chondritic radioactivity). The detailed parameters are given in Table 22.

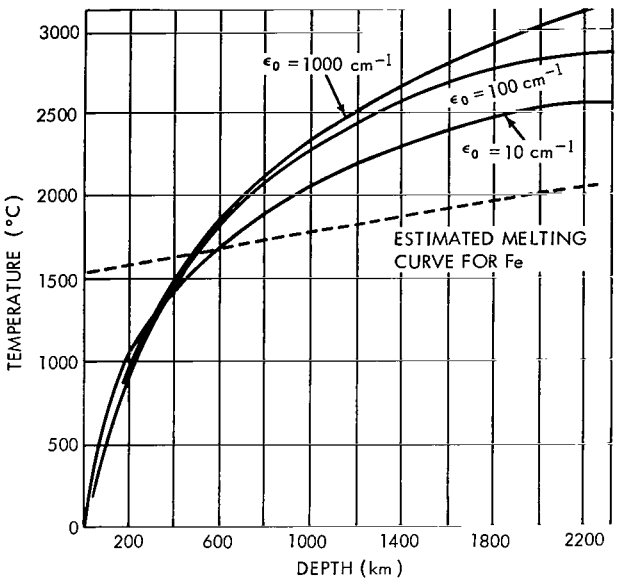

Figure 22–Calculated temperature distribution in Mars II model (uniform chondritic radioactivity and an initial temperature twice as high as the model shown in in Figure 19). The parameters are shown in Table 23.

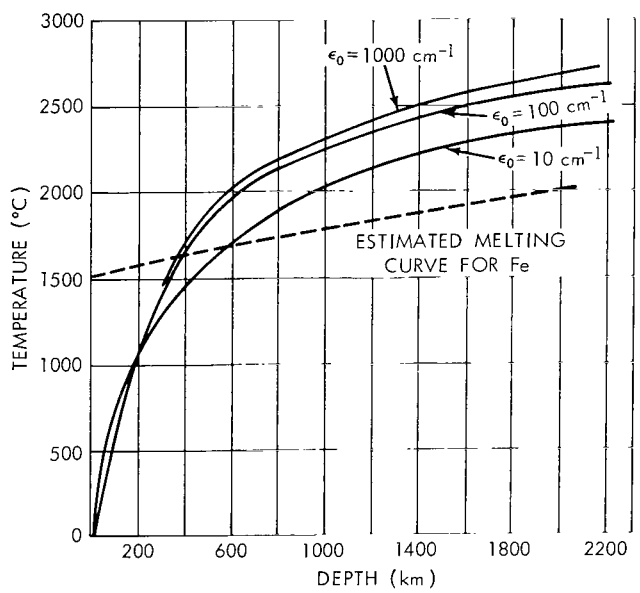

Figure 23–Calculated thermal distribution in Mars III model (radioactivity concentrated in the outer two thirds of the planet). Detailed parameters are given in Table 22.

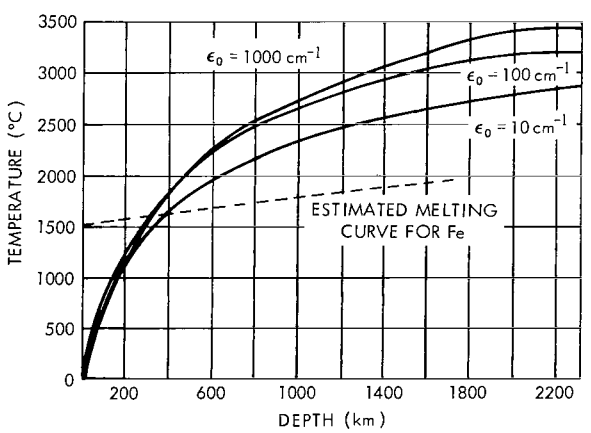

Figure 24–Calculated thermal distribution in Mars IV, the model for the thermal parameters listed in Table 23. The model is similar to that shown in Figure 23 but the initial temperature is twice as high.

The solution to the problem of the internal constitution of Mars awaits a definitive value for the radius of the solid body. From consideration of the mass and J_2 it would appear that the heavy element composition of Mars differs significantly from that of the moon and of the earth. The thermal calculations suggest a radioactivity substantially lower than that in chondrites.

Table 22

Thermal Parameters for Mars Models I and III
(Figures 21 and 23, Respectively).

Depth (km)	Initial Temperature (°C)	
0	-39	
330	100	
1040	400	
1750	700	
2000	800	
2300	910	
Radius	3313 km	
Surface Temperature (constant in time)	-39°C	
Radioactive Element Concentration (gm/gm)	Mars I	Mars III
Uranium	1.1×10^{-8}	1.35×10^{-8}
Thorium	4.4×10^{-8}	5.40×10^{-8}
Potassium	8.0×10^{-4}	9.8×10^{-4}
Time of Integration	4.51×10^{9} yr	
Lattice Conductivity	$2.5 \times 10^{5} \frac{\text{ergs}}{\text{cm deg}}$	
Density (uniform)	$3.9 \frac{\text{gm}}{\text{cm}^3}$	
Heat Capacity	$1.46 \times 10^{7} \frac{\text{ergs}}{\text{gm deg}}$	
Final Surface Heat Flow $\left(\frac{\text{ergs}}{\text{cm}^2\,\text{sec}}\right)$	Mars I	Mars III
ϵ_0 = 10 cm	17.0	19.7
ϵ_0 = 100 cm	12.5	16.0
ϵ_0 = 1000 cm	12.0	15.0

Table 23

Thermal Parameters for Mars Models II and IV
(Figures 22 and 24, Respectively).

Depth (km)	Initial Temperature (°C)	
0	-39	
330	200	
1040	800	
1750	1400	
2000	1600	
2300	1820	
Radius	3313 km	
Surface Temperature (constant in time)	-39°C	
Radioactive Element Concentration (gm/gm)	Mars II	Mars IV
Uranium	1.1×10^{-8}	1.35×10^{-8}
Thorium	4.4×10^{-8}	5.40×10^{-8}
Potassium	8.0×10^{-4}	9.80×10^{-4}
Time of Integration	4.51×10^{9} yr	
Lattice Conductivity	$2.5 \times 10^{5} \frac{\text{ergs}}{\text{cm sec deg}}$	
Density (uniform)	$3.9 \frac{\text{gm}}{\text{cm}^3}$	
Heat Capacity	$1.46 \times 10^{7} \frac{\text{ergs}}{\text{gm deg}}$	
Final Surface Heat Flow $\left(\frac{\text{ergs}}{\text{cm}^2 \text{ sec}}\right)$	Mars II	Mars IV
$\epsilon_0 = 10$ cm^{-1}	19.3	23.5
$\epsilon_0 = 100$ cm^{-1}	14.2	17.6
$\epsilon_0 = 1000$ cm^{-1}	13.3	16.1

Chapter 9

ROTATION OF THE PLANETS AND THE THERMAL STRUCTURE OF VENUS AND MERCURY

The rates of rotation of Mercury and Venus indirectly provide information about the thermal conditions within these planets. The argument is based on the observations that the rates of rotation of six of the planets are remarkably similar despite major differences in their orbital characteristics, masses, and moments of inertia (see Table 24). Mercury, Venus, and Pluto have exceptionally low rates of rotation. Little is known of the possible dynamical history of Pluto and, since it may have been a satellite of Neptune at one time, it will not be considered further. Mercury's rate of rotation is uncertain but available evidence indicates a period equal to the orbital period (Reference 100). The angular velocity of Venus is not known, but both spectroscopic and preliminary radar studies suggest that the rotational period is much longer than that of the earth (Reference 101).

Table 24

Rotation of the Planets.

Planet	Period (sec)	Mean Angular Velocity (radians/sec)
Mercury (Reference 100)	7.6×10^{6}	8.3×10^{-7}
Venus	–	–
Earth	8.616409×10^{4}	7.292115×10^{-5}
Mars (Reference 102)	8.86427×10^{4}	7.088×10^{-5}
Jupiter (Reference 103)	$3.54 \times 10^{4} - 3.57 \times 10^{4}$	1.77×10^{-4}
Saturn (Reference 104)	$3.68 \times 10^{4} - 3.83 \times 10^{4}$	1.67×10^{-4}
Uranus (Reference 100)	3.85×10^{4}	1.63×10^{-4}
Neptune (Reference 105)	4.58×10^{4}	1.37×10^{-4}
Pluto (Reference 106)	5.5×10^{5}	1.14×10^{-5}

ROTATION OF VENUS AND MERCURY

We will suppose that the *initial* angular velocity of rotation of Mercury and Venus equaled the *present* angular velocity of the major planets (a period in the order of 10 hours). On this hypothesis Mercury and Venus attained their present angular velocities through tidal interaction with the sun. Jeffreys has shown that the rate of change of the angular velocity of rotation should be proportional

to the product of the sixth power of the planet's apparent diameter (seen from the sun) and $\sin \epsilon$, where ϵ is the phase lag of the solar tide (Reference 20). The rate of change of angular velocity of Venus due to solar tidal interaction is about 7 times as great as that of the earth, provided the phase lag on Venus equals the phase lag on the earth. With equal phase lags, the present rate of deceleration of Venus would nearly equal that of the earth under the combined influences of the moon and the sun. The tidal deceleration of the earth due to the moon was greater in the past because of the closer approach of the moon. If the initial angular velocity of Venus were of the same order as that of the earth and if the internal properties of the two planets were similar, then the present angular velocity of Venus should be greater than that of the earth.

The apparent discrepancy can be resolved if it is assumed that the tidal dissipation takes place within the body of the planet and if anelastic dissipation in Venus is substantially greater than in the earth. In the earth, anelastic dissipation within the mantle is mainly due to solid friction (References 24 and 80). At temperatures near or at the melting temperature other mechanisms (e.g., creep, elastoviscosity) may become dominant. If there were large regions within the interior of Venus at or near the melting point, then tidal dissipation would be greater than in the earth. A mixture of molten and solid silicates would be particularly effective in dissipation since the energy loss would be through direct viscous interaction.

The observed angular velocity of Venus may be explained by supposing that temperatures within the depths of the planet surpass the melting point over considerable regions. It appears likely that in the earth the temperature comes closest to the melting temperature at a depth on the order of 100 to 200 km, but below this the temperatures may well be below the fusion temperature. Pressure at a given depth in Venus is probably only a few percent less than the pressure at the same depth within the earth. The melting temperature of silicates at a given depth in Venus will be approximately equal to the corresponding melting temperature within the earth.

If the concentration of heat-producing radioactive elements in Venus is similar to that in the earth, the actual temperature at a given depth in Venus should be higher than in the earth. Extensive observations show that the microwave emission spectrum of Venus is flat between 3 and 21 cm, corresponding to a brightness temperature of 600° K (Reference 107). If this high surface temperature has been maintained for an appreciable fraction of the history of the planet, then the internal thermal conditions have been affected in a major way. The higher surface temperature on Venus implies that the temperature in Venus would be higher than at the same depth in the earth.

A possible thermal structure within Venus is illustrated in Figures 25 and 26. The basic data for these models are given in Table 25. In Venus I the initial temperature (4.51×10^9 years ago) is taken as 1000° C, in Venus II it is 500° C. Three values of the opacity have been investigated. The range of ϵ_0 of 10 to 1000 cm^{-1} covers the values observed in silicates (see Chapter 5). The temperature at a depth of some 200 km is about 200° C higher than the temperature at the same depth for a similar thermal model of the earth. The variation of the melting temperature in silicates at these depths is uncertain, but the indicated temperatures are undoubtedly well above the melting temperature of common silicate materials.

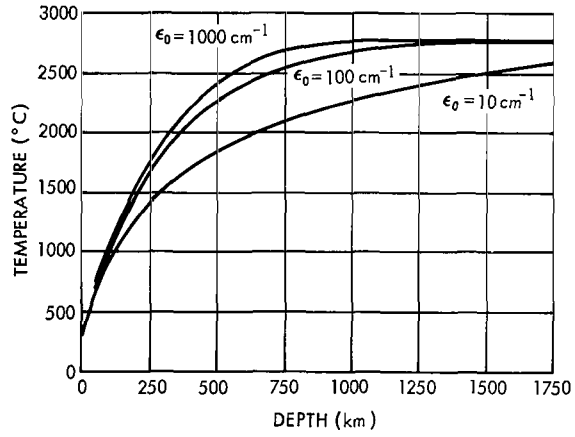

Figure 25–Calculated temperature distribution in the Venus I model (initial temperature of 1000°C). Chondritic radioactivity is assumed to be uniformly distributed. The detailed thermal parameters are listed in Table 25.

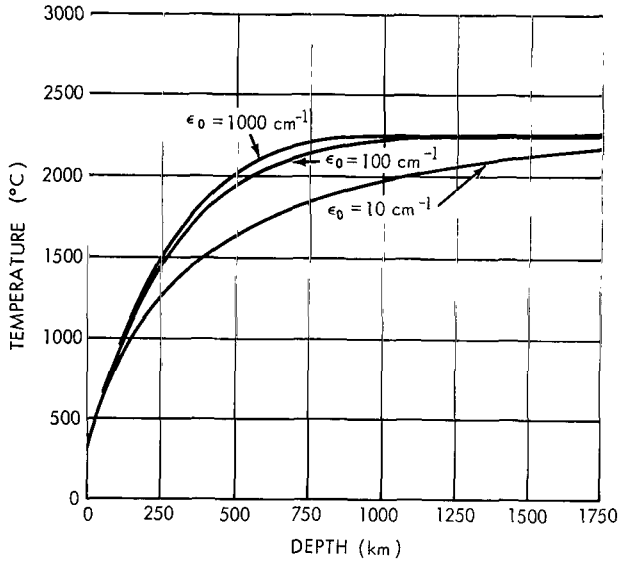

Figure 26–Calculated temperature distribution in the Venus II model (initial temperature of 500°C). Chondritic radioactivity is assumed to be uniformly distributed. The detailed thermal parameters are listed in Table 25.

Table 25

Thermal Parameters for Venus Models I and II (Figures 25 and 26, Respectively).

Initial Temperature (uniform)	Venus I - 1000°C; Venus II - 500°C
Surface Temperature (constant in time)	300°C
Radioactive Element Concentration (uniform, gm/gm)	
Uranium	1.1×10^{-8}
Thorium	4.4×10^{-8}
Potassium	8.0×10^{-4}
Time of Integration	4.51×10^{9} yr
Lattice Conductivity	$2.5 \times 10^{5}\ \frac{ergs}{cm\ sec\ deg}$
Density (uniform)	$4.0\ \frac{gm}{cm^3}$
Heat Capacity	$1.3 \times 10^{7}\ \frac{ergs}{gm\ deg}$

Final Surface Heat Flow $\left(\frac{ergs}{cm^2\ sec}\right)$	Venus I	Venus II
$\epsilon_0 = 10\ cm^{-1}$	17.2	14.4
$\epsilon_0 = 100\ cm^{-1}$	17.7	14.6
$\epsilon_0 = 1000\ cm^{-1}$	16.7	14.0

The inferred low rate of rotation of Venus is compatible with a model in which a substantial fraction of the planet is at or near the melting point. The high surface temperature combined with a radioactive composition equal to that of chondritic meteorites would provide a consistent model. Although evidence is sketchy, present data are consistent with the hypothesis that the radioactive chemical composition of Venus and the earth are similar but that the high surface temperature of Venus has raised the temperature within the planet above the melting point of the silicates.

Inferences regarding the internal structure of Mercury are even more uncertain. The solar tide acting on Mercury is about 50 times more effective than the combined lunar and solar tides acting on the earth, provided that the phase lag is the same. If Mercury had an initial angular velocity similar to that of the *present-day* earth, then the time required to reduce its rate of rotation to the present value is much too long if its anelasticity is equal to that of the earth. On the hypothesis of an *initial* angular velocity *equal* to that of the earth, we would require either: (1) that Mercury was initially molten and during this early time its periods of rotation and revolution were equalized by solar tidal friction; or (2) that the present thermal state of Mercury is such that it allows much greater dissipation of energy in it than in the earth. The thermal conditions within Mercury are most uncertain. The mean density makes it unlikely that the radioactive composition of Mercury is similar to that of chondrites. Indeed, it would seem that Mercury is largely metallic, and if this is the case then a lower concentration of radioactive elements is indicated. Since the effect of pressure on the melting point is far less in a planet the size of Mercury than in larger bodies such as Venus and the earth, a lower concentration of radioactive elements (one half to one third) would still melt the small body or make it largely molten.

REFERENCES

1. Urey, H. C., "The Planets; Their Origin and Development," New Haven: Yale University Press, 1952.
2. Alfvén, H., "On the Origin of the Solar System," Oxford: Clarendon Press, 1954.
3. Lüst, R., and Schlüter, A., "Drehimpulstransport durch Magnetfelder und die Abbremsung Rotierender Sterne," *Zeitschrift Astrophysik* 38(3):190-211, December 12, 1955.
4. Hoyle, F., "On the Origin of the Solar Nebula," *Quart. J. Roy. Astronom. Soc.* 1(1):28-55, September 1960.
5. Cameron, A. G. W., "The Formation of the Sun and Planets," *Icarus* 1(1):13-69, May 1962.
6. Fowler, W. A., Greenstein, J. L., and Hoyle, F., "Nucleosynthesis During the Early History of the Solar System," *Geophys. J.* 6(2):148-220, February 1962.
7. Reynolds, J. H., "Determination of the Age of the Elements," *Phys. Rev. Letters* 4(1):8-10, January 1, 1960.
8. Reynolds, J. H., "Isotopic Composition of Primordial Xenon," *Phys. Rev. Letters* 4(7):351-354, April 1, 1960.
9. Reynolds, J. H., "I-Xe Dating of Meteorites," *J. Geophys. Res.* 65(11):3843-3846, November 1960.
10. Jeffreys, H., "The Density Distributions in the Inner Planets," *Monthly Not. Roy. Astronom. Soc., Geophys. Suppl.* 4(1):62-71, January 1937.
11. O'Keefe, J. A., Eckels, A., and Squires, R. K., "The Gravitational Field of the Earth," *Astronom. J.* 64(1272):245-253, September 1959.
12. Kozai, Y., "The Gravitational Field of the Earth Derived from Motions of Three Satellites," *Astronom. J.* 66(1286):8-10, February 1961.
13. King-Hele, D. G., "The Earth's Gravitational Potential, Deduced from the Orbits of Artificial Satellites," *Geophys. J.* 4:3-16, 1961.
14. Kaula, W. M., "Celestial Geodesy," NASA Technical Note D-1155, March 1962; also in: *Advances in Geophysics*, ed. by H. E. Landsberg and J. Van Mieghem, New York: Academic Press, 1962, Vol. 9, pp. 191-293 (In Press).
15. King-Hele, D. G., "The Earth's Gravitational Potential, Deduced from the Orbits of Artificial Satellites," *Geophys. J.* 6(2):270-272, February 1962.
16. Newton, R. R., "Ellipticity of the Equator Deduced from the Motion of Transit 4A," *J. Geophys. Res.* 67(1):415-416, January 1962.
17. Henriksen, S. K., "The Hydrostatic Flattening of the Earth," in: *Annals Internat. Geophys. Yr.*, New York: Pergamon Press, 1960, Vol. 12, Pt. 1, pp. 197-198.
18. O'Keefe, J. A., "Zonal Harmonics of the Earth's Gravitational Field and the Basic Hypothesis of Geodesy," *J. Geophys. Res.* 64(12):2389-2392, December 1959.

19. Munk, W. H., and MacDonald, G. J. F., "Continentality and the Gravitational Field of the Earth," *J. Geophys. Res.* 65(7):2169-2172, July 1960.

20. Jeffreys, H., "The Earth: Its Origin, History and Physical Constitution," 4th Ed., Cambridge: University Press, 1959.

21. Vening Meinesz, F. A., "Continental and Ocean-Floor Topography; Mantle-Convection Currents," *Proc. K. Nederlandse Akademie van Wetenschappen* 63B(4):410-421, 1960.

22. Vacquier, V., Raff, A. D., and Warren, R. E., "Horizontal Displacements in the Floor of the Northeastern Pacific Ocean," *Bull. Geol. Soc. Amer.* 72(8):1251-1258, August 1961.

23. Bullard, E. C., "The Figure of the Earth," *Monthly Not. Roy. Astronom. Soc., Geophys. Suppl.* 5(6):186-192, January 1948.

24. Munk, W. H., and MacDonald, G. J. F., "The Rotation of the Earth," Cambridge: University Press, 1960.

25. Haskell, N. A., "The Motion of a Viscous Fluid Under a Surface Load," *Physics* 6(8):265-269, August 1935.

26. Haskell, N. A., "The Motion of a Viscous Fluid Under a Surface Load. Part 2," *Physics* 7(2):56-61, February 1936.

27. Lyustikh, E. N., "Isostasy and Isostatic Hypotheses," *Trudy Geologicheskogo Instituta, Akademiya Nauk SSSR* No. 38 (165) 1957 (In Russian).

28. Chandler, S., "On the Variation of Latitude," *Astronom. J.* 11(251):83-86, December 23, 1891.

29. Jeffreys, H., and Jeffreys, B., "Methods of Mathematical Physics," 3rd Ed., Cambridge: University Press, 1956.

30. Jeffreys, H., and Vicente, R. O., "The Theory of Nutation and the Variation of Latitude," *Monthly Not. Roy. Astronom. Soc.* 117(2):142-161, 1957.

31. Bondi, H., and Gold, T., "On the Damping of the Free Nutation of the Earth," *Monthly Not. Roy. Astronom. Soc.* 115(1):41-46, 1955.

32. Munk, W., and Hassan, E. S. M., "Atmospheric Excitation of the Earth's Wobble," *Geophys. J.* 4:339-358, 1961.

33. Takeuchi, H., Saito, M., and Kobayashi, N., "Statical Deformations and Free Oscillations of a Model Earth," *J. Geophys. Res.* 67(3):1141-1154, March 1962.

34. Bullen, K. E., "An Introduction to the Theory of Seismology," 2nd Ed., Cambridge: Univ. Press, 1953.

35. Gutenberg, B., "Physics of the Earth's Interior," New York: Academic Press, 1959.

36. Benioff, H., Press, F., and Smith, S., "Excitation of the Free Oscillations of the Earth by Earthquakes," *J. Geophys. Res.* 66(2):605-619, February 1961.

37. Alsop, L. E., Sutton, G. H., and Ewing, M., "Free Oscillations of the Earth Observed on Strain and Pendulum Seismographs," *J. Geophys. Res.* 66(2):631-641, February 1961.

38. Pekeris, C. L., Alterman, Z., and Jarosch, H., "Comparison of Theoretical with Observed Values of the Periods of Free Oscillation of the Earth," *Proc. Nat. Acad. Sci.* 47(1):91-98, January 1961.

39. Ness, N. F., Harrison, J. C., and Slichter, L. B., "Observations of the Free Oscillations of the Earth," *J. Geophys. Res.* 66(2):621-629, February 1961.

40. MacDonald, G. J. F., "The Earth's Free Oscillations," NASA Technical Note D-1336, June 1962; also *Science* 134(3491):1663-1668, November 24, 1961.

41. Backus, G., and Gilbert, F., "The Rotational Splitting of the Free Oscillations of the Earth," *Proc. Nat. Acad. Sci.* 47(3):362-371, March 1961.

42. MacDonald, G. J. F., and Ness, N. F., "A Study of the Free Oscillations of the Earth," NASA Technical Report R-136, 1962; also *J. Geophys. Res.* 66(6):1865-1911, June 1961.

43. Gerling, E. K., and Polkanov, A. A., "The Absolute Age Determination of the Precambrian of the Baltic Shield," *Geokhimiya* No. 8:695-717, 1958; Translation in *Geochemistry* No. 8:867-896, 1958.

44. Russell, R. D., and Farquhar, R. M., "Lead Isotopes in Geology," New York: Interscience, 1960.

45. Murthy, V. R., and Patterson, C. C., "Primary Isochron of Zero Age for Meteorites and the Earth," *J. Geophys. Res.* 67(3):1161-1167, March 1962.

46. Patterson, C., "Age of Meteorites and the Earth," *Geochim. et Cosmochim. Acta* 10(4):230-237, October 1956.

47. Birch, F., "The Present State of Geothermal Investigations," *Geophysics* 19(4):645-659, October 1954.

48. Von Herzen, R., "Heat-Flow Values from the South-Eastern Pacific," *Nature* 183(4665):882-883, March 28, 1959.

49. Birch, F., and Clark, H., "The Thermal Conductivity of Rocks and its Dependence Upon Temperature and Composition," *Amer. J. Sci.* 238(8):529-558, August 1940; 238(9):613-635, September 1940.

50. Clark, S. P., Jr., and Niblett, E. R., "Terrestrial Heat Flow in the Swiss Alps," *Monthly Not. Roy. Astronom. Soc., Geophys. Suppl.* 7(4):176-195, August 1956.

51. Birch, F., "Flow of Heat in the Front Range, Colorado," *Bull. Geol. Soc. Amer.* 61(6):567-630, June 1950.

52. Clark, S. P., Jr., "Absorption Spectra of Some Silicates in the Visible and Near Infrared," *Amer. Mineralogist* 42(11-12):732-742, November-December 1957.

53. Boyd, F. R., and England, J. L., "Effect of Pressure on the Melting of Diopside and Albite," *J. Geophys. Res.* 67(9):3544, August 1962 (Abstract).

54. Carslaw, H. S., and Jaeger, J. C., "Conduction of Heat in Solids," 2nd Ed., Oxford: Clarendon Press, 1959.

55. Lubimova, H. A., "Thermal History of the Earth With Consideration of the Variable Thermal Conductivity of its Mantle," *Geophys. J.* 1(2):115-134, June 1958.

56. MacDonald, G. J. F., "Calculations on the Thermal History of the Earth," *J. Geophys. Res.* 64(11):1967-2000, November 1959.

57. MacDonald, G. J. F., "Surface Heat Flow from a Differentiated Earth," *J. Geophys. Res.* 66(8):2489-2493, August 1961.

58. Jeffreys, H., "The Structure of the Earth Down to the 20° Discontinuity," *Monthly Not. Roy. Astronom. Soc., Geophys. Suppl.* 3(9):401-422, April 1936.

59. Roy, D. M., and Roy, R., "An Experimental Study of the Formation and Properties of Synthetic Serpentines and Related Layer Silicate Minerals," *Amer. Mineralogist* 39(11-12):957-975, November-December 1954.

60. Bragg, W. L., "Atomic Structure of Minerals," Ithaca, N. Y.: Cornell University Press, 1937.

61. Dachille, F., and Roy, R., "High Pressure Studies of the System Mg_2GeO_4-Mg_2SiO_4 with Special Reference to the Olivine-Spinel Transition," *Amer. J. Sci.* 258(4):225-246, April 1960.

62. Dachille, F., and Roy, R., "System Mg_2SiO_4-Mg_2GeO_4 at 10,000, 60,000 and about 300,000 psi," *Bull. Geol. Soc. Amer.* 67(12, pt. 2):1682-1683, December 1956 (Abstract).

63. Dachille, F., and Roy, R., "Experimental Study of the Olivine-Spinel Inversion in Mg_2SiO_4," *Bull. Geol. Soc. Amer.* 69(12, pt. 2):1550, December 1958 (Abstract).

64. Ringwood, A. E., "The System Mg_2SiO_4-Mg_2GeO_4," *Amer. J. Sci.* 254(11):707-711, November 1956.

65. Ringwood, A. E., "The Constitution of the Mantle-II. Further Data on the Olivine-Spinel Transition," *Geochim. et Cosmochim. Acta* 15(1/2):18-29, 1958.

66. Ringwood, A. E., "Olivine-Spinel Transition in Fayalite," *Bull. Geol. Soc. Amer.* 69(1):129, January 1958.

67. Birch, F., "Elasticity and Constitution of the Earth's Interior," *J. Geophys. Res.* 57(2):227-286, June 1952.

68. MacDonald, G. J. F., "Quartz-Coesite Stability Relations at High Temperatures and Pressures," *Amer. J. Sci.* 254(12):713-721, December 1956.

69. Boyd, F. R., and England, J. L., "The Quartz-Coesite Transition," *J. Geophys. Res.* 65(2):749-756, February 1960.

70. Zoltai, T., and Buerger, M. S., "The Crystal Structure of Coesite, the Dense, High-Pressure Form of Silica," *Zeitschrift für Kristallographie* 111(2):129-141, February 1959.

71. Stishov, S. M., and Popova, S. V., "A New Dense Modification of Silica," *Geokhimiya* No. 10:837-839, 1961; Translation in *Geochemistry* No. 10:923-926, 1961.

72. Chao, E. C. T., Fahey, J. J., et al., "Stishovite, SiO_2, a Very High Pressure New Mineral from Meteor Crater, Arizona," *J. Geophys. Res.* 67(1):419-421, January 1962.

73. Kennedy, G. C., and LaMori, P. N., "Some Fixed Points on the High Pressure Scale," in: *Progress in Very High Pressure Research: Proc. Internat. Conf., Bolton Landing, New York, June 1960,* ed. by F. P. Bundy, W. R. Hibbard, Jr., and H. M. Strong, New York: Wiley, 1961, pp. 304-313.

74. MacDonald, G. J. F., "A Critical Review of Geologically Important Thermochemical Data," Doctoral Dissertation, Harvard University, 1954.

75. King, E. G., "Heats of Formation of Manganous Metasilicate (Rhodonite) and Ferrous Orthosilicate (Fayalite)," *J. Amer. Chem. Soc.* 74(17):4446-4448, September 5, 1952.

76. Kuhn, W., and Rittmann, A., "Über den Zustand des Erdinnern und seine Entstehung aus einem Homogenen Urzustand," *Geologische Rundschau* 32(3):215-256, August 25, 1941.

77. Ramsey, W. H., "On the Constitution of the Terrestrial Planets," *Monthly Not. Roy. Astronom. Soc.* 108(5):406-413, 1948.

78. Ramsey, W. H., "On the Nature of the Earth's Core," *Monthly Not. Roy. Astronom. Soc., Geophys. Suppl.* 5(9):409-426, October 1949.

79. Ramsey, W. H., "The Planets and the White Dwarfs," *Monthly Not. Roy. Astronom. Soc.* 110(5):444-454, 1950.

80. Knopoff, L., and MacDonald, G. J. F., "An Equation of State for the Core of the Earth," *Geophys. J.* 3(1):68-77, March 1960.

81. Birch, F., "Composition of the Earth's Mantle," *Geophys. J.* 4:295-311, 1961.

82. MacDonald, G. J. F., and Knopoff, L., "On the Chemical Composition of the Outer Core," *Geophys. J.* 1(4):284-297, December 1958.

83. Baldwin, J. E., "Thermal Radiation From the Moon and the Heat Flow Through the Lunar Surface," *Monthly Not. Roy. Astronom. Soc.* 122(6):513-522, 1961.

84. Urey, H. C., "Lines of Evidence in Regard to the Composition of the Moon," in: *Space Research: Proc. 1st Internat. Space Sci. Sympos., Nice, January 1960,* ed. by H. K. Bijl, Amsterdam: North-Holland Publ. Co., 1960, pp. 1114-1122.

85. Urey, H. C., and Craig, H., "The Composition of the Stone Meteorites and the Origin of the Meteorites," *Geochim. et Cosmochim. Acta* 4(1/2):36-82, 1953.

86. Aller, L. H., "Solar and Stellar Abundances of the Elements," in: *Physics and Chemistry of the Earth,* ed. by L. H. Ahrens, F. Press, et al., London: Pergamon Press, 1961, Vol. 4, pp. 1-26.

87. Jeffreys, H., "On the Figure of the Moon," *Monthly Not. Roy. Astronom. Soc.* 122(5):421-432, 1961.

88. MacDonald, G. J. F., "Interior of the Moon," *Science* 133(3458):1045-1050, April 7, 1961.

89. Urey, H. C., Elsasser, W. M., and Rochester, M. G., "Note on the Internal Structure of the Moon," *Astrophys. J.* 129(3):842-848, May 1959.

90. Bolt, B. A., "Spheroidal Oscillations of the Moon," *Nature* 188(4757):1176-1177, December 31, 1960.

91. Takeuchi, H., Saito, M., and Kobayashi, N., "Free Oscillations of the Moon," *J. Geophys. Res.* 66(11):3895-3897, November 1961.

92. MacDonald, G. J. F., "Stress History of the Moon," *Planet. Space Sci.* 2(4):249-255, August 1960.

93. Urey, H. C., "Boundary Conditions for Theories of the Origin of the Solar System," in: *Physics and Chemistry of the Earth,* ed. by L. H. Ahrens, F. Press, et al., London: Pergamon Press, 1957, Vol. 2, pp. 46-76.

94. Rabe, W., "Untersuchungen über die Durchmesser der Grossen Planeten," *Astronomische Nachrichten* 234(5606):153-200, 1928.

95. Trumpler, R. J., "Observations of Mars at the Opposition of 1924," *Lick Observ. Bull.* 13(387):19-45, April 26, 1927.

96. Dollfus, A., "Un Micromètre à Double Image Permettant un Grand Dédoublement," *Comptes Rendus, Académie des Sciences* (Paris) 235(23):1477-1480, December 10, 1952.

97. Camichel, H., "Détermination Photographique du Pôle de Mars, de son Diamètre et des Coordonnées Aréographiques," *Bulletin Astronomique* 18(2):83-174, 1954.

98. Woolard, E. W., "The Secular Perturbations of the Satellites of Mars," *Astronom. J.* 51(1150):33-36, August 1944.

99. MacDonald, G. J. F., "On the Internal Constitution of the Inner Planets," *J. Geophys. Res.* 67(7):2945-2974, July 1962.

100. Russell, H. N., Dugan, R. S., and Stewart, J. Q., "Astronomy; a Revision of Young's Manual of Astronomy, Vol. I, The Solar System," Boston: Ginn and Co., 1945.

101. Victor, W. K., Stevens, R., and Golomb, S. W., (Ed.) "Radar Exploration of Venus: Goldstone Observatory Report for March-May 1961," Calif. Inst. Tech., Jet Propulsion Lab. Tech. Rept. No. 32-132, August 1, 1961.

102. Ashbrook, J., "A New Determination of the Rotation Period of the Planet Mars," *Astronom. J.* 58(1210):145-155, August 1953.

103. Peek, B. M., "The Planet Jupiter," New York: Macmillan, 1958.

104. Camichel, H., "Mesure de la Durée de Rotation de Saturne d'Après une Tache," *Bulletin Astronomique* 20(2):141-144, 1956.

105. Günther, O., "Der Rotationslichtwechsel des Neptun," *Astronomische Nachrichten* 282(1):1-14, 1955.

106. Walker, M. F., and Hardie, R., "A Photometric Determination of the Rotational Period of Pluto," *Publ. Astronom. Soc. Pacific* 67(397):224-231, August 1955.

107. Mayer, C. H., "Radio Emission of the Moon and Planets," in: *Planets and Satellites,* ed. by G. P. Kuiper and B. M. Middlehurst, Chicago: University of Chicago Press, 1961, pp. 442-472.

Appendix A

Detailed Analysis of the Free Oscillations

Elastic Vibrations of a Sphere

At frequencies for which the spectrum is recognizably discrete, the normal modes involve a major part of the earth. The characteristic length associated with these vibrations is large compared with the inhomogeneities of the continent-ocean system. Hence, it is customary to assume spherical symmetry for the earth. The earth is then defined by the radial functions determining the initial distribution of unperturbed density, $\rho(r)$, and the Lamé constants, $\mu(r)$ and $\lambda(r)$.

In the analysis of the free vibrations of the solid earth we first describe the equilibrium state and then superimpose on the static solution a perturbation velocity field v_i controlled by the elastic gravitational and rotational restoring forces. As we shall see, the rotational restoring forces can be treated as a perturbation, but for the low frequency vibrations the effect of gravity must be explicitly taken into account.

Consider a rotating isotropic solid. The equilibrium conditions, referred to a coordinate axis rotating at angular velocity Ω_j, are

$$\left.\begin{aligned} \text{grad } U &= -\frac{1}{\rho} \text{ grad } p \ , \\ U &= U_g(r) - \frac{1}{2} r^2 \Omega^2 \cos^2 \theta \ , \end{aligned}\right\} \tag{A1}$$

where p is the hydrostatic pressure and ρ is the density. The potential U is made up of two parts. $U_g(r)$ is the spherically symmetrical potential of the gravitational forces satisfying Poisson's equation,

$$\nabla^2 U_g = 4\pi G\rho \ . \tag{A2}$$

The second term in the equation for the total potential U is proportional to the square of the angular velocity Ω, and represents the cylindrically symmetrical centrifugal forces; r is the distance from the earth's center; θ is the latitude.

The surfaces, U = constant, are ellipsoids of revolution with the maximum ellipticity at the surface. An approximate representation of the equilibrium surface is

$$r = a\left[1 + \epsilon_T\left(\frac{1}{3} - \sin^2 \theta\right)\right], \tag{A3}$$

where ϵ_T is the hydrostatic value for the flattening of the ellipsoid. The theoretical value for the flattening of a body rotating at the angular velocity of the earth and also having the internal density distribution of the earth is 1/299.8. The observed value is 1/298.2 (Chapter 2). Thus the actual surface approximates the surface of hydrostatic equilibrium to within 2 parts in 300, and the surfaces of equilibrium deviate from spherical surfaces by only one part in 300 throughout the earth.

The free oscillations are studied by superimposing a small stress on the hydrostatic configuration described by Equations A1*. The total stress tensor, p_{ij}, at any point within the earth is the sum of a hydrostatic pressure $p\delta_{ij}$ and τ_{ij}, an elastic stress tensor measured from the initially compressed equilibrium state:

$$p_{ij} = -p\,\delta_{ij} + \tau_{ij} \quad . \tag{A4}$$

It is assumed that τ_{ij} is linearly related to the strain tensor ϵ_{ij} through the local elastic parameters. At any point the divergence of the elastic stress tensor is

$$\frac{\partial \tau_{ij}}{\partial x_j} = (\lambda + \mu)\frac{\partial^2 u_j}{\partial x_i\,\partial x_j} + \mu\frac{\partial^2 u_i}{\partial x_j{}^2} \quad , \tag{A5}$$

where λ and μ are the Lamé constants. The element u_1 is the displacement vector measured from the initial equilibrium stress state.

The equations of motion referred to a coordinate system fixed to the mean body are

$$\rho\frac{\partial^2 u_i}{\partial t^2} + 2\rho\,\epsilon_{ijk}\,\Omega_j\frac{\partial u_k}{\partial t} = -\rho\frac{\partial U}{\partial x_i} + \frac{\partial p_{ij}}{\partial x_j} \quad , \tag{A6}$$

provided that the ellipticity and the quadratic terms in the displacement are neglected. Neglecting the ellipticity implies that the initial pressure distribution, p_0, and initial density distribution, ρ_0, are spherically symmetrical functions of the radius. In addition, we will assume that the elastic constants are radial functions. The assumed spherical symmetry of the earth neglects the near-surface continent-ocean structure. The supposition is that the inhomogeneities of the near-surface material do not extend to great depths. The low frequency vibrations involve the earth as a whole and are not affected in any major way by surface inhomogeneities.

The equations of motion referred to a rotating system differ from the nonrotating case because of two terms involving the angular velocity. The total potential U includes a term varying as the square of the angular velocity. The smallness of the cylindrically symmetrical centrifugal force terms follows from

*Pekeris, C. L., Alterman, Z., and Jarosch, H., "Rotational Multiplets in the Spectrum of the Earth," *Phys. Rev.* 122(6):1692-1700, June 15, 1961. MacDonald, G. J. F., and Ness, N. F., "A Study of the Free Oscillations of the Earth," NASA Technical Report R-136, 1962; also *J. Geophys. Res.* 66(6):1865-1911, June 1961.

$$\left.\begin{aligned} \frac{\partial^2 U}{\partial x_1^2} &= 4\pi\epsilon\rho - 2\Omega^2 \quad , \\ \frac{2\Omega^2}{4\pi\epsilon\rho} &\approx \frac{1}{300} \quad . \end{aligned}\right\} \tag{A7}$$

The term involving the angular velocity of the left-hand side of Equation A6 is the Coriolos or gyroscopic force. Its effect is to couple motion along the various coordinate axes since the rotation deflects the oscillating particles. The rotational coupling introduces a complexity in the motion that is important in interpreting the detailed observations of the earth's free vibrations.

Assume a time variation of the displacement of

$$u_k = q_k e^{i\omega t} \quad , \tag{A8}$$

where q_k is a complex amplitude and ω, the angular frequency of vibration, assumes only discrete values. In terms of the complex amplitude the equations of motion are

$$-\omega^2 \rho q_k + 2i\omega\epsilon_{krs}\Omega_r q_s = -\rho\frac{\partial U}{\partial x_k} + \frac{\partial p_{kj}}{\partial x_j} \quad . \tag{A9}$$

The gyroscopic forces couple the motion along the coordinate axes and, in spherical coordinates, Equation A9 is not separable. However, the strength of the coupling depends upon the ratio of the angular velocity to the frequency of oscillation. A rough estimate of the period of the fundamental oscillation is provided by the ratio of the circumference to the average elastic wave velocity,

$$\frac{2\pi a}{\bar{V}} = \frac{2\pi(6.3 \times 10^8)}{8 \times 10^5} = 4 \times 10^3 \text{ sec} \quad . \tag{A10}$$

Thus the lowest order oscillation should have a period on the order of an hour. This frequency is an order of magnitude greater than 2Ω and we may suppose that the effect of the earth's rotation can be treated as a perturbation of the solution for a nonrotating earth. Let

$$\delta = \frac{\Omega}{\omega^0} \quad , \tag{A11}$$

where ω^0 is the frequency of oscillation in the absence of rotation. The perturbation expansions are

$$\left.\begin{aligned} q_k &= q_k{}^0 + \delta q_k{}^1 + \cdots \quad , \\ \omega &= \omega^0 (1 + \alpha\delta + \cdots) \quad , \end{aligned}\right\} \tag{A12}$$

where q_k^0 is the complex amplitude in the absence of rotation. Introducing Equations A12 into Equation A9 we note that the gyroscopic terms are of order δ whereas the centrifugal terms are of order δ^2. The term α in Equations A12 determines the magnitude of the frequency shift resulting from rotation. The equations of motion to zero and first order in δ are:

$$\left.\begin{aligned} &-\rho\,(\omega^0)^2\,q_k^0 + \rho\,\frac{\partial U^0}{\partial x_k} - \frac{\partial p_{kj}^0}{\partial x_j} = 0\,, \\ &-\rho\,(\omega^0)^2\,q_k^1 + \rho\,\frac{\partial U^1}{\partial x_k} - \frac{\partial p_{kj}}{\partial x_j} = -2\rho\,(\omega^0)^2\,\alpha q_k^0 + 2\rho i(\omega^0)^2\,\epsilon_{krs}\,z_r\,q_s^0\,, \\ &\Omega_j = \Omega z_j\,. \end{aligned}\right\} \qquad \text{(A13)}$$

The motion to zero order in δ is governed by elasticity, by the gravitational forces arising from the alteration of the density field by the motion, and by the attraction of the deformed interfaces. Equations A13 and A2 determine the displacement and the gravitational potential. These solutions are subject to the conditions that: (1) The solution is regular at the origin. (2) The stresses vanish on the deformed surface of the earth. (3) The internal and external gravitational potentials and their gradients are equal at the deformed external surface. In addition, the stress components must be continuous at any internal surface of discontinuity, as must the gradient of the gravitational potential.

The equations of motion are separable in spherical coordinates if rotation is neglected. A solution with spherical symmetry is:

$$\left.\begin{aligned} q_j &= \sum_{l=0}^{\infty}\sum_{m=-l}^{l}\Big[\sqrt{l(l+1)}\,C_{j,l}^{m}(\theta,\lambda)\,{}_nT_l(r) \\ &\quad + P_{j,l}^{m}(\theta,\lambda)\,{}_nW_l(r) + \sqrt{l(l+1)}\,B_{j,l}^{m}(\theta,\lambda)\,{}_nV_l(r)\Big]\,, \\ U(r) &= \sum_{l=0}^{\infty}\sum_{m=-l}^{l} X_l^m(\theta,\lambda)\,{}_n\psi_l(r)\,, \end{aligned}\right\} \qquad \text{(A14)}$$

where the vector spherical harmonics C_i, B_i, and P_i are defined by*

$$\left.\begin{aligned} C_{i,l}^{m}(\theta,\lambda) &= \frac{1}{\sqrt{l(l+1)}}\,\epsilon_{ijk}\frac{\partial}{\partial x_k}(x_k\,X_l^m)\,, \\ P_{i,l}^{m}(\theta,\lambda) &= \frac{x_i}{r}\,X_l^m\,, \\ B_{i,l}^{m}(\theta,\lambda) &= -\frac{1}{\sqrt{l(l+1)}}\,r\frac{\partial}{\partial x_i}\,X_l^m\,. \end{aligned}\right\} \qquad \text{(A15)}$$

*Morse, P. M., and Feshbach, H., "Methods of Theoretical Physics," New York: McGraw-Hill, 1953.

X_l^m denotes the complex spherical harmonics. T, W, V, ψ are radial functions and the subscript n denotes the overtone or the number of radial zeros. It should be mentioned that in the notation adopted the letters l and m are reserved for the angular order of the spherical harmonics and are associated with the latitude θ and longitude λ, respectively. The coordinate subscripts are separated from the order subscripts by commas.

The vectors C_i, P_i, and B_i are mutually orthogonal. Motions described by

$$q_i^0 = \sum_{l=0}^{\infty} \sum_{m=-l}^{l} \sqrt{l(l+1)}\, C_{i;l}^m(\theta, \lambda)\, {}_nT_l(r) \tag{A16}$$

involve no radial component; the particles remain on a spherical surface throughout an oscillation. The density remains constant since

$$\frac{\partial q_i^0}{\partial x_i} = 0 . \tag{A17}$$

These oscillations are termed the toroidal oscillations. They are particulary simple since they do not involve coupling with the density field, and, as a result, the gravitational field remains constant.

The motions described by P_i and B_i are characterized by the vanishing of the radial component of the curl of the displacement. They are labeled *spheroidal* oscillations. They involve both radial and horizontal components of the displacement; therefore the gravitational forces come into play.

Numerical Methods For Obtaining The Eigen Frequencies

Two methods have been used to obtain the eigen frequencies for an earth with a radial variation of its elastic properties. In an approach taken from Pekeris the equations are reduced to a set of first-order ordinary differential equations which are integrated by the Runge-Kutta method. In an alternate scheme, matrix methods are used to join up solutions valid in homogeneous layers.

In order to illustrate the methods that have been applied, we will consider the simpler case of *toroidal* oscillations. The equation of motion for toroidal oscillation is

$$\mu\left(\frac{d^2T}{dr^2} + \frac{2}{r}\frac{dT}{dr}\right) + \frac{d\mu}{dr}\left(\frac{dT}{dr} - \frac{T}{r}\right) + \left[(\omega^0)^2 \rho^0 - \frac{l(l+1)}{r^2}\mu\right] T = 0 , \tag{A18}$$

where the subscripts of the radial function T have been omitted. The boundary conditions require that the stress should vanish at the outer surface of the elastic mantle and, since the core is fluid, should also vanish at the inner surface.

Alterman, Jarosch, and Pekeris* formally obviated the need to evaluate the empirically obtained derivative of rigidity by introducing the variables

$$\left.\begin{aligned} y_1 &= T \ , \\ y_2 &= \mu\left(\frac{\partial T}{\partial r} - \frac{T}{r}\right) . \end{aligned}\right\} \tag{A19}$$

Equation A18 is then equivalent to the system

$$\left.\begin{aligned} \frac{dy_1}{dr} &= \frac{1}{r} y_1 + \frac{1}{\mu} y_2 \ , \\ \frac{dy_2}{dr} &= \left[\frac{\mu(l^2 + l - 2)}{r^2} - (\omega^0)^2 \rho^0\right] y_1 - \frac{3}{r} y^2 \ , \end{aligned}\right\} \tag{A20}$$

where the boundary conditions are that y_2 must vanish at the outer and inner boundaries of the earth's mantle. Equations A20 can be integrated by the Runge-Kutta method and the eigen frequencies determined as a function of the integer l. The analysis of the spheroidal oscillations is similar, but it involves the simultaneous solution of six first-order equations.

An alternative method, used by Gilbert and MacDonald†, employs the known solution for a homogeneous spherical shell. The earth is assumed to be a number of concentric spherical elastic shells. The solution for each shell is continued to the next shell by use of the appropriate boundary condition.

The displacement in a toroidal oscillation for a homogeneous elastic shell is

$$g_i^0 = \sum_{l=1}^{\infty} \sum_{m=-l}^{l} \sqrt{l(l+1)}\, C_{i,l}^{m} (\theta, \lambda) \left[a_l^m\, j_l(kr) + b_l^m\, y_l(kr)\right] , \tag{A21}$$

where

$$k = \frac{\omega^0}{V_s} \tag{A22}$$

is the wave number. The values j_l and y_l are spherical Bessel functions of the first and second kind. The coefficients a and b are determined by the boundary conditions that the radial traction vanish, i. e.,

$$\sum_{l=1}^{\infty} \sum_{m=-l}^{l} \sqrt{l(l+1)}\, C_{i,l}^{m} (\theta, \lambda) \cdot$$

$$\cdot \left\{\mu k a_l^m \left[j_l'(kr) - (kr)^{-1} j_l(kr)\right] + \mu k b_l^m \left[y_l'(kr) - (kr)^{-1} j_l(kr)\right]\right\} = 0 , \tag{A23}$$

*Alterman, Z., Jarosch, H., and Pekeris, C. L., "Oscillations of the Earth," *Proc. Roy. Soc. London* 252A(1268):80-95, August 25, 1959.
†Gilbert, F., and MacDonald, G. J. F., "Free Oscillations of the Earth: I. Toroidal Oscillations," *J. Geophys. Res.* 65(2):675-693, February 1960.

at the inner and outer surfaces. If we denote the bracketed terms in Equations A21 and A23 by R and S respectively, then

$$\begin{bmatrix} R \\ S \end{bmatrix} = \begin{bmatrix} j_l(kr) & y_l(kr) \\ \mu k\left[j_l'(kr) - (kr)^{-1} j_l(kr)\right] & \mu k\left[y_l'(kr) - (kr)^{-1} y_l(kr)\right] \end{bmatrix} \begin{bmatrix} a \\ b \end{bmatrix} . \tag{A24}$$

Let s denote the s spherical shell; r_s and r_{s+1} identify the bottom and top radii of the s spherical shell, respectively. Equations A24 take the form

$$\begin{bmatrix} R_s(r) \\ S_s(r) \end{bmatrix} = \mathfrak{A}_s(r) \begin{bmatrix} a_s \\ b_s \end{bmatrix} , \tag{A25}$$

where $\mathfrak{A}$ is a 2, 2 matrix. $\mathfrak{A}_s$ is a function of the density and rigidity of the layer whose inner radius is r_s. Equation A25 can be written

$$\begin{bmatrix} a_s \\ b_s \end{bmatrix} = \mathfrak{A}_s^{-1}(r) \begin{bmatrix} R_s(r) \\ S_s(r) \end{bmatrix} , \tag{A26}$$

provided $\mathfrak{A}_s$ is not singular. By combining Equations A25 and A26 we relate the stress and displacement at the level r_s to the same quantities at r_{s+1}:

$$\begin{bmatrix} R_s(r_s) \\ S_s(r_s) \end{bmatrix} \quad \mathfrak{A}_s(r_s)\, \mathfrak{A}_s^{-1}(r_{s+1}) \begin{bmatrix} R_s(r_{s+1}) \\ S_s(r_{s+1}) \end{bmatrix} . \tag{A27}$$

In terms of the inner, r_I, and outer, r_0, radii of the mantle,

$$\begin{bmatrix} R_1(r_I) \\ S_1(r_I) \end{bmatrix} = \mathcal{C} \begin{bmatrix} R_N(r_0) \\ S_N(r_0) \end{bmatrix} , \tag{A28}$$

where

$$\left.\begin{aligned} \mathcal{C} &= \mathfrak{B}_1\, \mathfrak{B}_2 \cdots \mathfrak{B}_N , \\ \mathfrak{B}_s &= \mathfrak{A}_s(r_s)\, \mathfrak{A}_s^{-1}(r_{s+1}) , \end{aligned}\right\} \tag{A29}$$

The stress must vanish at both the inner and outer surfaces. Therefore Equations A28 become

$$\left.\begin{aligned} \begin{bmatrix} R_1(r_I) \\ 0 \end{bmatrix} &= \mathcal{C} \begin{bmatrix} R_N(r_0) \\ 0 \end{bmatrix} , \\ \mathcal{C}_{21} &= 0 . \end{aligned}\right\} \tag{A30}$$

The roots of Equations A30 are, then, resonant frequencies for the toroidal oscillations.

Spheroidal oscillations may be treated similarly. The matrices are 6×6 and the roots are determined by the vanishing of a partition of the matrix. In this method the elements of the matrices and the inversions are evaluated numerically.

Effect of Rotation on the Eigen Frequencies

The numerical calculations of the previous section can be used to obtain the eigen frequencies for the nonrotating earth. For this case the solution is degenerate with respect to the ordinal number m (see Equations A14); the two possible signs of m are symmetrical for a stationary sphere. Rotation removes the degeneracy with respect to the azimuthal number m. Each line in the spectrum is split into a multiplet of $2l + 1$ lines where the frequencies are given by

$$\omega_l{}^m = \omega_l{}^0 + m\sigma(l)\Omega \quad . \tag{A31}$$

A perturbation calculation* shows that for toroidal oscillations σ is

$$\sigma(l) = \frac{1}{l(l+1)} \quad , \tag{A32}$$

whereas in the case of spheroidal oscillations,

$$\sigma(l) = \frac{\int_0^{r_0} \rho r^2 (2WV + V^2)\,dr}{\int_0^{r_0} \rho r^2 \left[W^2 + l(l+1)V^2\right] dr} \quad , \tag{A33}$$

where r_0 is the outer radius. W and V are the radial functions in Equations A14. Table A1 illustrates the splitting of the spheroidal and toroidal oscillations for the Gutenberg model earth.

Table A1

Rotational Splitting
of Toroidal and Spheroidal Oscillations ($l = 2$)

m	Period (min.)	
	Toroidal	Spheroidal
2	41.9	52.1
1	42.1	52.9
0	42.3	53.7
-1	42.5	54.5
-2	42.7	55.3

*Backus, G., and Gilbert, F., "The Rotational Splitting of the Free Oscillations of the Earth," *Proc. Nat. Acad. Sci.* 47(3):362-371, March 1961. Pekeris, C. L., Alterman, Z., and Jarosch, H., "Rotational Multiplets in the Spectrum of the Earth," *Phys. Rev.* 122(6):1692-1700, June 15, 1961. MacDonald, G. J. F., and Ness, N. F., "A Study of the Free Oscillations of the Earth," NASA Technical Report R-136, 1962; also *J. Geophys. Res.* 66(6):1865-1911, June 1961.